1-1-1982

Measurements of liquid contact in atmospheric pool boiling of water on copper surfaces using a fast response, flush mounted surface temperature probe.

Leo Yu-Wan Lee

MEASUREMENTS OF LIQUID CONTACT IN ATMOSPHERIC POOL BOILING OF WATER ON COPPER SURFACES USING A FAST RESPONSE, FLUSH MOUNTED SURFACE TEMPERATURE PROBE

by

Leo Yu-Wan Lee

A Thesis

Presented to the Graduate Committee

of Lehigh University

in Candidacy for the Degree of

Master of Science

in

Mechanical Engineering

September 1982

This thesis is accepted and approved in partial fulfillment of the requirements for the degree of Master of Science in Mechanical Engineering.

Sept. 13, 1982
(date)

John C. Chen
Professor in Charge

Douglas Abbott
Department Chairman

ACKNOWLEDGEMENTS

The author wishes to thank Dr. R. A. Nelson, Prof. S. Neti, Prof. O. Badr, Dr. K. Tuzla, Mr. J. Kerner and Mr. T. Butrie for their valuable suggestions and helpful comments at various stages of the present experiment.

Prof. J. C. Chen provided careful guidance and encouragement, without which the satisfactory completion of the current study might not have been possible.

The author also thanks Sharon Cawley for this expertly typed report and for her charming assistance in other areas of my graduate work.

I also acknowledge the sponsorship given by EG&G of Idaho for the current research.

TABLE OF CONTENTS

NOMENCLATURE

At	atomic weight
C, C_p	specific heat capacity
DNB	departure from nucleate boiling
E	energy
f	frequency
F	fraction
g	gravitational acceleration
h	heat transfer coefficient, film coefficient
h	specific enthalpy
ID	internal diameter
k,K	thermal conductivity
ℓ	length
Leid	Leidenfrost point, Leidenfrost temperature, the boiling conditions where liquid solid contact in film boiling is first observed
OD	outer diameter
q	heat transfer rate per unit area
Q	heat transfer per unit area
R	radius
S	sum of squares in error
t	time
T	temperature
TC	thermocouple
x	distance, length

X	sensitivity coefficient, defined as $\partial T/\partial Q_{surf}$
Y	measured temperature
α	thermal diffusivity of material $\equiv k/\rho c_p$
β	shorthand for $k\rho C_p$
β	coefficient of volumetric expansion
σ	surface tension
ρ	density
Δ	"change in"
χ	quality $\equiv m_{gas}/m_{TOT}$
∞	infinity
Σ	summation of
π	product of
θ	liquid contact duration

Superscripts

s	iteration count
*	nondimensional quantity
m	future steps in time

Subscripts

b	bulk
c	contact
crit., DNB:	critical point
i	initial condition
int	interface
L, LIQ	liquid

max	maximum
MIN	minimum
n	nodal designation
W	wall

LIST OF TABLES

LIST OF FIGURES

ABSTRACT

A flush mounted, fast responding surface temperature probe was developed. From the measured transient local surface temperatures it was possible to detect liquid-solid contact in film and transition boiling. In pool boiling of saturated deionized water on copper surface, no liquid contact was observed with the surface superheat higher than 200°C. Below that temperature, average liquid contact time fraction increased with decreasing surface superheat and reached a value of 0.4 at critical-heat-flux before attaining full liquid contact in nucleate boiling. With a suitably large sample size, frequency of liquid contacts, duration of liquid contacts and their stochastic distribution could be found. Dependence of the liquid contact behavior on surface superheat and on surface condition was also demonstrated.

I. INTRODUCTION

I.1 Boiling Heat Transfer

Boiling heat transfer has been of technical interest for many decades. In the recent years, with the increasing applications in cryogenics, metal forming, and nuclear engineering, where high heat transfer rates and high surface superheats are encountered, the boiling heat transfer mechanisms, especially for high temperature regimes, have come under intensive investigations.

The boiling process is dependent on many variables and to some extent is stochastic in nature. Current methods to attack the problem tend to be empirical or semi-empirical in nature. Berenson [1] in his well known experiments demonstrated the importance of surface roughness and liquid solid wetting properties. The dependence of the boiling process on thermophysical properties of the heating wall and boiling liquid, pressure, gravitational force, and depth of liquid are well demonstrated in the literature [2,3,4,5].

1.2 Boiling Regimes

Using electric heated wires in pool boiling experiments, Nukiyama [6] first observed the existence of several modes of boiling in 1934. A typical boiling curve (Figure 1) illustrates the nucleate, transition, and film boiling regimes.

1.2.1 Nucleate Boiling

Nucleate boiling occurs with relatively low surface superheats. A liquid continuum is found on the boiling surface with

vapor bubbles generating at preferred nucleation sites. Some researchers believe the agitation provided by the growing and collapsing vapor bubbles accounts for the highly efficient mode of heat transfer in nucleate boiling, while other researchers [7] suggested that the evaporation of liquid micro-layer under a bubble generate the heat flux observed. Excellent surveys and discussions are given by Hsu and Graham [2], Westwater [3], and Leppert and Pitts [4].

I.2.2 Film Boiling

When the surface superheat is very high, all liquid in the vicinity of the hot surface is vaporized and a layer of vapor blanket exists between the liquid bulk and the hot wall. This boiling regime is called film boiling. Due to the insulating properties of the vapor, film boiling mechanism is inefficient and the heat transfer coefficient is typically two orders of magnitude lower than that of nucleate boiling.

Utilizing the concept of free laminar convection and Nusselt's treatment of film condensation, Bromley [8] and Chang [9] analyzed film boiling heat transfer on vertical surfaces. Bromley's model was later improved by Hsu and Westwater[1] to take into account of transition of turbulence for longer vertical walls.

Stable film boiling on horizontal surfaces was modelled by Chang [9], Berenson [10], and Hamill and Baumeister [11]. All

[1]Referred from Hsu and Graham [2], page 74.

three models employ the concept of wavy vapor film and assume a regular pattern of distribution of bubble domes. Correlations for laminar film boiling were also given by the above authors.

I.2.3 Transition Boiling

Transition boiling occupies a regime between nucleate and stable film boiling. Unlike the two other boiling regimes, transition boiling does not seem to have a recognizable boiling pattern. High speed motion pictures by Westwater and Santangelo [12] and by Stock [13] showed the presence of vapor micro-explosions in this boiling regime. Experimental data by Berenson [1] demonstrated that surface condition has strong effects on the transition boiling process, suggesting the possibility of some intimate liquid-solid contacts in this regime.

It is widely believed that transition boiling can be modelled as an oscillatory state between local film boiling and nucleate boiling, with a significant portion of heat transfer through transient conduction to the contacting liquid. No widely accepted correlation isyet available for this boiling regime.

I.3 Objectives of Present Investigation

While liquid contact heat transfer has important contributions to transition and low temperature film boiling regimes, experimental data on liquid contact parameters has been largely lacking. The objectives of the present investigations are:

(1) To develop a surface phase probe capable of

detecting local liquid contacts in pool boiling environment.

(2) To verify the liquid contact phenomenon.

(3) To quantitatively measure the liquid contact durations, frequency, and averaged-time-fraction of liquid contact as functions of surface temperature and surface aging effects on pool boiling of water on copper surfaces.

II. PREVIOUS INVESTIGATION

A brief survey of previous investigations on the subject of liquid-solid contact during boiling is presented in this chapter. Emphasis is placed on highly superheated solid surfaces, corresponding to film and transition boiling conditions.

II.1 Leidenfrost Temperatures

Traditionally, the limiting surface temperature below which liquid contact can occur on the hot wall is known as the Leidenfrost temperature. Spiegler et al. [14] suggested that the Leidenfrost temperature is a function of the thermophysical properties of the fluid alone and can be related to the critical temperature.

$$T_{Leid} = (27/32)T_{crit} \tag{II.1}$$

Baumeiser, Henry and Simon [15] improved Spiegler's equation to take into account the surface properties and obtained

$$T_{Leid} = \frac{(27/32)T_{crit}\{1-\exp(-0.52[10^4(\rho/At)^{4/3}/\sigma_{LV}]^{1/3})\}-T_{LIQ}}{\exp(0.00175\beta)\operatorname{erfc}(0.042\sqrt{\beta})} \tag{II.2}$$

where

$$\beta \equiv (k\rho c)_{SOLID}$$

and

At = atomic weight of boiling fluid

Manson [16] demonstrated that a periodic, spatially non-uniform vapor film could introduce periodic disturbance on the hot surface, resulting in the formation of local cold spots which leads to the collapse of stable film boiling. Manson's model also explains the discrepancies between predicted and measured Leidenfrost temperatures and is included in Henry's [17] discussion on minimum film boiling temperatures.

II.2 Heat Transfer in Metastable Film and Transition Boiling

Due to the presence of local rewetting in transition boiling regime, the total surface heatflux is made up by two parts:

$$Q_{TOT} = Q_{LIQ} + Q_{VAP} \tag{II.3}$$

or

$$Q_{TOT} = F_{L,A}q_{LIQ} + (1-F_{L,A})q_{VAP} \tag{II.4}$$

where $F_{L,A}$ is the average area fraction of liquid contact on the hot surface.

It seems reasonable to assume q_{VAP} to be equivalent to the film boiling heat flux. Heat transfer to the contacting liquid is mostly by transient conduction due to the short durations involved. Bankoff and Mehra [18], in their quenching theory for transition boiling, suggested that heat transfer by transient

conduction to the quenching liquid could be the principal mode of heat transfer in transition boiling regime.

When the semi-infinite material are suddenly brought into contact, classical theory by Carslaw and Jaeger [19] and by Myers [20] predicts the interface will be brought to the temperature

$$T_{int} = T_{2,i} + (T_{1,i}-T_{2,i})(1+\sqrt{\beta_2/\beta_1})^{-1} \qquad (II.5)$$

and

$$T_1 = T_{2,i} + (T_{int}-T_{2,i})\text{erfc}\ (\frac{x_1}{2\sqrt{\alpha_1 t}}) \qquad (II.6)$$

where

int = interface

i = initial temperature

1 = metal part

2 = liquid bulk

By taking derivative of T and integrating in time, we get heat transfer for each liquid contact

$$Q_{LIQ} = 2k_1(T_{int}-T_{2,i})(\frac{\theta}{\pi\alpha_1})^{\frac{1}{2}} \qquad (II.7)$$

θ = contact duration

If all liquid contacts have the same duration and contact frequency (f) are known, then heat transfer to liquid per second

per unit area

$$q_{LIQ} = F_{L,A} f q_{LIQ} \tag{II.8}$$

The presence of liquid motion and eddies will change the effective conductivity of liquid

$$k_{2,eff} = (1+\eta) K_{2,SOLID} \tag{II.9}$$

and η is a function of turbulence level and has a non-negative value.

II.3 Measurements of Liquid Contacts- Previous Attempts

In light of the importance of liquid contact heat transfer as discussed in the previous section, several pioneering experiments were attempted to obtain information on the liquid contact parameters. Most of these attempts were limited to steady-state nucleate boiling systems and only a few were conceived with film/transition boiling. Two types of probes were used:

(1) electrical conductance probe

(2) surface temperature probe

II.3.1 Electrical Conductance Probes

The electrical conductance probe senses the changes in resistance across two electrodes. Different designs were used by Hewitt et al. [21] and Griffith [22] to measure liquid film thickness and transition between annular flow and slug flow.

Using a unique micro-conductance probe, Iida et al. [23,24] was able to "map" the vapor void fraction of boiling water at various locations above the boiling surface.

Yao and Henry [25,26] used a grid of conductance probes in the pool to measure the frequency, durations, and contact area fraction in pool boiling of ethanol and water. In their excellent discussions they demonstrated liquid contact phenomenon is liquid depth dependent, and area of liquid contact decreases exponentially with interface temperature (Figures, 3,4,5). However, the probe calibration (Figure 2) has high degree of uncertainties and only permit order-of-magnitude measurement of area averaged contact (Figure 3).

A flush mounted electrical conductance probe was used by Ragheb [27] and Regheb and Cheng [28] in force convective flow boiling experiments for the detection of phase change at the wall. Both of their probe designs -- the probe to wall method and the two electrode method -- were flush mounted in the wall. Due to the slow response time of their recording system, only time averaged information on F_L was obtained (presumably by a linear interpolation between minimum film boiling point and the DNB point). Their flow boiling F_L is given in Figure 6 (together with Kalnin's and Tong's inferred values).

II.3.2 Surface Temperature Probe

Liquid contacts in high temperature boiling regimes invariably introduce sharp transient temperature drops on the hot surface.

When the local surface temperature is properly monitored, liquid contacts can be detected. This method is advantageous in that most liquid, including electrically non-conductive fluids, can use this method with success. The surface temperature probe method also eliminates the need for calibration of contact area vs. conductance, which could cause large uncertainties.

Using an external thermocouple probe in direct contact with the boiling surface, Hsu and Schmidt [29] measured the time dependent fluctuations in nucleate boiling. Hsu and Schmidt, however, did not claim high quantitative accuracy due to the disturbance in the hydrodynamic boundary conditions by the presence of the probe and the fin-conduction in the thermocouple.

Yu and Mesler [30] also conducted surface temperature measurements in high heat flux nucleate boiling regime (Figures 7 and 8). The flush mounted temperature probe they developed was novel in design and had quick response time. By superimposing the probe trace and the cinephotography of the boiling process they were able to verify the presence of macrolayer and microlayer indirectly. It is interesting to note that their probe signal trace near critical heat flux (Figure 8) is similar to those obtained in this study.

II.4 Correlations on Liquid Contact Fraction

Transition boiling heat transfer is a relatively new research subject, even the importance of liquid contact parameters (the fraction of liquid contact, frequency of liquid

contact, durations of liquid contact, and their stochastic distributions) are widely recognized in liquid contact heat transfer calculations, the experimental data are largely lacking.

Two proposed correlations by Kalnin et al. [31] and by Tong and Young [32] attempts to give an estimate on liquid contact fraction in high temperature boiling.

By separating heat transfer to liquid and vapor in contact with the wall

$$q_{tot} = F_{L,A} q_{LIQ} + (1-F_{L,A}) q_{vap} \tag{II.4}$$

Kalnin approached the problem by assuming

$$F_{L,A} = 1 \quad \text{at} \quad q = q_{max} \tag{II.10a}$$

$$F_{L,A} = 0 \quad \text{at} \quad q = q_{min} \tag{II.10b}$$

and the proposed correlation is

$$F_{L,A} = \left(\frac{\Delta T_{min} - \Delta T_N}{\Delta T_{min} - \Delta T_{max}}\right)^7 \tag{II.10c}$$

Equation (II.10c) is not in a particularly useful form since ΔT_{min} and ΔT_{max} may not be readily available.

To improve $F_{L,A}$ correlations at film boiling regime, it is sensible to suggest $F_{L,A}$ asymptotically approaches zero at film boiling regime with increasing superheat. Considering flow

boiling situations, the form

$$F_{L,A} = c\ell^{-f(\Delta T,x)} \qquad \text{(II.11)}$$

satisfies the boundary condition at high temperature end. Tong and Young [32] evaluated c and f empirically and proposed

$$F_{L,A} = \exp[-0.001\ (\frac{x_E^{2/3}}{dx_E/d\ell})(\frac{\Delta T_{SAT}}{100})^{(1+0.0016\Delta T_{SAT})}] \qquad \text{(II.12)}$$

where

T is in °F

ℓ is length in inches

x_E is the equilibrium quality

Equation (II.12) is defined only in flow boiling and is subjected to experimental modifications.

III. EXPERIMENT

III.1 Purpose

The two objectives of the present experiment were:

a) To develop a surface phase probe which can distinguish individual liquid on vapor contacts on a hot surface in a high temperature boiling experiment.

b) Quantitatively measure the local liquid-contact time-averaged fraction ($F_{L,t}$), liquid contact frequency, and residence durations in pool boiling experiments.

III.2 Probe Development

Several types of probe designs were tried, including the capacitance probe, the electrical-conductance probe, and the surface temperature probe. Scoping experiments demonstrated all three types of probes have inherent shortcomings and fabrication difficulties. It was determined that a surface-temperature probe using a micro-thermocouple offered the unique advantage that the surface temperature and the liquid contact could be detected simultaneously, though the signal analysis was less straightforward.

Regardless of the type of probe used, the characteristics desired were:

a) The probe must be sensitive only to a very small

area such that a local, time dependent signal is measured. This "point probe" requirement enables the determination of the stochastic nature of the liquid contacts.

b) The probe must be mounted internally and in good thermal contact with the test block.

c) Probe tip should be flush with the solid surface to prevent interference to the fluid mechanics of boiling.

d) Probe tip must be made of material similar to other parts of the boiling surface. The surface texture is preferably the same as the adjacent surface.

e) The probe must be rugged enough to withstand the thermal shocks introduced by liquid contacts, it also must be usable to high temperatures (corresponding to film boiling superheats).

A fast-response surface thermocouple probe design was chosen since all of the above criteria were reasonably well met. The dimensions of the test probe are given in Figures 9, 10, and 11. The construction of the probe consisted of three steps:

a) Mounting the microthermocouple in place

b) Resurface the top surface

c) Form thermocouple junction by coating a thin layer of metal across the two thermocouple leads.

Fabrication technique of the microthermocouple surface temperature probe is described in Appendix I.

III.3 Experimental Apparatus and Procedure

In the present experiment, liquid contact measurements in transition and film boiling regimes were performed using the transient method. Initially, the test block-probe assembly (Figure 12) was heated up to and maintained at 450°C for a ten minute period in a clam shealth oven (Figure 13). After uniform block temperature was obtained, preboiled, saturated deionized water was introduced onto the block-probe surface, and was held in place by an aluminum skirt. A smooth transition from film boiling, transition boiling to nucleate boiling occurred as the copper block gradually lost its sensible enthalpy. With an initial block temperature of 450°C, a typical quench process lasted three to four minutes.

Two main experimental series were performed in the present study--Series I, which consisted run series 200's, 300's, 400's and 500's, differed from Series II (runs #1, 2, 3, 4 and 5) in thermal junction formation techniques and recording procedure. However, the two experimental series shared a common signal path configuration shown in Figure 14.

The probe signal was initially amplified with an Accudata

Model 122 DC Amplifier (Figure 16) and routed to a Nicholet Model 1091A "Explorer" digital oscilloscope (Figure 15) for monitoring and recording purposes. Once a signal was captured into the oscilloscope's memory, it could be recorded onto a Techran 817 data cassette through a Nicholet model 194A buffer unit. Data in the digital cassette, which is in standard IEEE format, could then be interfaced with the mainframe computer (a Zyper 720) for calculation purposes. In order to record the whole quench history with a sampling frequency of 5000 Hz, a minimum of one mega words solid-state memory, or a data transmission/recording rate exceeding 60,000 bits/sec (to a hard disk or tape) was needed. Both of the above requirements exceeded the capability of the present equipment used.

For the chronologically earlier Series I runs, the overall quench history was only recorded with a slower sampling frequency of 20 samples/sec. To evaluate liquid contact data, a 0.8 second window of the transient surface temperaturehistory can be captured in the 4096 words oscilloscope's memory (at 5000 samples/sec), the fast scan permitted the determination of individual liquid contacts at that particular surface condition and surface superheat. However, due to the slow data transfer rate from the oscilloscope to the cassette tape, only one record (and hence one data point) could be obtained for a given quench run. A collection of these liquid contact data (from different runs but at similar surface conditions) was used to study the liquid

contact phenomena. It should be noted that after the preparatory runs (Series 100's), the quench block surface was highly oxidized and reached equilibrium state before final data runs began. The fact that the surface aging effects reached an equilibrium was reflected by the boiling curves, as calculated from the overall quench history obtained at various stages of Series I, agreed with each other within experimental error.

Run Series II utilized an Ampex 265 FM recorder to assist the data recording process. The FM recorder, when running at 30 ips, has a minimum bandwidth of DC to 10 KHz, and could record the entire quench history at real time in analog form. It was thus possible, by analyzing the playback signal in segments, to obtain a complete set of liquid contact data for a given quench run. Furthermore, the surface aging effects could be studied by comparing liquid contact and heat flux data of the consecutive quench runs (run #1 had a newly coated surface).

To minimize water deposits, the block surface was lightly wiped with cotton swab and iso-propyl alcohol solution. All unnecessary equipment were turned off and disconnected from the signal path to minimize electrical noise pick-up.

IV. SIGNAL ANALYSIS

IV.1 Liquid-contacts

By using a fast sweep rate (5000 samples/sec), transient local surface temperature at the probe tip was recorded. The large fluctuations in this temperature can be used to detect liquid solid contacts in film and transition boiling. Figure 17 represents a typical expanded trace of the probe signal. When the hot surface was covered by a layer of vapor film, local surface heat flux was quite low. For pool boiling of water on copper surface at 250°C, film boiling correlations by Bromley [8], Zuber [33] and Berenson [34] predicted heat flux values from 2×10^4 W/m^2 to 4×10^4 W/m^2, and was confirmed by Yao's [25,26] experimental data. Due to the low surface heat flux and high thermal diffusivity of copper, the surface temperature registered a value close to the center block temperature (Regime A in Figure 17). When the vapor film was temporarily displaced, direct liquid contact on the surface resulted in a large transient local surface heat flux. With initial wall temperature of 250°C, transient conduction to the liquid is estimated to average 8.5×10^6 W/m^2 over the first millisecond of contact. The sudden heat loss caused a rapid drop in surface temperature (regime B in Figure 17). When local film boiling condition was reestablished (regime C), the surface temperature asymptotically recovered to nearly its original temperature.

Given a sufficient sample period, averaged time fraction of liquid contacts, frequency of liquid contacts, and durations of

individual contacts can be determined by counting in the manner illustrated in Figure 18. It should be noted that the time fraction of liquid contact ($F_{L,t}$) measured in the current study, could be defined by

$$F_{L,t} \equiv \frac{\text{total time of liquid-solid contact}}{\text{total time elipsed}} \qquad \text{(IV.1)}$$

at a local point on the boiling surface over a statistically determinent sample period under quasi-steady or steady-state situation. $F_{L,t}$ differs from $F_{L,A}$ used in (II.4) conceptually where

$$F_{L,A} \equiv \frac{\text{total area under liquid-solid contact}}{\text{total area of boiling surface}} \qquad \text{(IV.2)}$$

for a sufficiently large and statistically determinant surface sample area.

A closer examination of $F_{L,t}$ and $F_{L,A}$ is discussed in Chapter VI in the current report.

As shown in Figures 19, 20, 21 and 22, the frequency of liquid-solid intimate contacts occurred with a value close to 20 contacts/sec at deep transition boiling (illustrated in Figures 19 and 20). It gradually increased to over 40 contacts/sec at 113°C (Figure 21) and at 155°C (Figure 22) surface superheat. It appeared that a 0.819 second probe signal provided the necessary large sample period for the determination of $F_{L,t}$ defined by equation (IV.1), and was used for all current $F_{L,t}$ measure-

ments unless otherwise noted.

A Fortran program was developed to aid calculations of liquid contact parameters from the digitized probe signal. The program (FLDATA) was divided into three parts:

Part (a): With the knowledge of the reference junction temperature, the gain and DC offset of the amplifier, and any nonlinearity in the signal circuit, the original surface temperature trace was reconstructed. The average surface temperature and superheat (from which the measured liquid contact parameters were correlated to), average maximum surface temperature (which was used to estimate the transient liquid-solid contact heat transfer in equation (II.7)), and other related statistics were determined.

Part (b): Liquid contacts were determined and related parameters calculated from the surface temperature trace. Several criteria were used and intimate liquid-solid contact was considered when:

(i) Surface temperature registered a value below 110°C

(ii) A continuous drop in surface temperature with magnitude greater than 15°C

(iii) Surface temperature drop rate exceeded 10°C/msec for a surface temperature drop between 5-15°C.

Also note that any surface temperature fluctuations less than

±3°C was considered noise, and has no calculation consequence. Liquid contacts with a smaller temperature drop was considered not occurring at the measurement junction.

Part (c): This part was the output stage, where hard copies of liquid contact statistics were printed and plotted.

IV.2 Surface Heat Flux

Using a slow sampling rate (20 samples/sec), the overall quench history could be recorded into the memory of the digital oscilloscope. A typical probe signal trace for the overall quench process, as shown in Figure 23, started with the introduction of saturated water and proceeded through stable film boiling, transition boiling, and into nucleate boiling regime as the quench block cooled. For this particular run, initial liquid contact occurred at 75 second and full liquid rewet on the surface was observed around 190 seconds.

When the temperature history of one or more locations in the test block are known, the surface heat flux in a transient experiment can be calculated by solving an inverse conduction problem. For one-dimensional heat transfer, several schemes have been used and some are included in the excellent review by Beck [35].

The inverse conduction program used in the present investigation is a variation of the "CONTA" code developed and discussed by Beck. The operation principles of the present program are:

(i) Use a reasonable estimate of the surface heat flux, and solve the direct conduction problem; an internal temperatureprofile is calculated for the assumed surface heat flux.

(ii) Calculate a "sensitivity coefficient" W (Beck used X), defined as

$$\left.\frac{\partial T_x}{\partial Q_{surf}}\right]_{t=\tau}$$

at given location x and at time τ.

(iii) Compare the measured temperature profile to the calculated temperature profile. The assumed surface heat flux is varied to minimize the sum of temperature discrepancies squared.

Formulation of the basic heat conduction equation in one-dimensional heat transfer without internal heat generation can be written

$$\frac{\partial}{\partial x}\left[K\frac{\partial T}{\partial x}\right] = \rho C_p \frac{\partial T}{\partial t} \qquad \text{(IV.3)}$$

For equal-nodal configuration illustrated in Figure 25, energy balance on a typical interior node n, at time step m, is

$$q_{n-1,n}^{m+\frac{1}{2}} - q_{n,n+1}^{m+\frac{1}{2}} = \frac{dE_n^{m+\frac{1}{2}}}{dt} \qquad \text{(IV.4)}$$

where $q_{n-1,n}^{m+\frac{1}{2}}$ is the heat flux from node n-1 to node n at time

step $n+\frac{1}{2}$ etc., and E_n is the sensible enthalpy for node n.

Using Crank-Nicholson approximation, various terms in (IV.4) can be approximated by:

$$q^{m+\frac{1}{2}}_{n-1,n} = \frac{1}{2}\left[K^{m}_{n-}\frac{T^{m}_{n-1}-T^{m}_{n}}{\delta x} + K^{m}_{n-}\frac{T^{m+1}_{n-1}-T^{m+1}_{n}}{\delta x}\right] \qquad \text{(IV.5)}$$

$$q^{m+\frac{1}{2}}_{n,n+1} = \frac{1}{2}\left[K^{m}_{n+}\frac{T^{m}_{n}-T^{m}_{n+1}}{\delta x} + K^{m}_{n+}\frac{T^{m+1}_{n}-T^{m+1}_{n+1}}{\delta x}\right] \qquad \text{(IV.6)}$$

and

$$\frac{dE^{m+\frac{1}{2}}_{n}}{dt} = \rho C^{m}_{p_n}(\delta x)\frac{T^{m+1}_{n}-T^{m}_{n}}{\delta t} \qquad \text{(IV.7)}$$

where K^{m}_{n-} is the thermal conductivity evaluated at temperature $\frac{1}{2}[T^{m}_{n-1} + T^{m}_{n}]$, similarly K^{m}_{n+} is evaluated at temperature $\frac{1}{2}[T^{m}_{n}+T^{m}_{n+1}]$.

Equation (IV.4) can then be rearranged into the form

$$A_n T^{m+1}_{n-1} + B_n T^{m+1}_{n} + C_n T^{m+1}_{n+1} = D_n \qquad \text{(IV.8)}$$

where

$$A_n = K^{m}_{n-} \qquad \text{(IV.9a)}$$

$$C_n = K^{m}_{n+} \qquad \text{(IV.9b)}$$

$$B_n = 2\rho C^{m}_{p_n}(\delta x)^2/\delta t - A_n - C_n \qquad \text{(IV.9c)}$$

and

$$D_n = -A_n T_{n-1}^m - B_n T_n^m - C_n T_{n+1}^m \qquad \text{(IV.9d)}$$

Following similar treatment, equation of the surface node can be written as

$$q_s^{m+\frac{1}{2}} + \frac{1}{2}\left[K_{1+}^m \frac{T_2^{m+1} - T_1^{m+1}}{\delta x} + K_{1+}^m \frac{T_2^m - T_1^m}{\delta x}\right]$$

$$= (\rho C_p)_1^m \lambda \delta x\left[\frac{T_1^{m+1} - T_1^m}{\delta t}\right] + (\rho C_p)_2^m (1-\lambda)\delta x\left[\frac{T_2^{m+1} - T_2^m}{\delta t}\right] \qquad \text{(IV.10)}$$

Rearranging (IV.10) we have

$$B_1 T_1^{m+1} + C_1 T_2^{m+1} = D_1 \qquad \text{(IV.11)}$$

where

$$B_1 = K_{1+}^m + 2\rho C_{p_1}^m \lambda \frac{(\delta x)^2}{\delta t} \qquad \text{(IV.12a)}$$

$$C_1 = -K_{1+}^m + 2\rho C_{p_1}^m (1-\lambda) \frac{(\delta x)^2}{\delta t} \qquad \text{(IV.12b)}$$

and

$$D_1 = 2(\delta x) q_s^{m+\frac{1}{2}} - B_1 T_1^m - C_1 T_2^m \qquad \text{(IV.12c)}$$

q_s is the surface heat flux and is taken to be positive for heat transfer into the block.

For the end node at the bottom insulated surface, we have

$$A_n T_{n-1}^{m+1} + B_n T_n^{m+1} = D_n \qquad \text{(IV.13)}$$

where

$$B_n = K_{n-}^m + 2\rho C_{p_n}^m \lambda \frac{(\delta x)^2}{\delta t} \qquad \text{(IV.14a)}$$

$$A_n = -K_{n-}^m + 2\rho C_{p_{n-1}}^m (1-\lambda) \frac{(\delta x)^2}{\delta t} \qquad \text{(IV.14b)}$$

and

$$D_n = -B_n T_n^m - C_n T_{n-1}^m \qquad \text{(IV.14c)}$$

A system of equations can thus be formed.

$$\begin{bmatrix} B_1 & C_1 & 0 & & & 0 \\ A_2 & B_2 & C_2 & & & 0 \\ 0 & & & & & \\ & 0 & A_{n-1} & B_{n-1} & C_{n-1} & \\ 0 & & & A_n & B_n & \end{bmatrix} \begin{Bmatrix} T_1^{m+1} \\ T_2^{m+1} \\ \\ \\ T_n^{m+1} \end{Bmatrix} = \begin{Bmatrix} D_1 \\ \\ \\ \\ D_n \end{Bmatrix} \qquad \text{(IV.15)}$$

Equations (IV.15) can be solved by any efficient numerical algorithms, such as Gauss elimination and Thomas algorithm.

The "Error" of the calculated temperature profile, as the solutions of (IV.15), when compared to the experimental value, can be measured by the sum of deviations squared, the function ξ,

$$\xi \equiv \sum_{j=1}^{J} \sum_{i=1}^{I} (Y_{j,m+i-1} - T_{j,m+i-1})^2 \qquad \text{(IV.16)}$$

Subscript j is for the jth thermocouple location and i is for ith future times. $Y_{j,m+i-1}$ is the jth measured temperature at time t_{m+i-1} and $T_{j,m+i-1}$ is the jth calculated temperature (at node j) at time t_{m+i-1} for a prescribed surface heat flux q_m.

The use of future temperature smooth out random measurement errors. Consider the present case, where one thermocouple at the surface was used (J=1), choosing two future temperatures (I=2), we have, from equation (IV.16)

$$\xi \equiv \sum_{i=1}^{2} (Y_{m+i-1} - T_{m+i-1})^2 \qquad \text{(IV.17)}$$

and minimizing ξ for a given ξ_m, get

$$\frac{\partial \xi}{\partial q_m} = 0 = -2 \sum_{i=1}^{2} [(Y_{m+i-1} - T_{m+i-1}^{*s}) W_{m+i-1}^{*s}] \qquad \text{(IV.18)}$$

where s is the iteration index.

$$T_{m+i-1}^{*s} \equiv T_{m+i-1}^{*(s-1)} + W_{m+i-1}^{*s} (q_m^s - q_m^{s-1}) \qquad \text{(IV.19)}$$

and

$$W_{m+i-1}^{*s} \equiv \frac{\partial T_{m+i-1}^{s}}{\partial q_m} \qquad \text{(IV.20)}$$

as discussed in Section (IV.2ii).

For the direct conduction problem we have the system

$$\frac{\partial}{\partial x}\left(K \frac{\partial T}{\partial x}\right) = \rho C_p \frac{\partial T}{\partial t} \qquad \text{(IV.21a)}$$

with

$$\text{B.C.'s} \qquad -K \frac{\partial T(0,t)}{\partial x} = q_m \qquad \text{(IV.21b)}$$

$$- K \frac{\partial T(L,t)}{\partial x} = 0 \qquad \text{(IV.21c)}$$

$$\text{I.C.} \qquad T(x,t_{m-1}) = f(x) \qquad \text{(IV.21d)}$$

Differentiating (IV.21) with respect to q_m, we have a new system of equation

$$\frac{\partial}{\partial x}\left(K \frac{\partial w}{\partial x}\right) = \rho C_p \frac{\partial w}{\partial t} \qquad \text{(IV.22a)}$$

$$\text{B.C.'s} \qquad -K \frac{\partial w(0,t)}{\partial x} = 1 \qquad \text{(IV.22b)}$$

$$-K \frac{\partial w(L,t)}{\partial x} = 0 \qquad \text{(IV.22c)}$$

$$\text{I.C.} \qquad w(x,t_{m-1}) = 0 \qquad \text{(IV.22d)}$$

Equation IV.22s' can be solved in the exact same manner as system IV.21 discussed error, only difference in RHS vector is resulted.

$$q_m^s = q_m^{s-1} + \frac{\sum_{i=1}^{2} (Y_{m+i-1} - T_{m+i-1}) w_{m+i-1}^{s-1}}{\sum_{i=1}^{2} (w_{m+i-1}^{s-1})^2} \qquad \text{(IV.23)}$$

When the thermal properties at all nodes does not change appreciably with one time step, we have a linear system and only one iteration is needed (predictor-corrector).

The inverse conduction problem outlined above involved differentiation process in the surface temperature history, which would greatly exagerate uncertainties, noise, and random errors in the original data. Due to the large fluctuations in surface temperature history introduced by liquid contacts, the original data, as shown in Figure 23, had to be smoothed to assume differentiability. Two steps were involved:

(i) The signal was short-time-averaged over one second intervals.

(ii) The short-time-averaged signal was then fitted by a second order polynomial piecewise, correlation over twelve time steps were used to generate the best fitted curve, from which temperature at center six time steps were recalculated. A smoothed surface temperature trace, corresponding to the raw data shown in Figure 23, is illustrated in Figure 24. The surface heat flux history calculated from the smoothed surface

temperature trace was cross-correlated with the short-time-averaged temperature to generate the boiling curves.

V. RESULTS

Two groups of data are presented. The first run series, which consisted run series 200's, 300's, 400's and 500's, investigated the feasibility of using a fast response surface microthermocouple probe for the measurement of local, transient liquid contacts in pool boiling environment. The second run series, which included runs 1, 2, 3, 4 and 5, investigated the progressive surface aging effects on liquid contact phenomenon. A summary comparison of test conditions between series I and series II is outlined in Table 1. Since series I and series II runs had different surface conditions, probe formation techniques, and used different recording procedure, their results are presented separately.

Of prime interest, the parameters which are important to the study of liquid-solid contact behavior and liquid contact heat transfer included

(i) the time-fraction of liquid contact at a local point on the boiling surface ($F_{L,t}$)

(ii) the average duration of liquid contacts, and

(iii) the frequency of liquid contact.

In conjunction of the above three parameters, the calculated surface heat flux and, for series I, the distribution of liquid contact durations are also reported.

V.1 Series I Results

Figure 26 shows the liquid contact time-fraction data for run series I at various short-time-averaged surface superheat.

	Series I	Series II
Runs:	200's,300's,400's & 500's.	runs 1,2,3,4 & 5
water:	200's-400's tap water 500's distilled.	distilled, deionized.
block:	oxygen-free copper	oxygen-free copper
recording method:	1 sample over a given window taken each run by Nicholet 1090A digital oscilloscope.	overall quench stored real-time into ampex 265 FM recorder.
surface cond. :	fully oxidized	progressive oxidation with increasing run no.
roughness :	lapped with 320 grade emery paper (initial)	lapped with 320 grade emery paper (initial)
junction form. :	brush tape electroplating with copper plating solution.	vacuum vapor deposition with pure aluminum (multi-coated six times)
thickness :	5×10^{-5} meter	1.7×10^{-5} meter
cleaning :	wiped with cotton swab and iso-propanol sol. before heating.	wiped with cotton swab and sio-propanol sol. before heating.

Table 1: comparisions between series I & II runs

It could be seen that at low surface superheat, $F_{L,t}$ value was quite high; at and around the critical heat flux point (30-40°C superheat), $F_{L,t}$ processed a value of 0.3-0.6, it decreased rapidly to a typical value of 0.1 around 90°C surface superheat. At even higher surface superheat, $F_{L,t}$ continued to decrease but with a slower rate. For all series I runs, $F_{L,t}$ hovered around a value of 0.03-0.1 at 90-150°C surface superheat. The smoothed $F_{L,t}$ value, shown in Figure 27, combined 300's and 400's series into one curve, for the reason that the 300's and 400's series used identical experimental procedure, and both had highly oxidized surfaces.. (The only difference was that they were taken on consecutive days.) While a maximum surface superheat up to 160°C was used for run series 200's, 300's and 400's, series 500's used a maximum superheat of 240°C. As shown in Figure 28, liquid contact frequency for series 500's fell from 50 Hz at 140°C superheat, to a vanishing 2 Hz at 200°C superheat. The infrequent and short contacts resulted in a dramatic drop in $F_{L,t}$ at 140-200°C superheat as shown in Figure 27.

The frequency of liquid contact for series I runs is shown in Figure 28. For surface superheat from 30°C to 140°C, a consistent increase in liquid contact frequency with increasing surface superheat is observed. Typically, liquid contact frequency has a value of 15-20 Hz at 30°C superheat, and increased almost linearly with respect to surface superheat and processed a maximum value around 60 Hz at 130°C superheat. For series 300's, a high

value of 90 Hz was observed. However, the frequency of liquid contacts dropped drastically from 150°C-200°C surface superheat to below 5 Hz, and vanished altogether at surface superheats higher than 230°C.

Figure 29 illustrates the functional dependence of the average liquid contact duration on the surface superheat. In general, liquid contact durations decreased monotonically with increasing surface superheat, but in a nonlinear manner. At 30-90°C superheat, average liquid contact duration dropped from a longest of 15 msec (50 msec for series 300's) to 2 msec; at surface superheat higher than 90°C, the average contact duration flattened out and hovered around a value of 0.3-2 msec.

The boiling curves for series I runs were calculated using the inverse conduction program discussed in Section IV.2, and are presented in Figure 29. While the boiling curve of the 500's series is flatter than the 300's and 400's series (boiling curves of the 300's and 400's series are almost in each agreement with each other), general agreement in trend and heat flux value is observed. By cross-plotting $F_{L,t}$ value with the surface heat flux, Figure 31 seeks a relationship of the two variables for the series I runs. It is interesting to note that at transition boiling regime (with $F_{L,t}$ from 0.08 to 0.3), close agreement between the different run series is observed. In general, surface heat flux increased with increasing $F_{L,t}$ value, but no conclusion could be drawn with $F_{L,t}$ greater than 0.3 (where little data was obtained due to the high heat flux and fast temperature drop).

V.2 Series II Results

As mentioned earlier in Section III.3, the major objective of the Series II runs were to observe surface aging effects on the liquid contact phenomenon. The chronologically arranged, and consecutively numbered runs (run 1 to run 5) had an increasing oxidized surface, and permitted qualitative studies of the surface aging effects. Since run 5 suffered from a sudden blast of electrical noise during data acquisition period, only the first four runs are reported.

Similar to Figure 26 of Series I, Figure 32 indicates a definite decrease of $F_{L,t}$ value with increasing surface superheat. With a new surface for Run 1, $F_{L,t}$ value decreased almost in an exponential manner from unity (at 25°C superheat) to 0.05 (at 190°C superheat). For the progressively oxidized surfaces, the $F_{L,t}$ values were similar to that of run 1 at low surface superheat (below 60°C). At higher superheat, however, time averaged liquid contact fraction for an oxidized surface is much lower when compared with an unoxidized surface. At 150°C superheat, run #4 has a $F_{L,t}$ of 0.003, while for run 1, it was 0.03, an order of magnitude difference. On the other hand, initial liquid-solid contact superheat for an aged surface was higher than the unoxidized surface (210°C for run 4 vs. 180°C for run 1).

Another interesting finding on surface aging effect is concerned about the liquid contact frequency. As shown in Figure 33, liquid contact frequency at low surface superheat (below 50°C) and

high surface superheat (above 160°C) is relatively independent of of surface oxidation. At medium superheat (50°C-150°C), liquid contacts on an oxidized surface occurred less frequently when compared with a less oxidized surface. It is unclear, at present, if the above discussed trend is a general phenomenon, or was it only unique to the boiling surface under study. A comparison of runs #3 and 4 with the Series I data (also an oxidized surface) seemed to suggest the different surface texture, material, and the oxide type might have strong effects on the liquid contact behavior. (Note that Series II runs had an aluminum vapor deposited surface, while series I had a copper electroplated surface).

The averaged liquid contact duration, presented in Figure 34 for the Series II runs, indicated shorter contact durations for oxidized surfaces at surface superheat higher than 60°C. For run #1, the average contact durations have a value of 1-2 msec, while run 2, 3, and 4 typically registered a value of about 40 percent lower. At surface superheat below 60°C, discrepancies on average contact durations for various surfaces were not significant.

Figure 35 presented the calculated boiling curve for each individual run in Series II. An increase in surface heat flux at high surface superheat (>60°C) was observed for an aged surface, and the trend was in agreement with Berenson's data [1].

The stochastic distributions of the liquid contact durations are shown graphically in Figures 35-38, and are listed in tabular form in Table 2. On the right hand side of Figures 36-39, the total

	File no.	Ave. superheat (^{o}C)	contact frequency (HZ)	occurance frequency(normalized)					
				t<1 (msec)	1≤t<2 (msec)	2≤t<4 (msec)	4≤t<8 (msec)	8≤t<16 (msec)	16≤t<32 (msec)
*** Run # 1 ***	R1T21	114.5	37.1	.3684	.3816	.2237	.0263	0	0
	R1T23	84.8	40.3	.3030	.1515	.0606	.2424	.1818	.0606
	R1T24	68.7	42.7	.2857	.2000	.0571	.2571	.1429	.0571
	R1T25	42.5	26.8	0	.0909	.0909	.1818	.1818	.3636
*** Run #4 ***	R4T94	109.6	13.4	.8182	.1818	0	0	0	0
	R4T95	89.8	19.5	.6250	.3125	.0625	0	0	0
	R4T103	66.6	13.4	.1818	.3636	.1818	.1818	.0909	0
	R4T105	37.0	25.6	.0476	.0952	.0952	.0476	.3809	.1905

Table 2: Statistical distrubition of contact durations

	File no.	Ave. superheat (^{o}C)	contact frequency (HZ)	occurance frequency(normalized)					
				t<1 (msec)	1≤t<2 (msec)	2≤t<4 (msec)	4≤t<8 (msec)	8≤t<16 (msec)	16≤t<32 (msec)
*** Run # 1 ***	R1T21	114.5	37.1	.3684	.3816	.2237	.0263	0	0
	R1T23	84.8	40.3	.3030	.1515	.0606	.2424	.1818	.0606
	R1T24	68.7	42.7	.2857	.2000	.0571	.2571	.1429	.0571
	R1T25	42.5	26.8	0	.0909	.0909	.1818	.1818	.3636
*** Run #4 ***	R4T94	109.6	13.4	.8182	.1818	0	0	0	0
	R4T95	89.8	19.5	.6250	.3125	.0625	0	0	0
	R4T103	66.6	13.4	.1818	.3636	.1818	.1818	.0909	0
	R4T105	37.0	25.6	.0476	.0952	.0952	.0476	.3809	.1905

Table 2: Statistical distrubition of contact durations

liquid contact frequency is also shown. On the horizontal axis, the following indices are used.

a: $\theta \leq 1$ msec

b: 1 msec $\leq \theta < 2$ msec

c: 2 msec $\leq \theta < 4$ msec

d: 4 msec $\leq \theta < 8$ msec

e: 8 msec $\leq \theta < 16$ msec

f: 16 msec $\leq \theta < 32$ msec

g: 32 msec $\leq \theta$

where θ is the liquid contact duration.

At higher surface superheat, as shown in Figures 36 and 37, liquid contact for run 4 was predominantly composed of very short contacts. At surface superheat of 85°C, Figure 36 illustrated almost half of the liquid contacts had durations longer than 4 msec for run #1 (least oxidized surface), while no similar contacts were observed on the highly oxidized surface of run #4; at lower surface superheats, as shown in Figure 38 and 39, longer contacts for oxidized surface occurred more frequently and little discrepancy was observed at 40°C superheat (Figure 39).

VI. DISCUSSION

VI.1 Analysis of Error and Uncertainties

In the present experiment, two types of errors were encountered. The first type of error was random in nature (i.e. electrical noise), and the second type was systematic in nature (i.e. nonlinearity in recording medium). While great care was taken to minimize both random and systematic errors during the design and execution stages, they could not be eliminated totally and the remaining inherited errors and uncertainties are summarized below.

Uncertainties in measured $F_{L,t}$ frequency of liquid contact, and durations of liquid contacts caused by the selection of liquid contact criteria (discussed in Section IV.1) were estimated at ±5%, ±2% and ±4% respectively. Quantization errors on $F_{L,t}$ and liquid contact durations were both estimated to be -0, +5% for an average contact duration less than 1 msec, and was expected to be less for longer contacts). On the surface temperature measurement, uncertainties due to electrical noise was ±1°C, and maximum systematic error due to amplifying and recording processes was 3°C, in either direction.

It was of major concern that the presence of the thermocouple probe itself might introduce thermal disturbance in the test block, and might result in liquid contact measurements whicn might be atypical to the actual values (without the probe).

Since electroplated/vapor deposited surfaces are homogeneous in nature, any systematic measurement errors will be due to the

inhomogenuity inside the test block.

Using a geometry shown in Figure 41, Beck and Huroviez [36] studied the effect of imbedded thermocouple void on surface temperature and heat transfer, and sample results were given in Figures 42 and 43. Compared to Figure 41, the present geometry has

$$R \approx 1.7 \times 10^{-4} \text{ meters}$$

$$E \approx 5 \times 10^{-5} \text{ meters} \quad \text{(Series I)}$$

or

$$E \approx 1.7 \times 10^{-5} \text{ meters} \quad \text{(Series II)}$$

and

$$g = \frac{R}{E} = 3.4 \quad \text{(Series I)}$$

$$= 10 \quad \text{(Series II)}$$

As shown in Figure 43

$$\frac{T_o - T_{o\infty}}{g q_o R/K} = 0.53 \quad \text{(Series I)}$$

$$= 0.4 \quad \text{(Series II)}$$

Table 3 illustrates some typical temperature change at the probe tip for the vapor-deposited probe (higher error of the two due to thinner junction). As shown in Table 3, RMS error for 180°C superheat was 3.3% (low), and was 2.67% to 5.7% low for surface superheat of 80°C (depended on contact durations and $F_{L,t}$). At a steady surface heat flux of 10^6 W/m^2, the probe tip was only 1.8°C low when compared without the presence of the probe.

Surface Superheat	Contact Duration	Average Heat Flux (W/m^2)	$T_o-T_{o\infty}$ (Error °C)	$\frac{T_o-T_{o\infty}}{\Delta T_{sat}}$ (%)	RMS (%)
180°C	1 msec s.s. vapor contact	$\sim 1 \times 10^7$	-17.7	-10	(F_L = 0.1)
		$\sim 1 \times 10^5$	-0.2	-0.1	-3.3
80°C	1 msec s.s. vapor contact	-4.5×10^6	-8.0	-10	(F_L = 0.3)
		$\sim 1 \times 10^5$	-0.2	-0.25	-5.7
	5 msec s.s. vapor contact	-2×10^6	-3.6	-4.5	(F_L = 0.3)
		$\sim 1 \times 10^5$	-0.2	-0.25	-2.67
Steady State Heat Transfer		1×10^6	-1.8		

TABLE 3 Typical values for surface temperature disturbance at probe tip: a conservative estimate

Surface Superheat	Contact Duration	Average Heat Flux (W/m^2)	$T_O-T_{O\infty}$ (Error °C)	$\frac{T_O-T_{O\infty}}{\Delta T_{sat}}$ (%)	RMS (%)
180°C	1 msec s.s. vapor contact	$\sim 1 \times 10^7$	-17.7	-10	(F_L = 0.1)
		$\sim 1 \times 10^5$	-0.2	-0.1	-3.3
80°C	1 msec s.s. vapor contact	$\sim 4.5 \times 10^6$	-8.0	-10	(F_L = 0.3)
		$\sim 1 \times 10^5$	-0.2	-0.25	-5.7
	5 msec s.s. vapor contact	$\sim 2 \times 10^6$	-3.6	-4.5	(F_L = 0.3)
		$\sim 1 \times 10^5$	-0.2	-0.25	-2.67
Steady State Heat Transfer		1×10^6	-1.8		

TABLE 3 Typical values for surface temperature disturbance at probe tip: a conservative estimate

The above estimates were conservative in nature due to the following reasons:

(i) Thermal conductivity of the ceramic insulating material was totally neglected.

(ii) Heat transfer through the two thermocouple leads was also neglected.

(iii) Averaged thermal deviation over the whole probe tip was lower than the deviation at the center of the probe tip.

It was thus expected, that the presence of the probe with the present geometry should not change the actual liquid contact parameters by more than 5 percent.

VI.2 Time-averaged and Area-averaged F_L

On a boiling surface, portion of the surface is in vapor contact (drg) and the other portion is under liquid contact. It was possible to define a liquid contact function, ε that

ε has a value of 1 on wetted surfaces, and has a value of 0 on dry surfaces. In general, ε is a function of location, time, surface condition, thermal properties of solid and liquid...etc., or

$$\varepsilon = \varepsilon(\vec{r},t,T,\alpha_s,\alpha_L,k_s,k_\ell,\sigma_{L,V},p...) \qquad (VI.1)$$

For a given boiling system, all solid and liquid properties, pressure

etc. are fixed, and assume fixed surface temperature

$$\varepsilon = \varepsilon(\vec{r},t) \tag{VI.2}$$

function of position and time only.

The time-averaged liquid contact fraction ($F_{L,t}$), such as measured by Ragheb [28] and in the present investigation, can be defined as

$$F_{L,t}(\vec{r}_o) \equiv \frac{\int_o^\tau \varepsilon(\vec{r}_o,t)dt}{\int_o^\tau dt} \tag{VI.3}$$

for a large enough sample period τ measured at location r_o.

Similarly, the area-average liquid contact fraction ($F_{L,A}$) measured by Yao and Henry [25,26] can be defined as

$$F_{L,A}(t_o) \equiv \frac{\int_o^{\vec{R}} \varepsilon(\vec{r},t_o)d\vec{r}}{\int_o^{\vec{R}} d\vec{r}} \tag{VI.4}$$

for some 'large enough measurement area R' at time $t = t_o$.

Assuming we have a homogeneous surface, thus $F_{L,t}$ cannot be a function of position, or

$$F_{L,t}(\vec{r}_o) = F_{L,t}(\vec{r}_o+\Delta\vec{r}) = C_1 = \frac{\int_o^T \varepsilon(\vec{r}_o+\vec{r},t)dt}{\int_o^T dt} \tag{VI.5}$$

Since $\Delta\vec{r}$ is arbitrary, $\vec{r}_o+\Delta\vec{r}$ can be at any location, equation (VI.5) can be rewritten as

$$F_{L,t}(\vec{r}_o) = F_{L,t}(\vec{r}) = C_1 = \frac{\int_o^T \varepsilon(\vec{r},t)dt}{\int_o^T dt} \qquad \text{(VI.6)}$$

Furthermore, if we have steady state or quasi-steady situation, $F_{L,A}$ by definition cannot be a function of time, or

$$F_{L,A}(t_o) = F_{L,A}(t_o+\Delta t) = C_2 = \frac{\int_o^{\vec{R}} \varepsilon(\vec{r},t_o+\Delta t)d\vec{r}}{\int_o^{\vec{R}} d\vec{r}} \qquad \text{(VI.7)}$$

Since Δt can be of any value, (IV.7) can be rewritten as

$$F_{L,A}(t_o) = F_{L,A}(t) = C_2 = \frac{\int_o^{\vec{R}} \varepsilon(\vec{r},t)dr}{\int_o^{R} d\vec{r}} \qquad \text{(VI.8)}$$

Since

$$C_1 = C_1 \frac{\int_o^{\vec{R}} d\vec{r}}{\int_o^{R} d\vec{r}} = \frac{\int_o^{\vec{R}} C_1 d\vec{r}}{\int_o^{\vec{R}} d\vec{r}} \qquad \text{(VI.9)}$$

Substituting into (VI.6) we have

$$F_{L,t}(\vec{r}_o) = C_1 = \frac{\int_o^{\vec{R}} \int_o^T \varepsilon(\vec{r},t)dt\, d\vec{r}}{\int_o^{\vec{R}} \int_o^T dt\, d\vec{r}} \qquad \text{(VI.10)}$$

also

$$C_2 = C_2 \frac{\int_0^T dt}{\int_0^T dt} = \frac{\int_0^T C_2\, dt}{\int_0^T dt} \qquad \text{(VI.11)}$$

Substituting into (VI.8), we have

$$F_{L,A}(t_o) = C_2 = \frac{\int_0^T \int_0^{\vec{R}} \varepsilon(\vec{r},t)\, d\vec{r}\, dt}{\int_0^T \int_0^{\vec{R}} d\vec{r}\, dt} \qquad \text{(VI.12)}$$

Note that the right hand side of (VI.10) and (VI.12) are equal, we have

$$F_{L,t}\,(\vec{r}_o) = F_{L,A}(t_o) \qquad \text{(VI.13)}$$

Thus, for a homogeneous surface and quasi-steady boiling situation, time-averaged liquid contact fraction measured at any surface location (for a long enough sample period) will be identical in value with the area-averaged liquid contact fraction (for a large enough measurement area) for a given surface superheat.

Since all assumptions were satisfied for the current investigation, the time-averaged liquid contact fraction obtained in this experiment permitted direct comparisons with area-averaged liquid contact data from other sources.

VI.3 Comparison with Previous Investigation

a. Boiling Curves

The calculated boiling curves for run series I shown in Figure 30, and that of series II shown in Figure 35, clearly indicated the important role of surface oxidation on the boiling heat flux. In general, Figure 35 showed an increase in surface heat flux value at high surface superheat with increasing oxidation. The copper-pentane data (Figures 37, 38) by Berenson [1] demonstrated similar trend. Note that at the surface superheat of 55°C ~(100°F) in Figure 38, the 'unclean' surface heat flux was more than an order of magnitude higher than that of the 'clean' surface. Figure 38 also demonstrated the surface superheat for stable film boiling was largely affected by the cleanliness of the boiling surface.

The peak pool boiling heat flux for the current investigation, which was between 1×10^6 to 2×10^6 W/m^2 (Figures 30,35) compares favorably with the 1.7×10^6 W/m^2 (538 K Btu/hr ft^2) obtained by Gambill [37]. Variations in surface critical heat flux values were typically within ±2 percent.

b. Maximum Surface Temperature for Liquid Contact

The incipient liquid contact surface superheat measured 180°C for run #1 (least oxidized surface) and progressively increased to 210°C for run #4 (highly oxidized surface). It is possible to explain the above observation by Manson's [16] model of nonuniform periodic heat transfer, which introduces local cold spots on the less conductive oxide film (and invites liquid contact). The

present measurements are in good agreement with Baumeister, Henry and Simon's [15] measured Leidenfrost temperature (165-225°C superheat). The maximum surface temperature predicted using Spiegler's equation (II.1) yield a value of 180°C superheat, and was again in good agreement with the present data.

c. *Liquid Contact Fraction*

At present, experimental data on liquid contact fraction are extremely limited. Aside from the pioneering effects by Yao and Henry [25,26], who measured area-averaged liquid contact fraction and other parameters in stable film boiling regime, the other liquid contact existed (to the knowledge of the present investigator) in Ragheb and Cheng's [28] time-averaged liquid contact fraction measurement in flow boiling regime.

To complicate matters further, Yao and Henry used a gold-plated boiling surface and correlated the normalized liquid contact data to the contact temperature (shown in Figures 3, 4, and 5). The presentation format on liquid contact fraction (Figure 3) also makes Yao's data not directly comparable with the present results given in Chapter V.

The flow boiling F_L data from Ragheb and Cheng [28], and the inferred values by Kalnin [31], and by Tong [32] are presented in Figure 6, and in Figure 46 with smoothed $F_{L,t}$ data from series II runs for comparison purposes. Note that the surface superheat value they used were the temperature measured a short distance away from the surface, which would correspond to the average

maximum surface temperature of the typical probe signal trace of the present investigation. For instance, Figure 20 illustrates a typical probe signal trace at late transition boiling regime, the averaged maximum surface temperature reads 150°C, as the temperature Ragheb's may intend to correlate his data with, as opposed to 139°C average surface superheat the present investigation used. At higher surface temperature, the average maximum temperature and the average surface temperature would be closer in value, due to the lower liquid contact fraction.

As shown in Figure 46, all measured and inferred liquid contact fraction agreed in trend and in general values. However, a direct comparison among the data was not sought due to different boiling situations and boiling surface conditions.

VI.4 Transient Conduction Liquid Contact Heat Transfer Model

After the liquid contact phenomenon was discovered by Bradfield [38] in the sixties, it was a widely accepted concept that (1) heat transfer to the liquid in contact with the hot wall is the major mode of heat transfer in transition boiling, and (2) the peculiar transition boiling regime is caused by a large increase in liquid contact area at lower surface superheat.

Due to the large amount of variables involved, heat transfer mechanisms to the contacting liquid are still not well understood. In an attempt to provide reasonable estimates on liquid contact heat transfer, Bankoff and Mehra [18] proposed a simple and elegant quenching theory for transition boiling regime. The central idea

of the quenching theory is that heat transfer to the liquid contacts is by transient conduction.

As shown earlier in Section II.2, transient conduction heat transfer for each contact per contact area is

$$Q_{L,Q} = 2k_1(T_{int} - T_{2,i})\left(\frac{\theta}{\pi\alpha_1}\right)^{\frac{1}{2}} \qquad (II.7)$$

where

θ = contact duration

subscript 1 indicates metal, and interface temperature

T_{int} was defined by equation (II.5).

The total heat flux contributions to unit boiling surface area via transient conduction will then be

$$q_\ell = F_{L,A} \sum_{j=1}^{f} Q_{L,j} = 2F_{L,A}(T_{w,i}-T_c)\sqrt{\frac{(k\rho c)_w}{TC}} \sum_{j=1}^{f} \theta_j^{\frac{1}{2}} \qquad (VI.14)$$

where

f = liquid contact frequency

$F_{L,A}$ = area-averaged liquid contact fraction

To evaluate (VI.14), the contact temperature must be calculated using equation (II.5) (which involved k_ℓ, the liquid thermal conductivity. In general, tabulated values for liquid thermal

conductivity, such as those obtained from CRC Handbook of Phy. and Chem., assumed minimum internal fluid motion. During transient liquid contact on the hot surface, vapor formation and the high temperature gradient are likely to enhance internal convection within the liquid body, and resulted in a higher effective liquid thermal conductivity due to internal circulation and eddies. Conceptually, a hypothetical limiting case existed that the effective thermal conductivity of contacting liquid become so high that the heat transfer rate is limited by the transport properties of the base metal. As $(k\rho c)_{\ell,eff}$ tends to ∞, the contact temperature defined by II.5 tends to T_{sat}, and the hypothetical "maximum" heat transfer to the liquid becomes

$$q_{\ell,max} = 2F_{L,A}(T_{w,i}-T_{sat})\sqrt{\frac{(k\rho c)_w}{\pi}} \sum_{j=1}^{f} \theta_j^{\frac{1}{2}} \qquad \text{(VI.15)}$$

When tabulated k_ℓ value is used, equation (VI.14) represents a "minimum" heat transfer by transient conduction, and the left hand side can be designated as $q_{\ell,MIN}$.

Common intuition may lead us to think that the $k_{\ell,eff}\to\infty$ case is very remote from reality, experimental data seem to indicate this was not the case at low surface heat flux. As shown in Figure 20, many liquid contacts did send the surface temperature down close to the saturated temperature of water: one possible explanation for the above phenomenon was that the liquid in contact with the surface were liquid microlayers under bubbles;

evaporation of the liquid microlayers constantly cool the thin layer film, and resulted in a surface temperature close to T_{sat} until the liquid film dry out. However, even under this seemingly different situations, equation (VI.15) would still apply.

Figures 47 and 48 present the calculated transient conduction liquid contact heat transfer for the above two limiting cases. Also shown are the typical calculated surface heat flux for run series I (Figure 47) and for series II (Figure 58). It is relieving to see the actual surface heat flux did lie between the two limiting cases discussed above. Using tabulated K_ℓ value only, as shown in Figures 47 and 48 (the squares), predicted a much lower transient conduction heat flux than the actual total heat flux.

It appeared that the above findings did not contradict the quenching theory proposed by Bankoff and Mehra, but to quantitatively predict the liquid contact heat transfer values, a more comprehensive quenching model which includes the change of effective liquid thermal conductivity value, microlayer evaporations, and possibly other considerations, is needed.

VI.5 Effect of Surface Superheat on Liquid Contact Parameters

As discussed earlier in Chapter V, it was found that both liquid contact fraction and liquid contact durations decreased monotonically with increasing surface superheat, while liquid contact frequency possessed a maximum at 60-120°C surface superheat and fell off rapidly with superheat higher than 140°C.

The above observations could be explained as follows:

a) At very high surface superheat, any liquid in the vicinity of the hot wall was vaporized, and a relatively stable layer of vapor film existed in between the hot wall and the liquid bulk, stable film boiling condition existed.

b) As the surface superheat gradually lowered to around 200°F, the spatially nonuniform periodic heat transfer effect discussed by Manson [16] introduce local cold spots on the heating surface. As liquid rushed in and contacted the hot wall, the very high heat transfer rate by transient conduction quickly vaporized any liquid in contact with the hot wall, resulting in short contacts.

c) The vapor bubbles generated from (b) expanded in an explosive manner, greatly enhancing the internal circulations and turbulence level in the liquid bulk. The liquid bulk, now with higher kinetic energy, can more easily penetrate the vapor film and resulted in a much higher frequency liquid contact.

d) As the surface superheat decreased to less than 80°C, the lowered thermal driving force cannot 'pump' heat into the contacting liquid at the same rate as before (at higher temperature), longer contacts were thus observed. The less violent vapor generation also

resulted in lower contact frequency, and a lower liquid kinetic energy level.

e) At even lower surface superheat (below 50°C), the low thermal driving force could not 'expell' the contacting liquid, vapor bubbles began to grow on the surface. Liquid microlayers might form under the bubble, which took a much longer time to evaporate. Much longer liquid contacts and higher time-averaged liquid contact fraction resulted.

VI.6 Surface Aging Effect

It was a well documented fact that the boiling heat transfer mechanisms, especially in nucleate and transition boiling regimes, are strongly affected by the condition of the boiling surfaces. By performing copper-pentane pool boiling experiments, Berenson [1] demonstrated (1) increasing surface roughness decreased the critical surface superheat and 'flatten' the boiling curve as shown in Figure 44; (2) an 'unclean' surface greatly enhanced the heat transfer in transition boiling regime. Figures 45 shows that at 55°C (~100°F) surface superheat, an 'unclean surface' has a surface heat flux almost an order of magnitude higher than the 'clean surface', while the minimum film boiling superheat rose by 100% (from 100°F to 200°F).

It was unclear how the surface aging affect the boiling heat transfer mechanism, the matter was further complicated by the fact that the chemistry and the surface texture of an aged surface was

hard to quantify. Qualitatively, several changes to the surface was thought to have occurred, and was summarized by Iloeje et al. [39].

(1) Oxidation and aging changes the chemistry and thermal properties of the boiling surface.

(2) Oxidation and aging alter the surface texture, in general, a rougher and more porous surface is resulted.

(3) Oxidation and aging changes the wetting properties of the boiling system.

As shown in Figure 35, the present investigation indicated higher surface heat flux values and 'flatter' boiling curves in the transition--film boiling regimes for an increasingly oxidized surface. Considering the three reasons stated above, the present results were compatible with Berenson's [1] findings and were in line with Iloeje's [39] experimental data.

While it is widely believed the liquid contact heat transfer is a major contributing factor on transition boiling heat transfer, it is logical to anticipate changes in the liquid contact behavior due to surface aging effect. In Figures 32-39, it was indeed shown that increasing oxidation decreased the average contact duration, frequency, and time-averaged fraction of liquid contact for the present boiling system.

Considering that oxide layer formation generally degrades the thermal properties of the boiling surface and lowers the transient conduction heat transfer (for a given superheat, surface

area, and liquid contact duration), it was puzzling to find that an increase in surface heat flux was accompanied by a decrease in the measured time-averaged liquid contact fraction. This apparently inconsistent trend could be partially explained by the model proposed below.

The layer of oxide formed on the block surface are rough and of low tensile strength, thus many vapor cavities and cracks could form. Referring to Figure 49, the fin cooling effect created local cold spots on the hot wall, and direct liquid contact might occur on the oxide surface at various locations. In between cracks, the boid was expected to be normally covered by vapor, but liquid could occasionally seep through the crack and flood the micro-canyon, while vapor bubbles were formed at different nucleation sites (Figure 49). Some first order estimate follows:

For CuO: $\rho \cong 6.76$ z/cc

$K \cong 13.5$ W/m°C

$C_p \cong 1000$ J/Kg°C

$\alpha \cong 2 \times 10^{-6}$ sec/m^2

oxide layer: copper oxide with 30% vapor void average oxide layer thickness ~0.1 mm effective oxide layer thermal conductivity

$\cong (0.7 \times 13.5 + 0.3 \times 0.0246)$ W/m°K = 9.5 W/m°K

conductive thermal resistance = $\Delta x/K \cong 1.05 \times 10^{-5}$ °K/w

$\alpha_{oxide,eff} \cong 1.45 \times 10^{-6}$ sec/m^2

For liquid contact time of 5 msec, the penetration depth into the oxide bulk is in the order of $\sqrt{\alpha t} \cong 0.666$ mm.

Since oxide layer thickness was assumed to be 0.1 mm, the liquid contact information might not be able to reach the thermocouple tip, even for a relatively long 5 msec contact.

The measured liquid contacts were due to liquid which flooded the canyon: notice heat can transfer into the liquid body from the metal surface and from the sides of the oxide canyon (Figure 50). The larger heat transfer area resulted in shorter duration contacts.

At lower surface superheat, liquid contact frqction on the oxide surface might approach unity, a very high temperature gradient in the oxide layer was set up. When liquid contacts on the probe tip surface occu-red, heat transfer to the liquid from the sides of oxide cavity was much less significant (Figure 51) due to the large temperature gradient and cooler oxide layer, longer contacts resulted, and discrepancies between oxidized surface and clean surfaces decreased to vanishing level.

The above model was developed due to the following observations:

(a) Liquid contact signals were sharp and distinct

(b) Liquid contacts were fewer and of shorter durations for oxidized surfaces

(c) Surface heat flux increased with oxidation

(d) All surface effects on liquid contact seemed to disappear at low surface superheat.

VII. SUMMARY AND CONCLUSIONS

A fast response, flush mounted surface temperature probe was developed, and was used in liquid-solid contact measurements in pool boiling of water through the measurement of transient local surface temperature. While it must be stressed that the probe developed was capable of other fast response surface temperature measurement applications, several conclusions on liquid contact behavior can be drawn from the present investigation.

(1) The time-averaged liquid contact fraction and the average duration of contact increased with decreasing surface superheat, while frequency of liquid contacts possessed a maximum at surface superheat around 60-100°C.

(2) Maximum surface superheat for liquid contact increased with oxidation.

(3) Surface condition and aging strongly affected the liquid contact behavior.

(4) The quenching theory appeared to predict the correct trend of the transition boiling heat flux, but the calculated transient conduction heat transfer via liquid contact was lower than the actual value, possibly due to internal fluid motion in the liquid bulk.

REFERENCES

1. Berenson, P.J., "Experiments on pool boiling heat transfer," Int. J. Heat Mass Transfer, vol. 5, pp. 985-999.

2. Hsu, Y.Y. and Graham, R.W., "Transport processes in boiling and two-phase flow systems," Hemisphere Publishing Corporation, 1976.

3. Westwater, J.W., "Boiling of liquids," T.B. Drew and J.W. Hoopes, editors, Advances in Chemical Engineering, vols. 1&2, Academic Press, New York, 1957-1958.

4. Leppert, G. and Pitts C.C., "Boiling," T.F. Irvine Jr. and J.P. Hartnett, editors, Advances in Heat Transfer, vol. 1, Academics, 1964, pp. 185-266.

5. Griffith, P. and Wallis, J.P., "The role of surface conditions in nucleate boiling," Chem. Eng. Progress Symp. Series 56, 30, pp. 49-63, 1960.

6. Nukiyama, S., "Maximum and minimum values of heat transmitted from a metal to boiling water under atmospheric pressure," J. Soc. Mech. Eng., Japan, 36, 206, 367, 1934.

7. Yu, C.L. and Mesler, R.B., "A study of nucleate boiling near the peak heat flux through measurement of transient surface temperature," Int. J. Heat Mass Transfer, vol. 20, pp. 827-840, Pergamon Press, 1977.

8. Bromley, L.A., "Heat transfer in stable film boiling," Chemical Engineering Progress, vol. 46, no. 5, pp. 221-227.

9. Chang, Y.P., "Wave theory of heat transfer in film boiling," J. of Heat Transfer, 81c(1) pp. 1-12, 1959.

10. Berenson, P.J., "Transition boiling heat transfer from a horizontal surface," J. of Heat Transfer, 83(c), pp. 351-358, 1961.

11. Hamill, T.D. and Baumeister, K.J., "Film boiling heat transfer from a horizontal surface as an optimal boundary value process," Proc. 3rd Int. Heat Transfer Conf., vol. 4, pp. 59-64, 1966.

12. Westwater, J.W. and Santangelo, J.G., "Photographic study of boiling," Ind. Eng. Chem., 47(8), pp. 1605-1610, 1955.

13. Stock, B.J., "Observations on transition boiling heat transfer phenomena," ANL 6175, Argonne National Lab, 1960.

14. Spiegler, P., Heponfeld, J., Silberborg, M., Bumpus, C.F., and Norman, A., "On-set of stable film boiling and the foam limit," Int. J. Heat Mass Transfer, 6(11), pp. 987-984, 1963.

15. Baumeiser, K.J., Henry, R.E., and Simon, F.F., "Role of the surface in the measurements of Leidenfrost temperature," ASME Symp., "Augmentation of Convective Heat and Mass Transfer," New York, 1970.

16. Manson, L., "A periodic nonuniform heat transfer mechanism in film boiling," J. of Heat Transfer, pp. 111-112, 1967.

17. Henry, R.E., "A correlation for the minimum film boiling temperatures," AIChE Symposium Series, Heat Transfer -- Research and Design No. 138, vol. 70, pp. 81-90.

18. Bankoff, S.G. and Mehra, V.S., "A quenching theory for transition boiling," I&EC Fundamentals, vol. 1, no. 1, pp. 38-40, Feb. 1962.

19. Carslaw, H.S. and Jaeger, J.C., "Conduction of heat in solids," 2nd ed., Clarendon, New York, 1959.

20. Myers, G.E., "Analytical methods in conduction heat transfer," McGraw-Hill, 1971.

21. Hewitt, G.F., King, R.D., and Lovegrove, P.G., "Techniques for liquid film and pressure drop studies in annular two-phase flow," AERE-R 3921, March 1962.

22. Griffith, P., "The sing annular flow regime transition at elevated pressure," ANL-6796, November 1963.

23. Iida, Y. and Kobayasi, K., "An experimental investigation on the mechanism of pool boiling phenomena by a probe method," Proc. 4th Int. Heat Transfer Conf., vol. 5, paper B1.3, Versailles, 1970.

24. Iida, Y., Kabayasi, K. and Kumagai, S., "A study on the measurement of void fraction by probe method," J. Atomic Society, Japan, vol. 9, no. 1, pp. 2-9, 1967.

25. Yao, S.C. and Henry, R.E., "Hydrodynamic instability induced liquid-solid contacts in film boiling," ASME Paper, 1976.

26. Yao, S.C. and Henry, P.E., "An investigation of the minimum film boiling temperature on horizontal surfaces," J. of Heat Transfer, vol. 100, pp. 260-267, May 1978.

27. Ragheb, H.S., "Development of electric probes to detect phase change at heated surfaces," M.S. Thesis, Dept. of Mechanical Engineering, University of Ottawa, 1976.

28. Ragheb, H.S. and Cheng, S.C., "Surface wetted area during transition boiling in forced convective flow," Transaction ASME, vol. 101, pp. 381-383, May 1979.

29. Hsu, S.T. and Schmidt, F.W., "Measured variations in local surface temperatures in pool boiling of water," J. of Heat Transfer, pp. 254-260, Aug. 1961.

30. Yu, C.L. and Mesler, R.B., "A study of nucleate boiling near the peak heat flux through measurement of transient surface temperature," Int. J. Heat and Mass Transfer, vol. 20, Pergamon Press, pp. 327-840, 1977.

31. Kalnin, E.K., Berlin, I.I., Kostyuk, V.V., and Nosova, E.M., "Heat transfer in transition boiling of cryogenic liquids," Proceedings cryogenics Eng. Conference, Queen's Univ., Kingston, Ontario, pp. 273-277, 1975.

32. Tong, I.S. and Young, J.D., "A phenomenological transition and film boiling heat transfer correlation," Proc. of the 5th Int. Heat Transfer Conference, vol. IV, Tokyo, Japan, pp. 120-124, 1974.

33. Zuber, N., "On the stability of boiling transfer," Trans. ASME, vol. 80, pp. 711-715, April 1958.

34. Berenson, P.J., "Film boiling heat transfer from a horizontal surface," J. of Heat Transfer, pp. 351-358, Aug. 1961.

35. Beck, J.V., "Review of six inverse heat conduction computer codes," A report to ANL, contract #31-109-38-5949, Feb. 1981.

36. Beck, J.V. and Hurwicz, H., "Effect of thermocouple cavity on heat sink temperature," J. of Heat Transfer, pp. 27-36, Feb. 1960.

37. Gambill, W., "An experimental investigation of the inherent uncertainty in pool boiling critical heat flux to saturated water," AIChE Journal, pp. 502-508, July 1964.

38. Bradfield, W.S., "Liquid-solid contacts in stable film boiling," I&EC, 5(2), pp. 200-204, 1966.

39. Iloeje, O.C., Plummer, D.N., Rohsenow, W.M., and Griffith, P., "An investigation of the collapse and surface rewet in film boiling in force vertical flow," J. of Heat Transfer, pp. 166-172, May 1975.

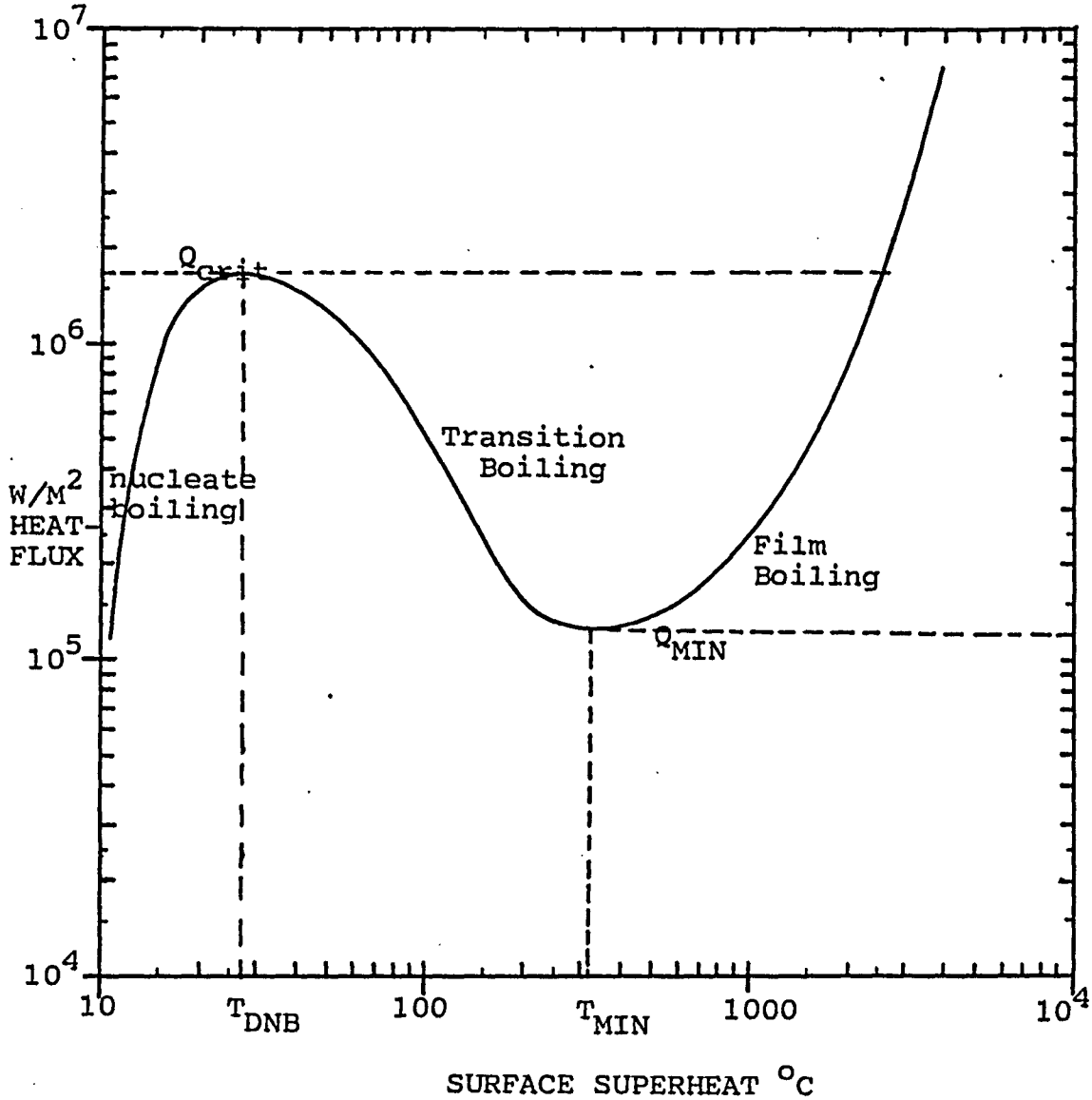

FIG. 1 : Typical boiling curve

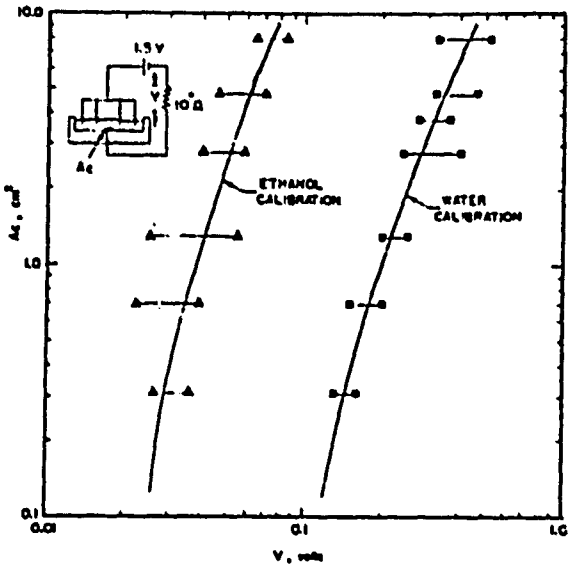

FIG 2 : Calibration of contact area and measured voltage for ethanol and water

FROM YAO & HENRY [26]

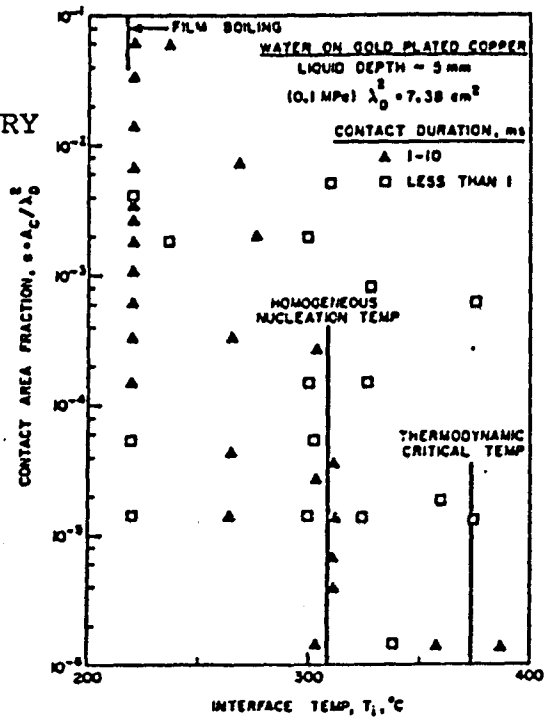

FIG 3: Measured contact areas as a function of interface temperature for water on a gold-plated copper surface

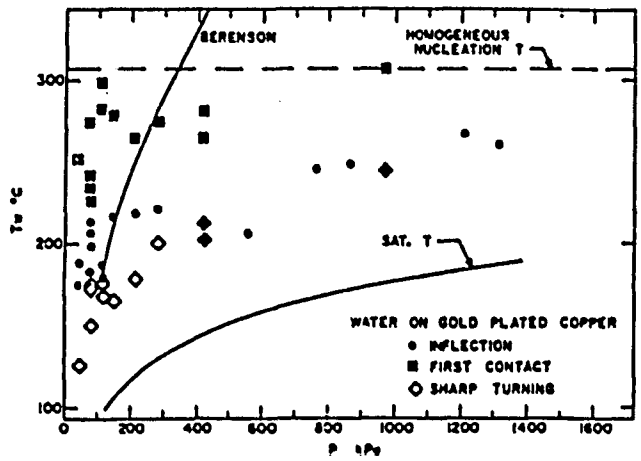

FIG 4: Temperature for initial contact in minimum film boiling for water on a gold-plated copper surface

FROM YAO & HENRY [26]

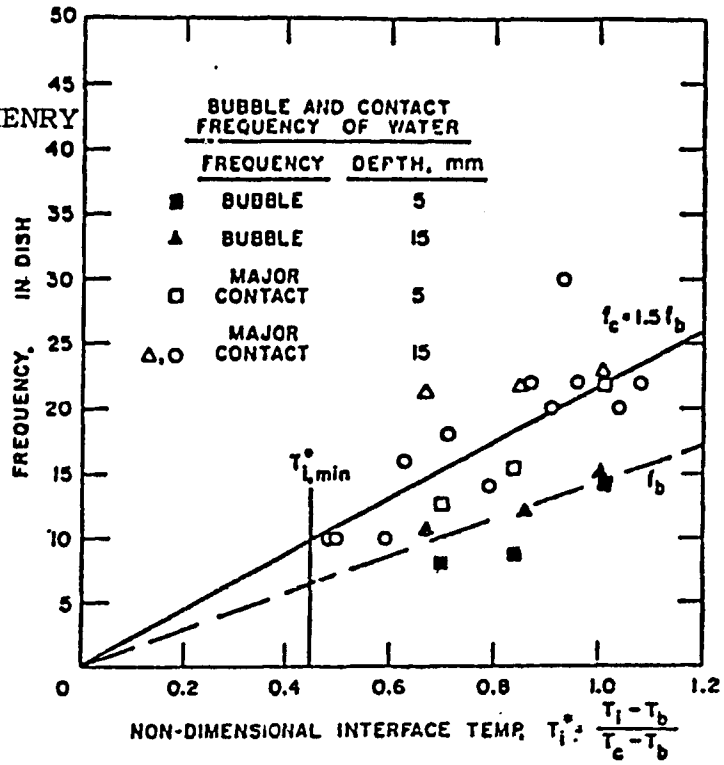

FIG 5: Film boiling bubble frequency and liquid-solid contact frequency of water.

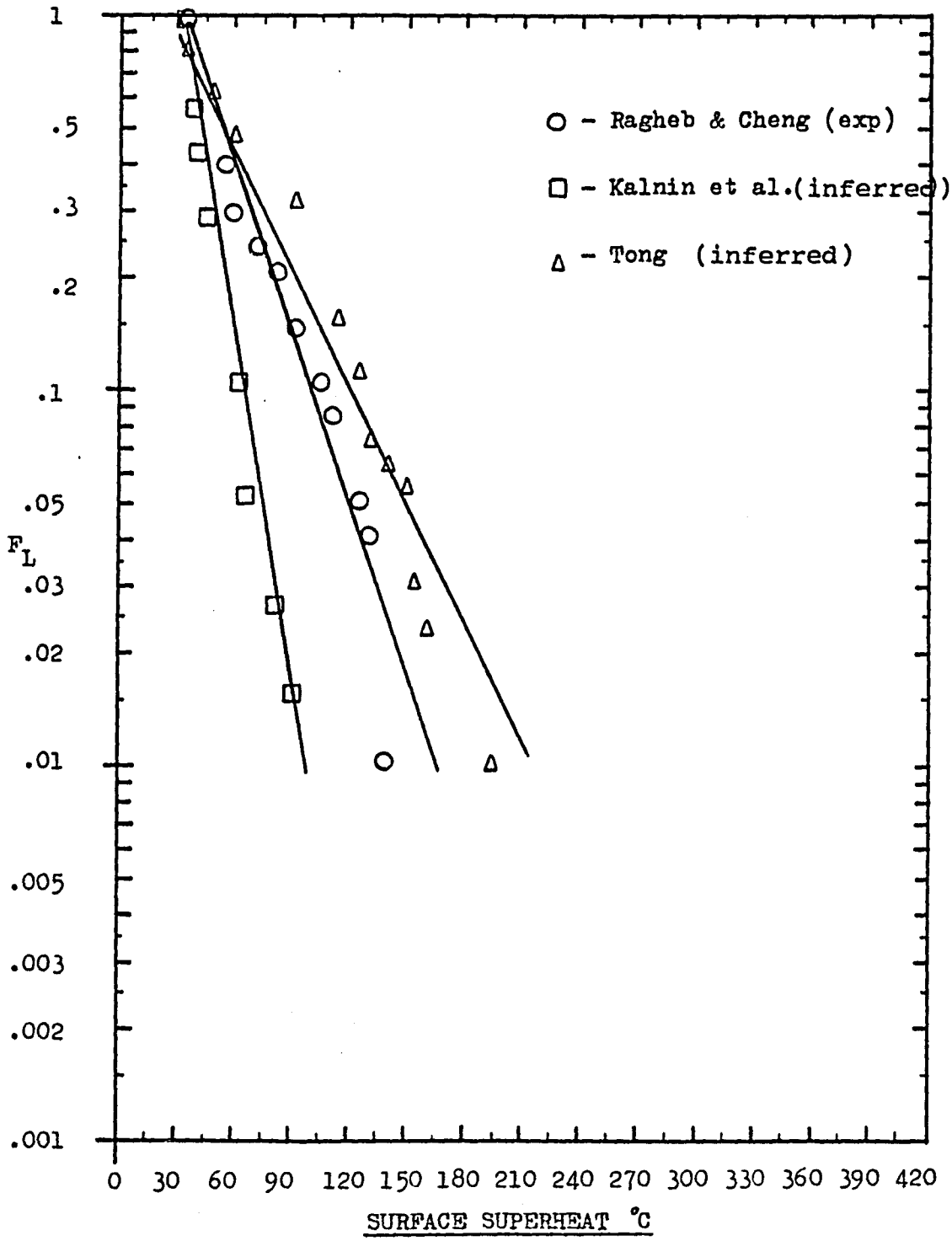

FIG 6: Presently availible F_L data.

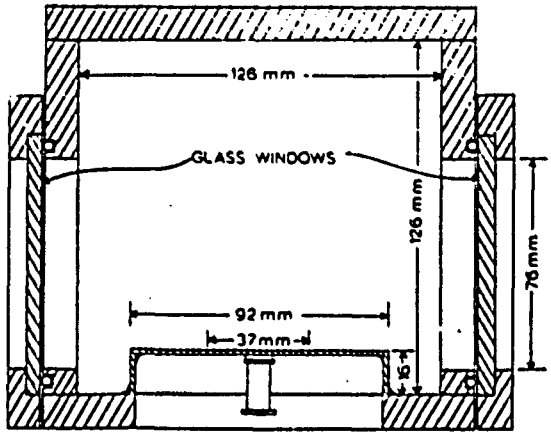

The boiling vessel.

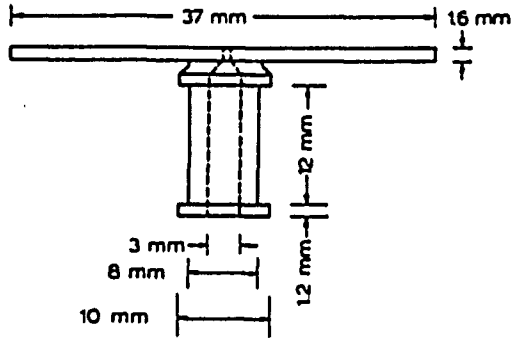

FIG 7: Dimensions of the boiling surface.

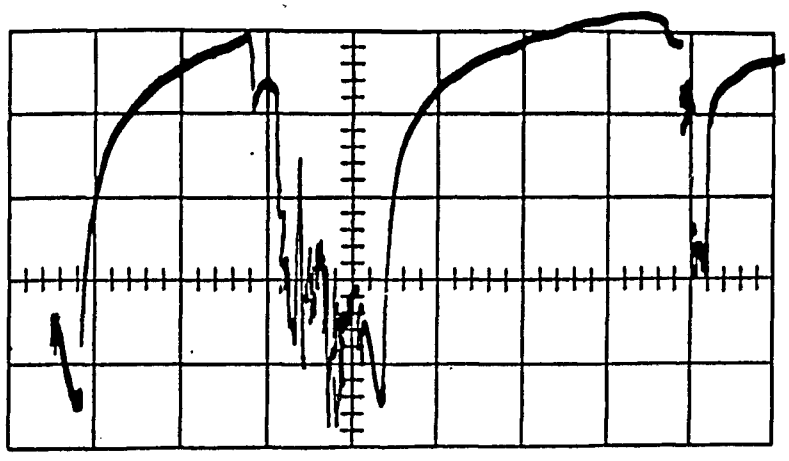

FIG 8 Transient surface temperature at 1.3 MW/m²

FROM YU & MESLER [30]

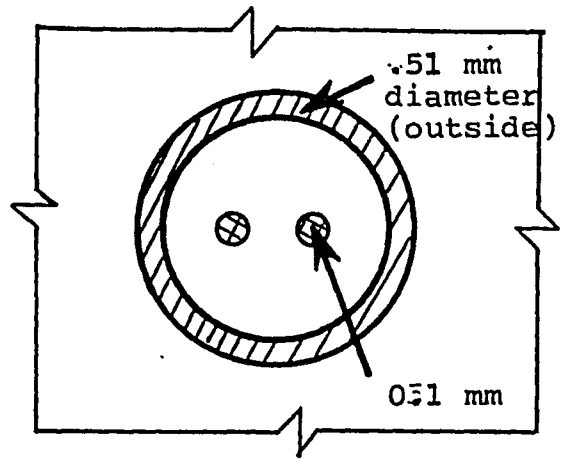

FIG 9: Top view of surface temperature probe (junction open)

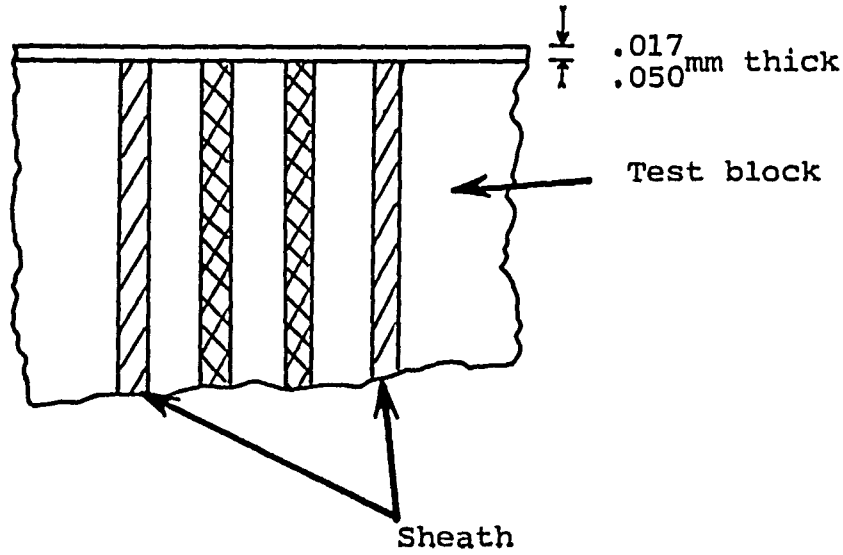

FIG 10: Side view of surface temperature probe (with closed junction)

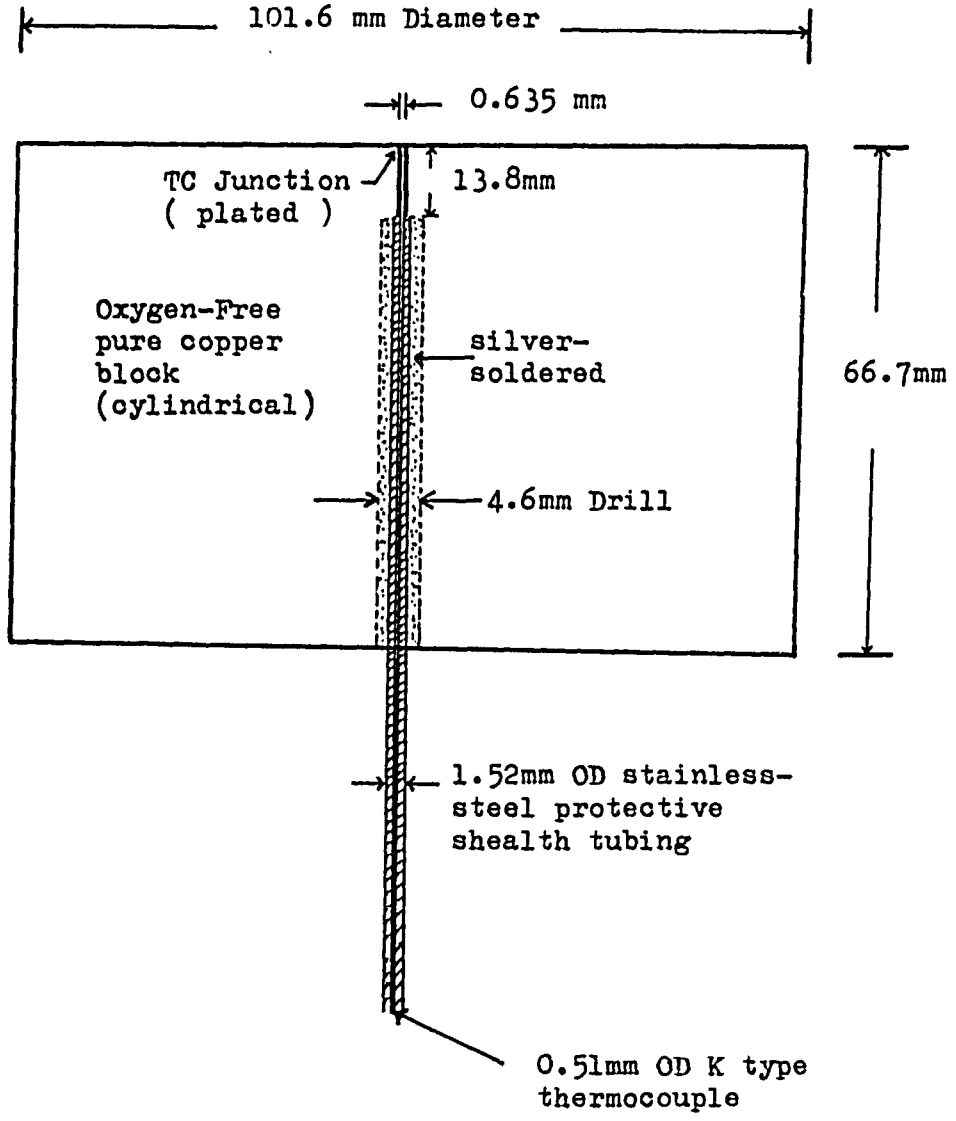

Fig 11 : CROSS SECTION OF QUENCH TEST BLOCK

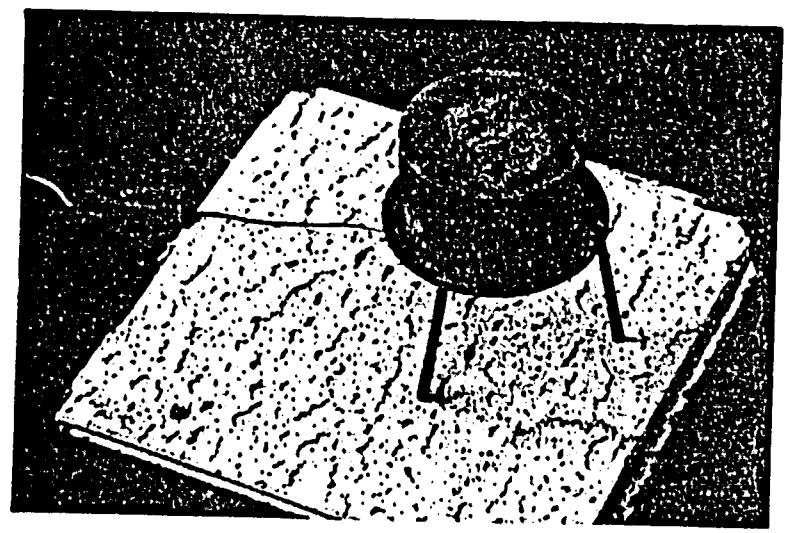

Fig. 12: Quench test block

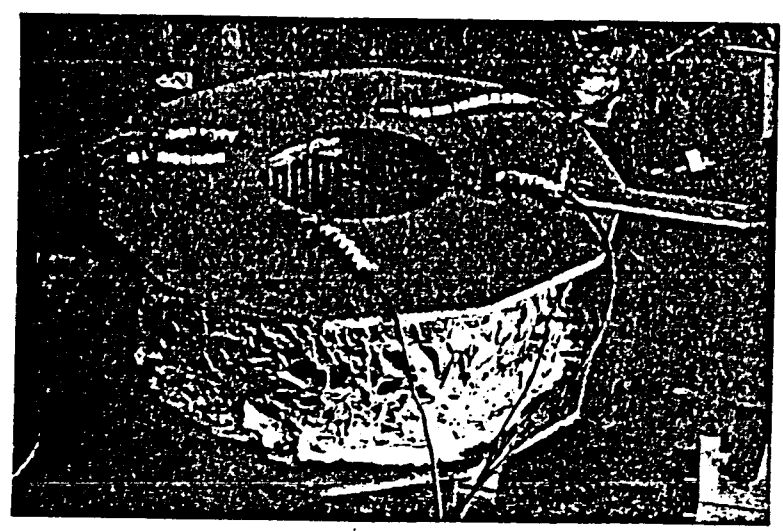

Fig. 13: Oven, lid removed

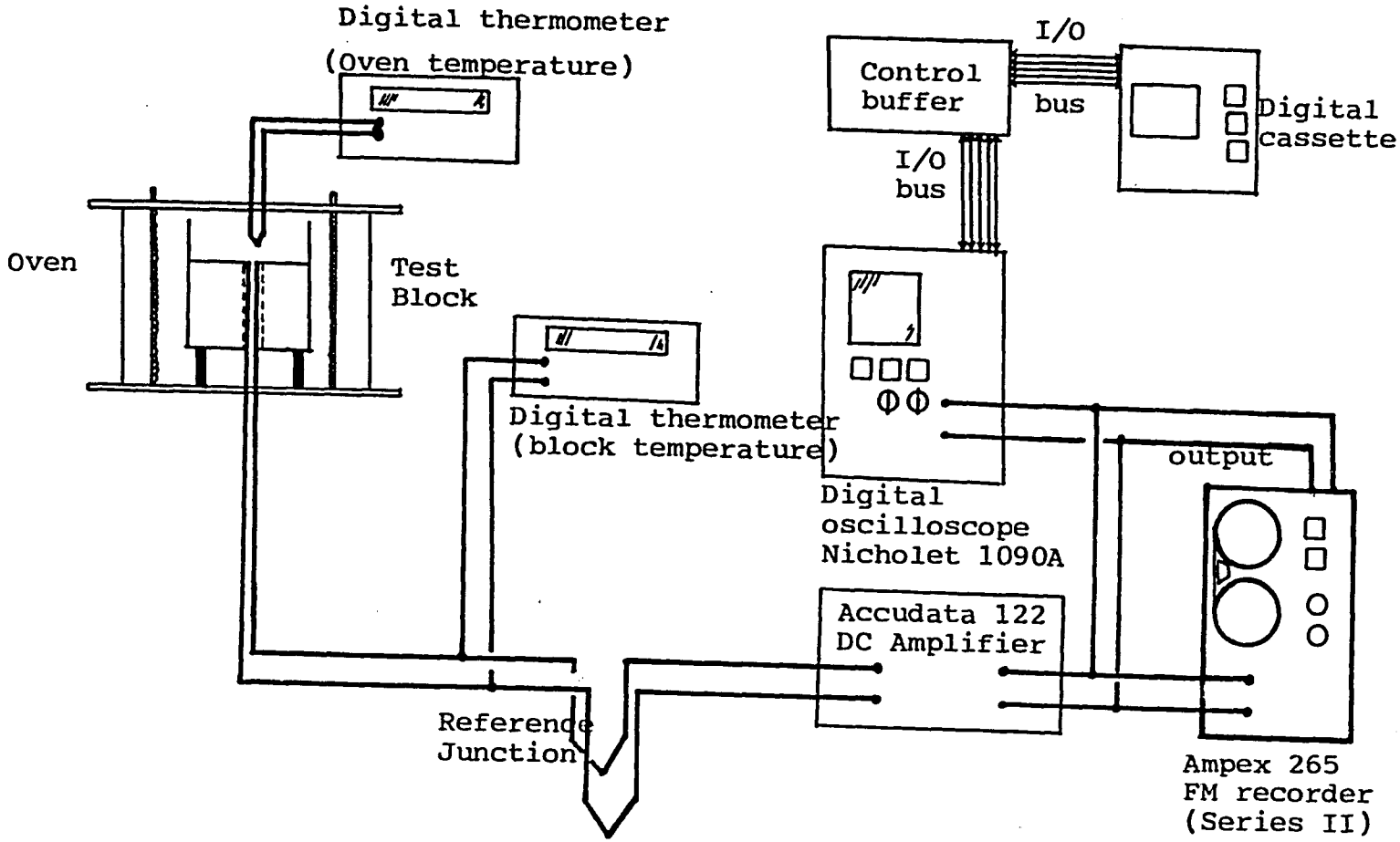

Fig 14: Experimental Set-up

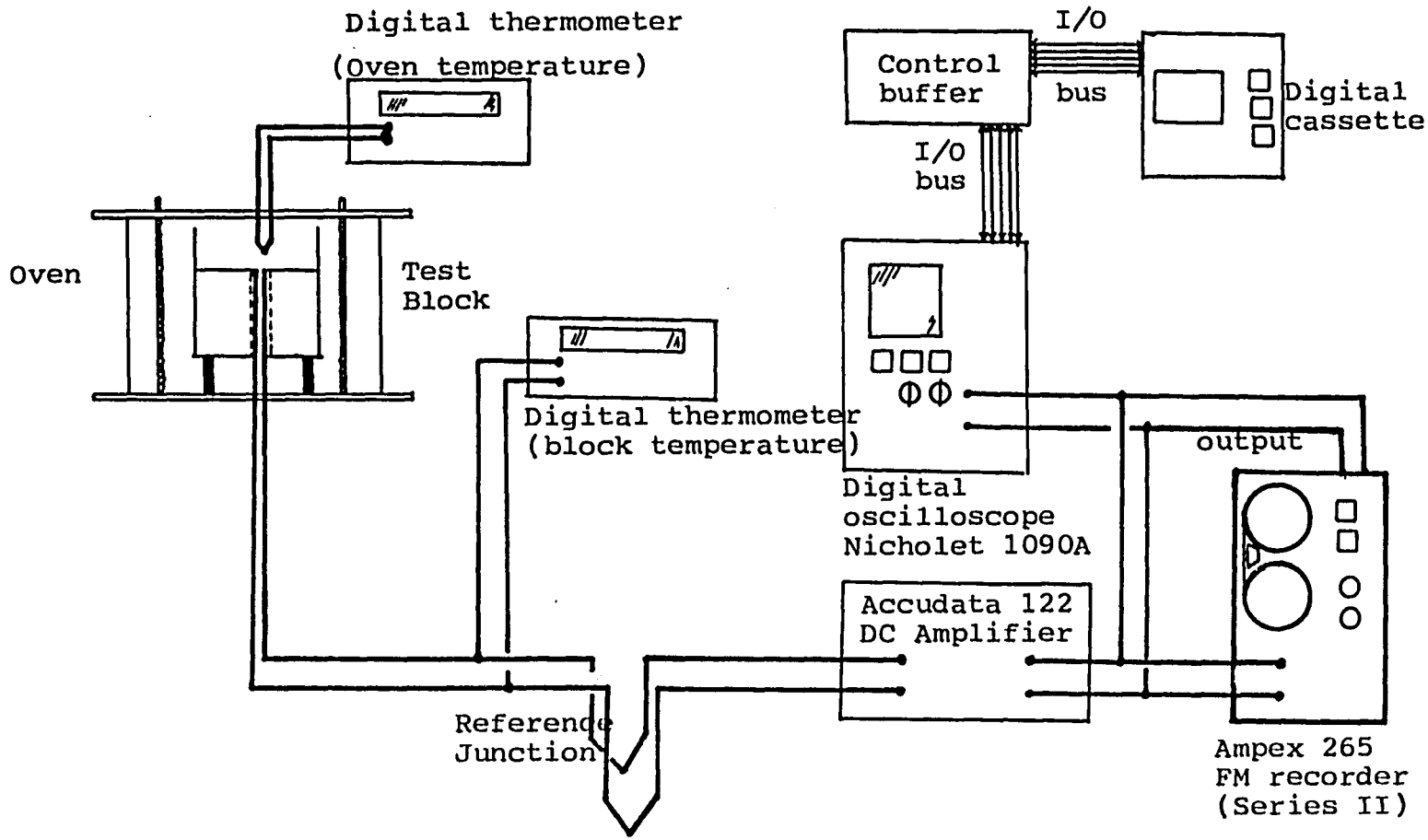

Fig 14: Experimental Set-up

Fig. 15

Nicholet 1090A digital oscilloscope

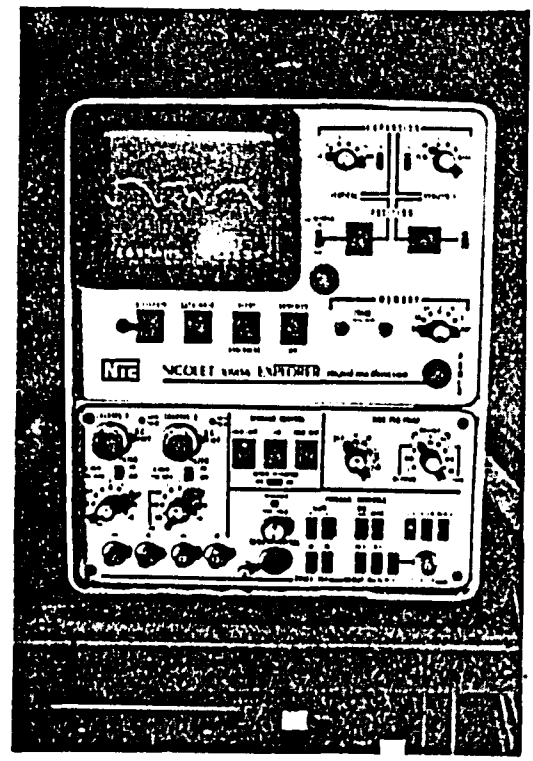

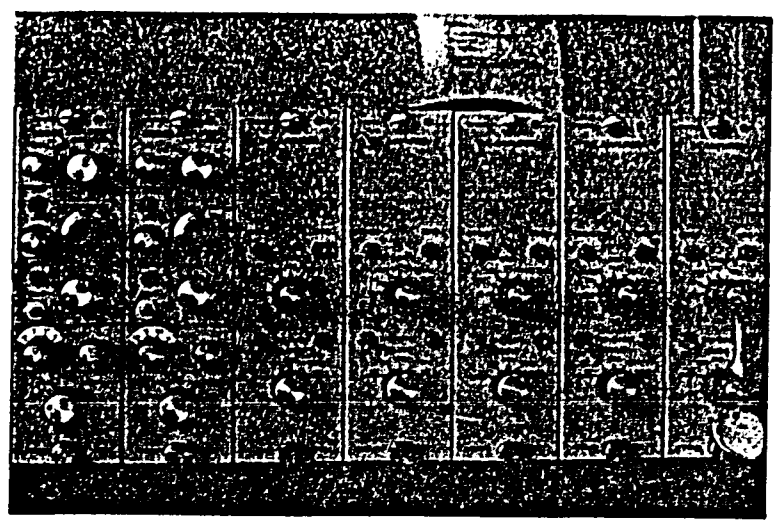

Fig. 16: Accudata 122 DC Amplifier

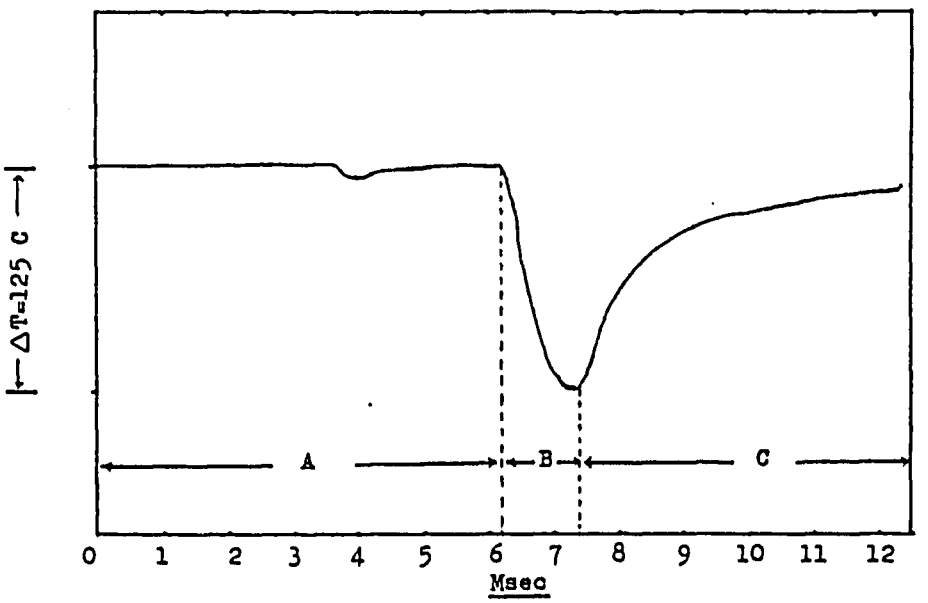

FIG 17: Transient local surface temperature on liquid contact

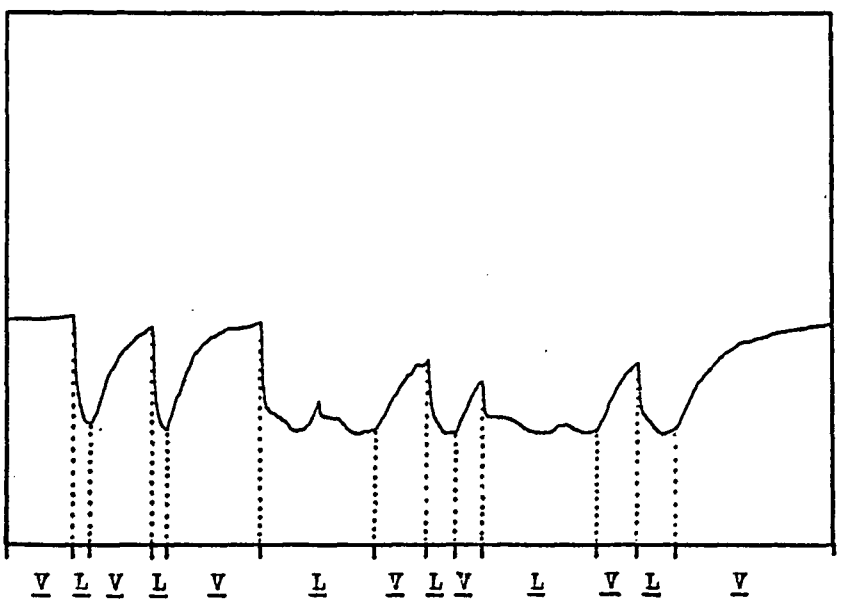

FIG 18 : Determination of liquid-solid contacts from probe signal

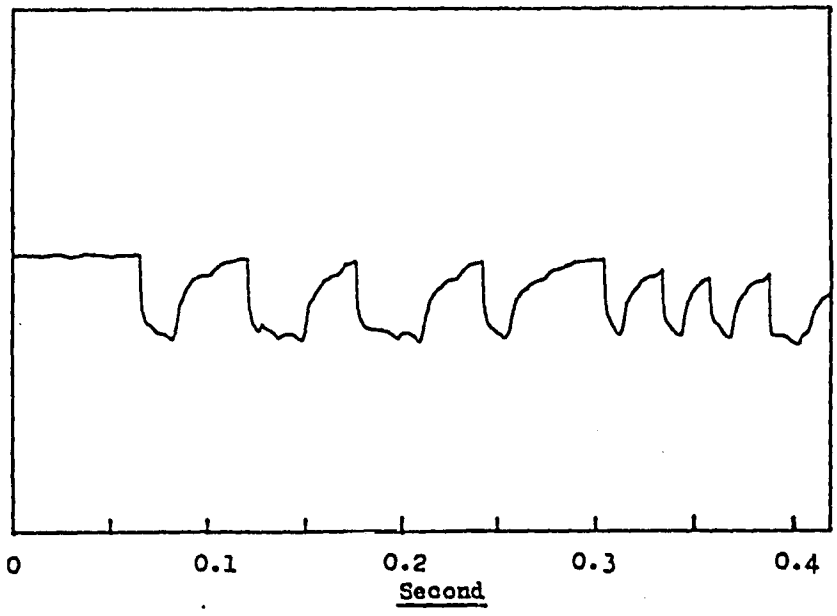

FIG 19: Probe signal at critical heat flux
Ave. surface superheat = 30 °C

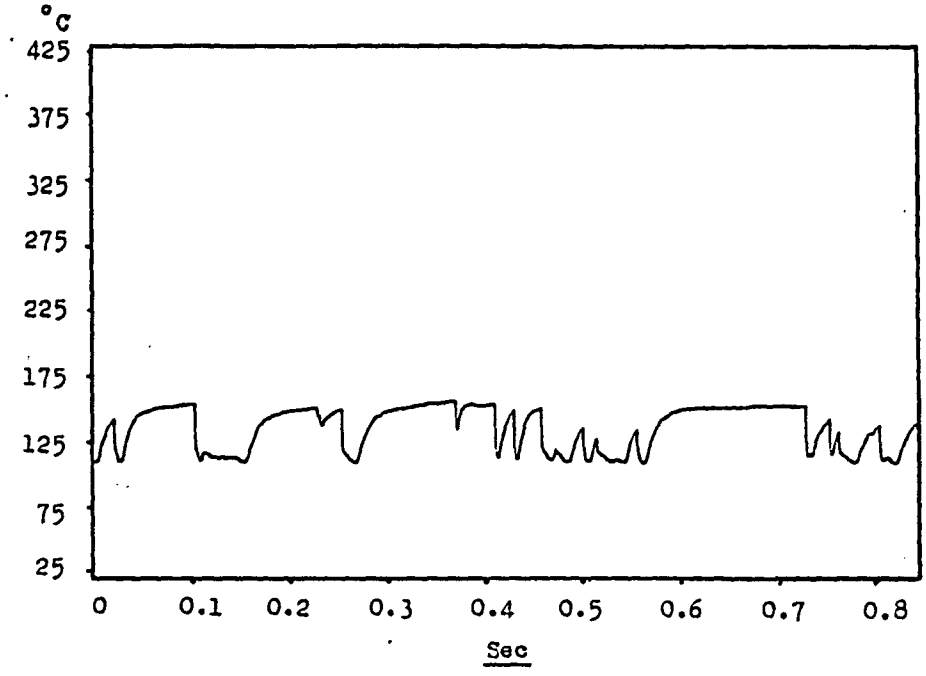

FIG 20: Probe signal at deep transition boiling, ave. superheat = 39 °C

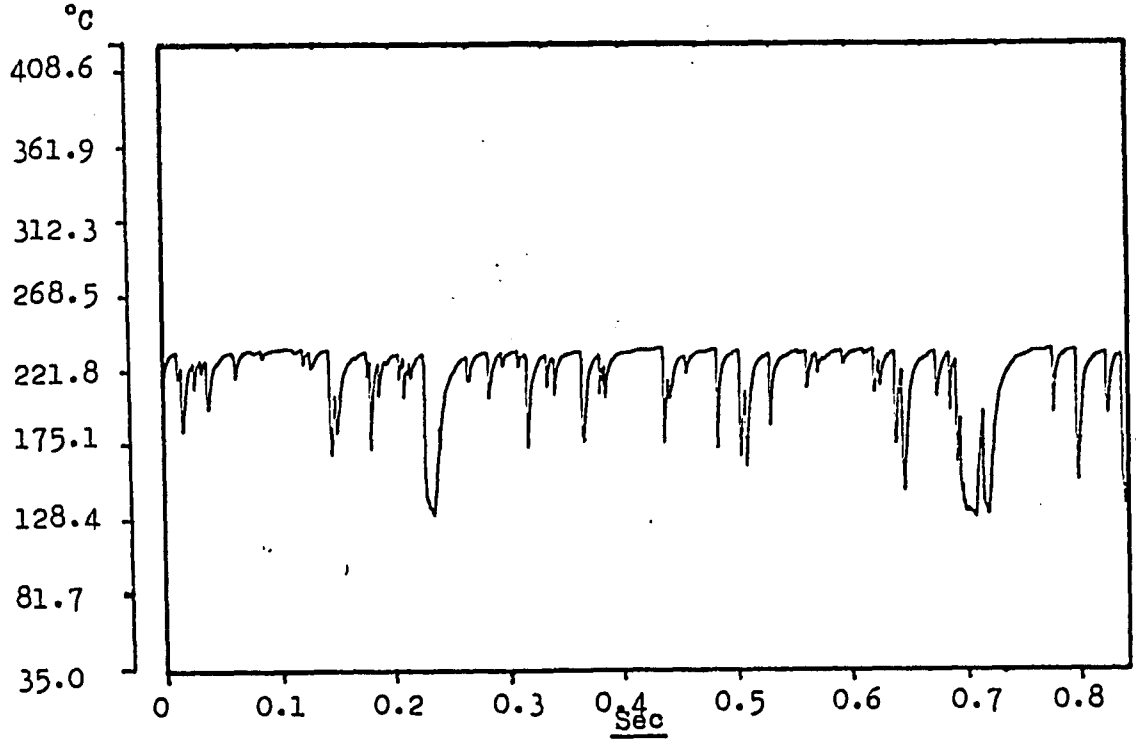

FIG 21: Probe signal, transition boiling
ave. surface superheat = 113 °C

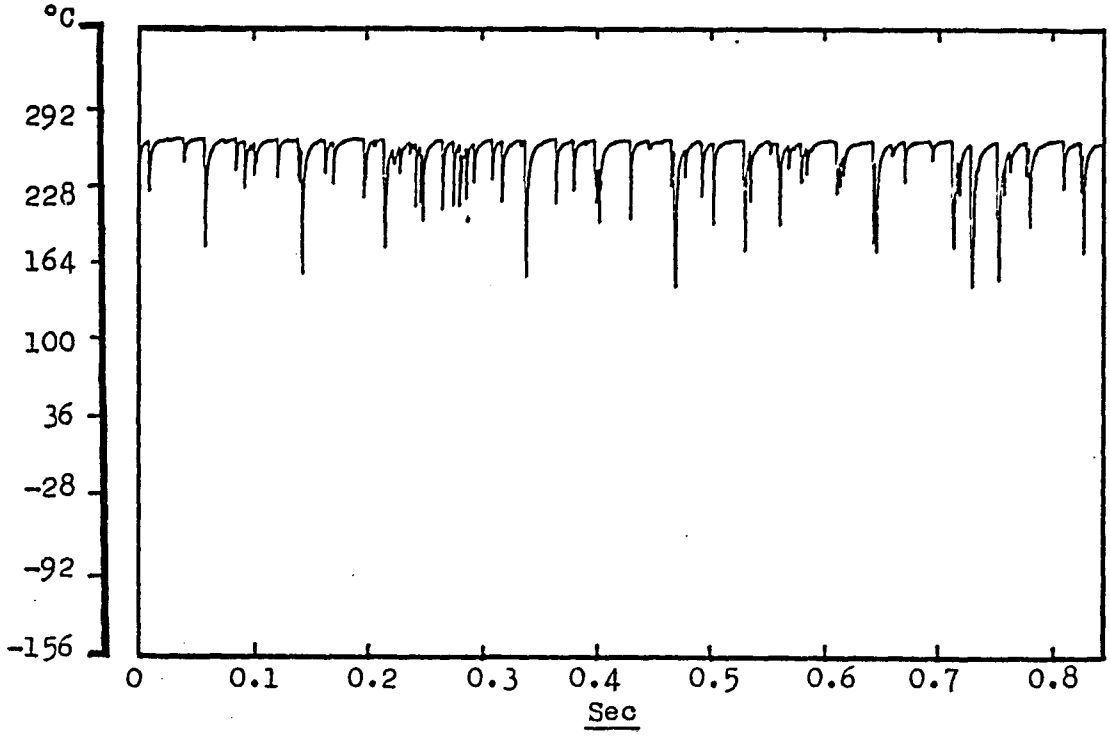

FIG 22; breaking down of film boiling,
ave. superheat = 155 °C

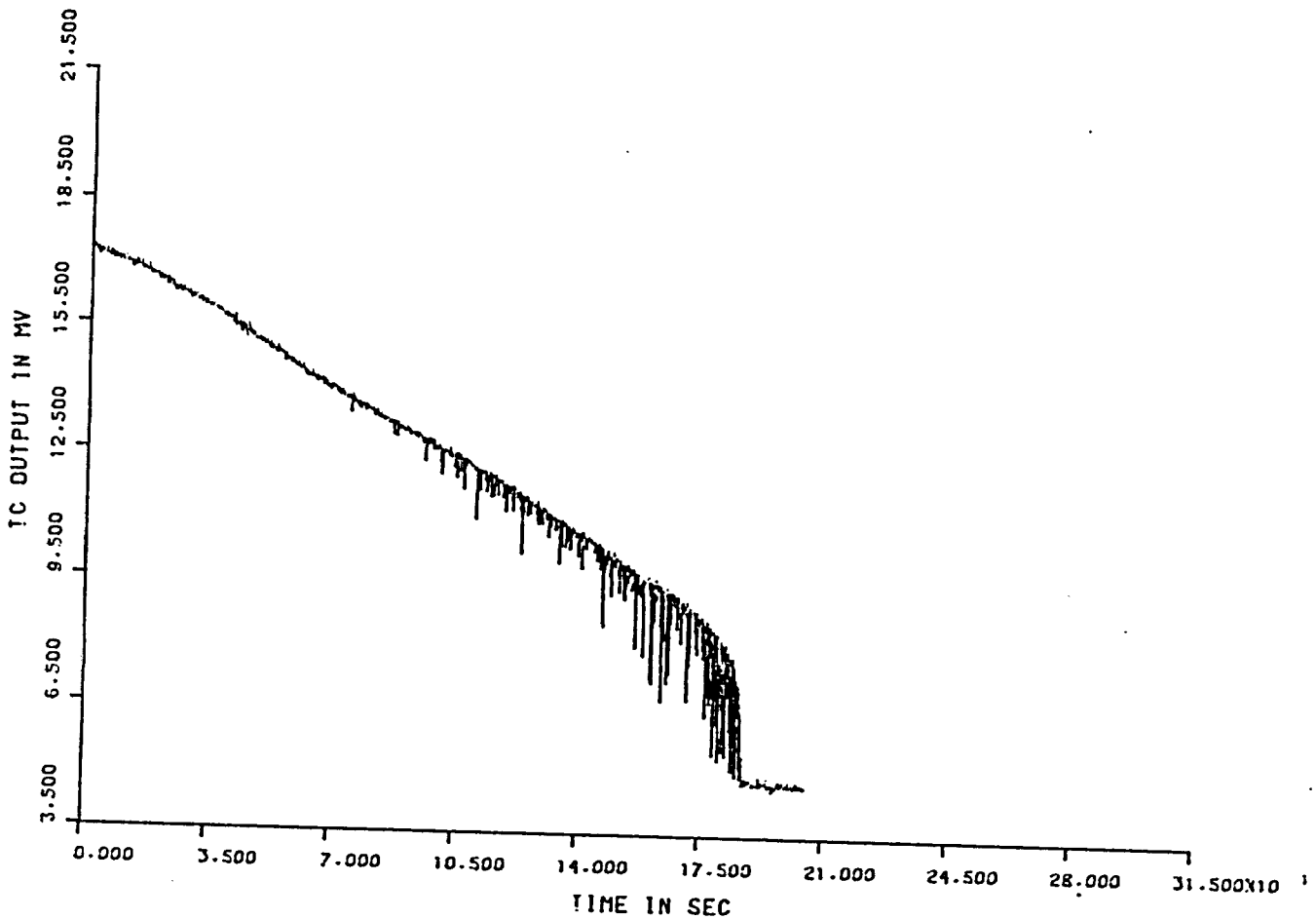

FIG 23: Overall quench history, run #1, Series II

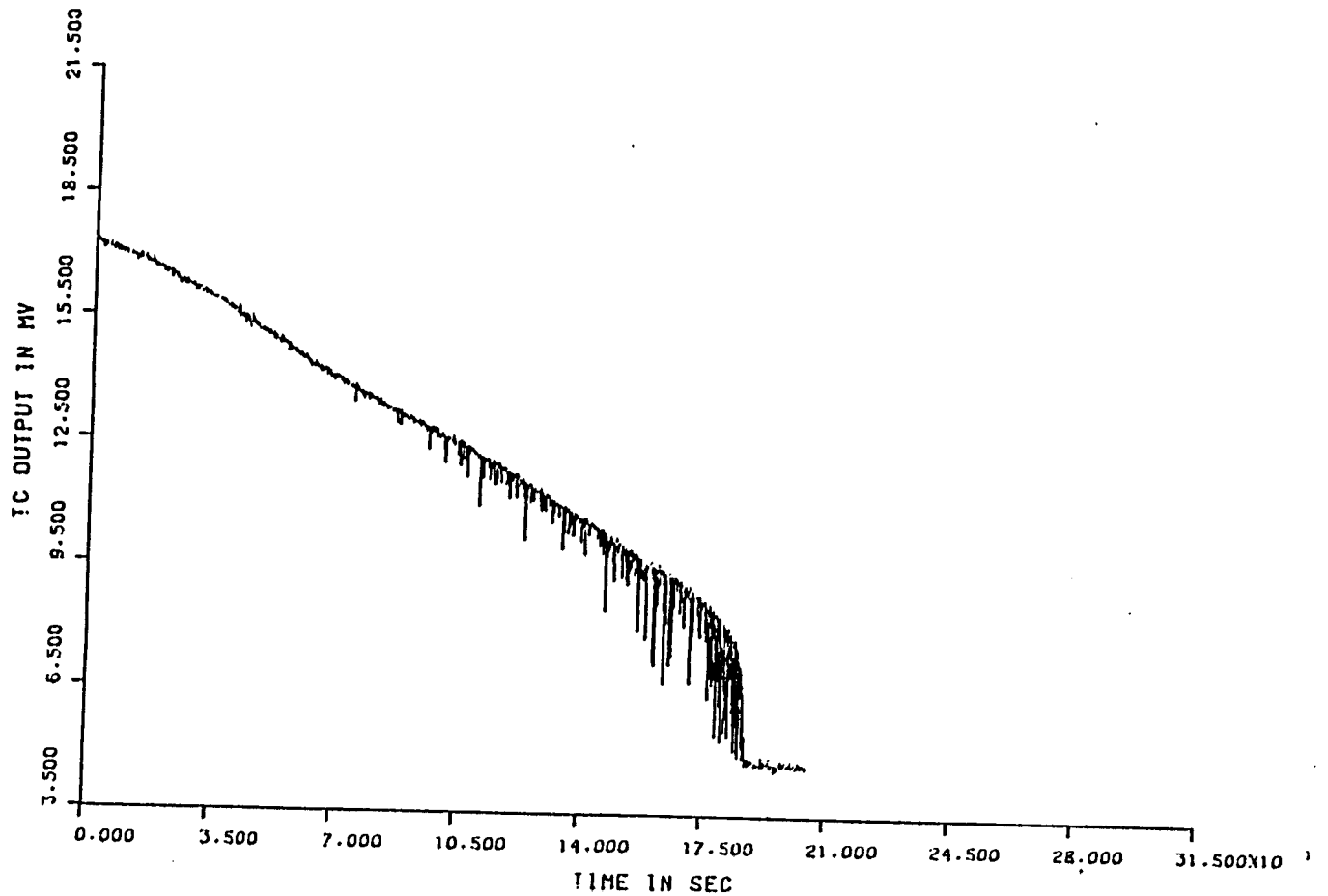

FIG 23: Overall quench history, run #1, Series II

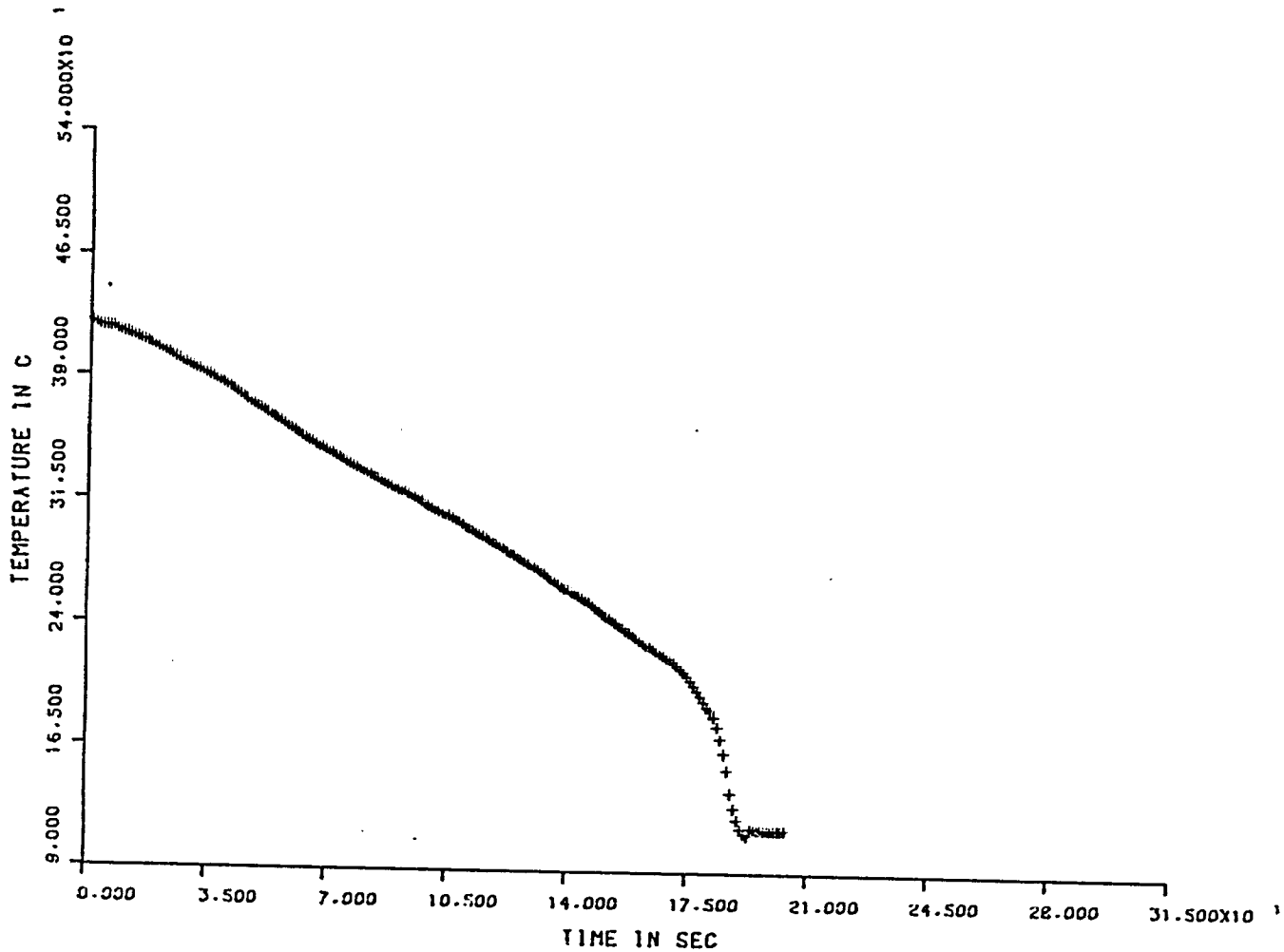

FIG 24: Smoothed overall quench history, run #1, SeriesII

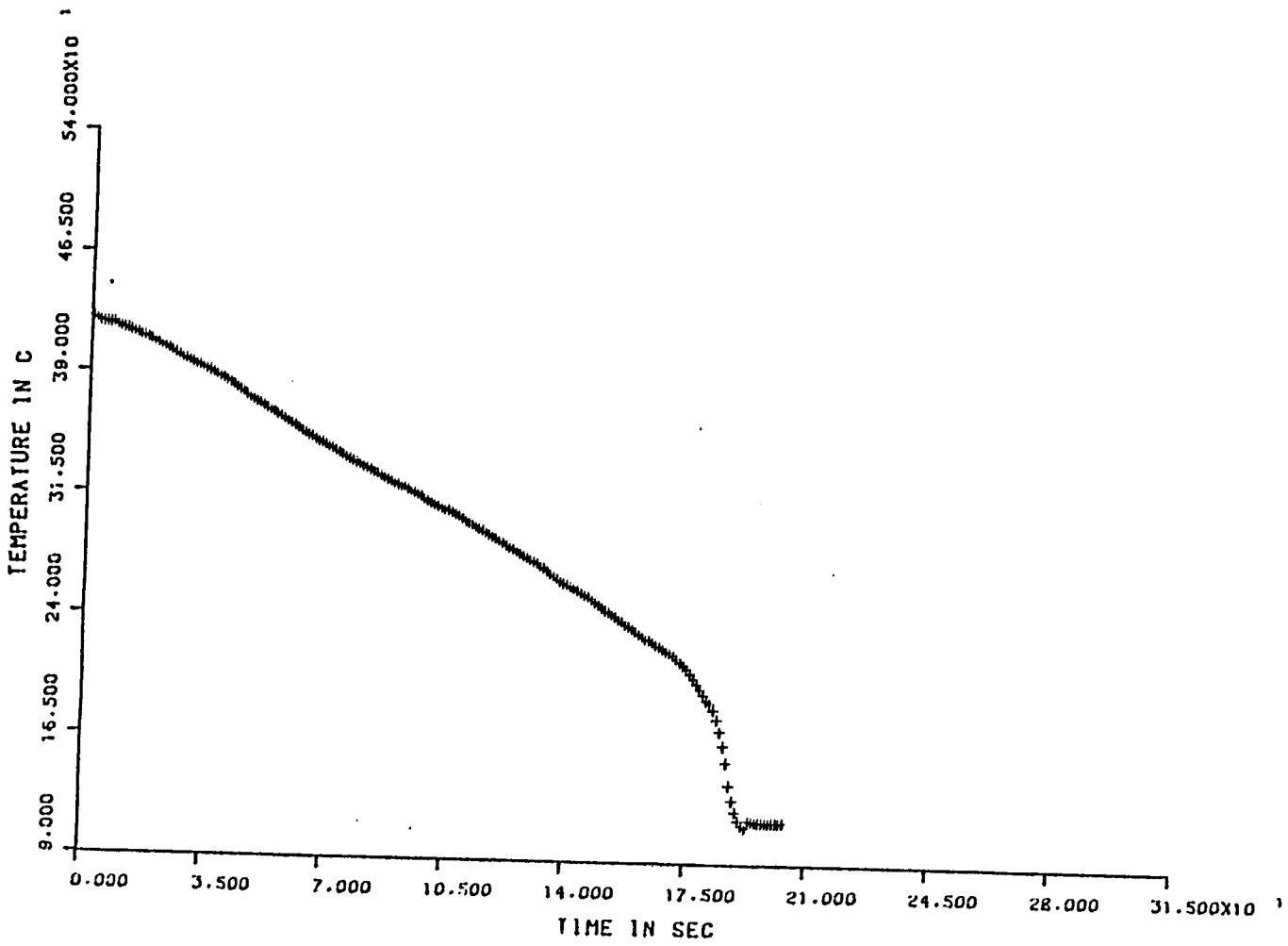

FIG 24: Smoothed overall quench history, run #1, SeriesII

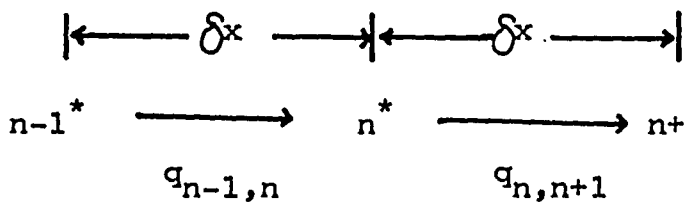

(a) spacing for typical interior node

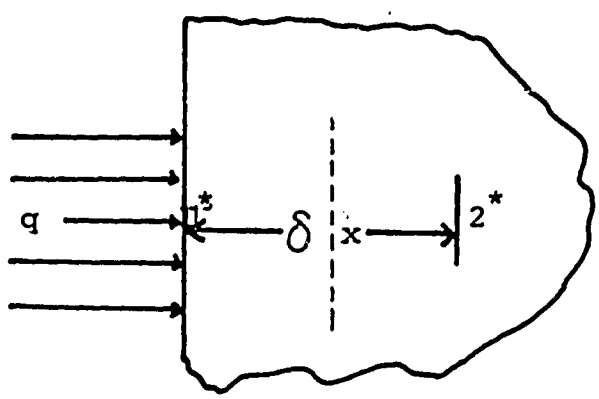

(b) Surface node with heat flux

FIG 25: Nodal configurations in the inverse condition problem , from Beck[35]

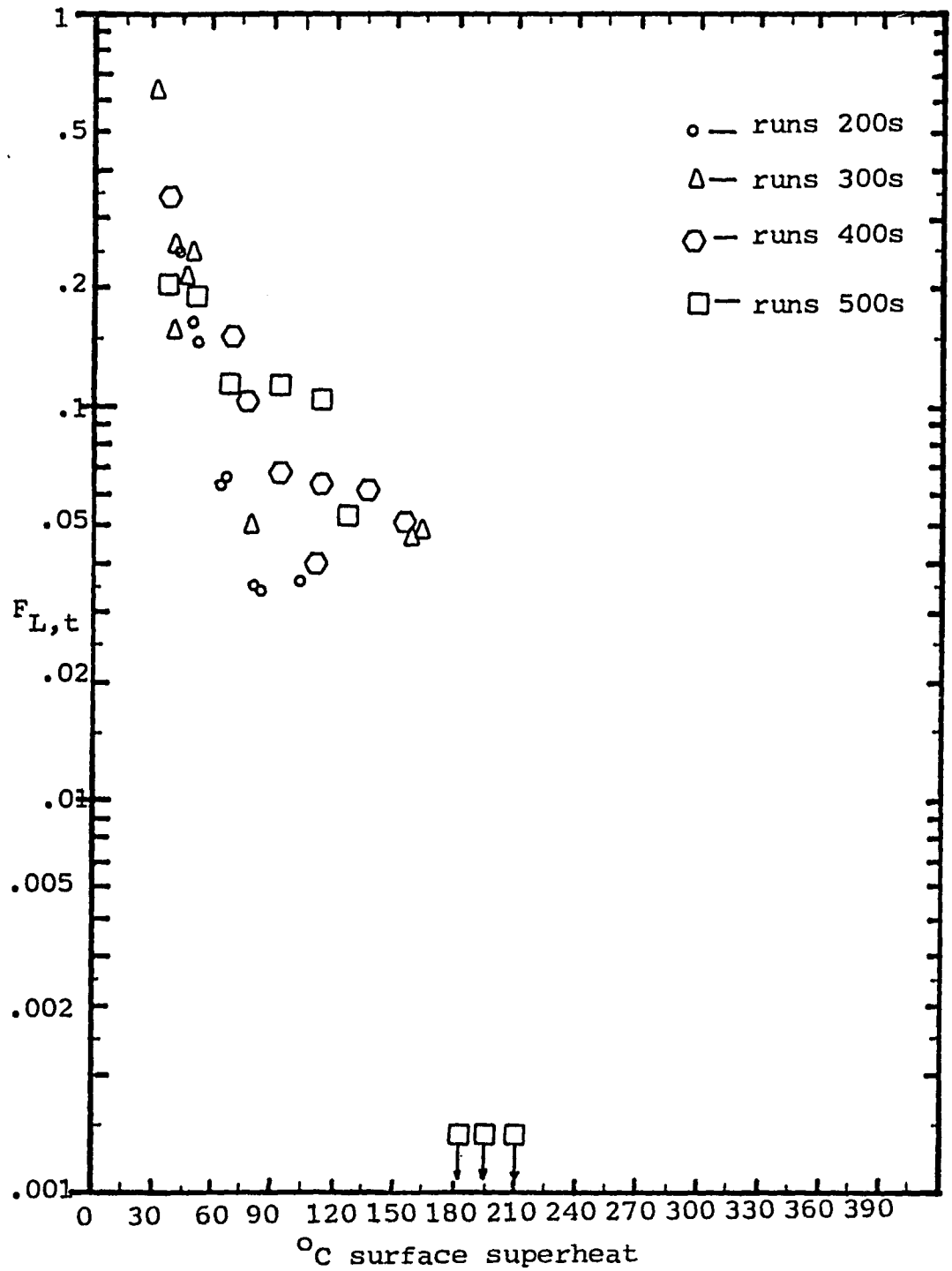

FIG. 26 : Liquid contact time-fraction, series I

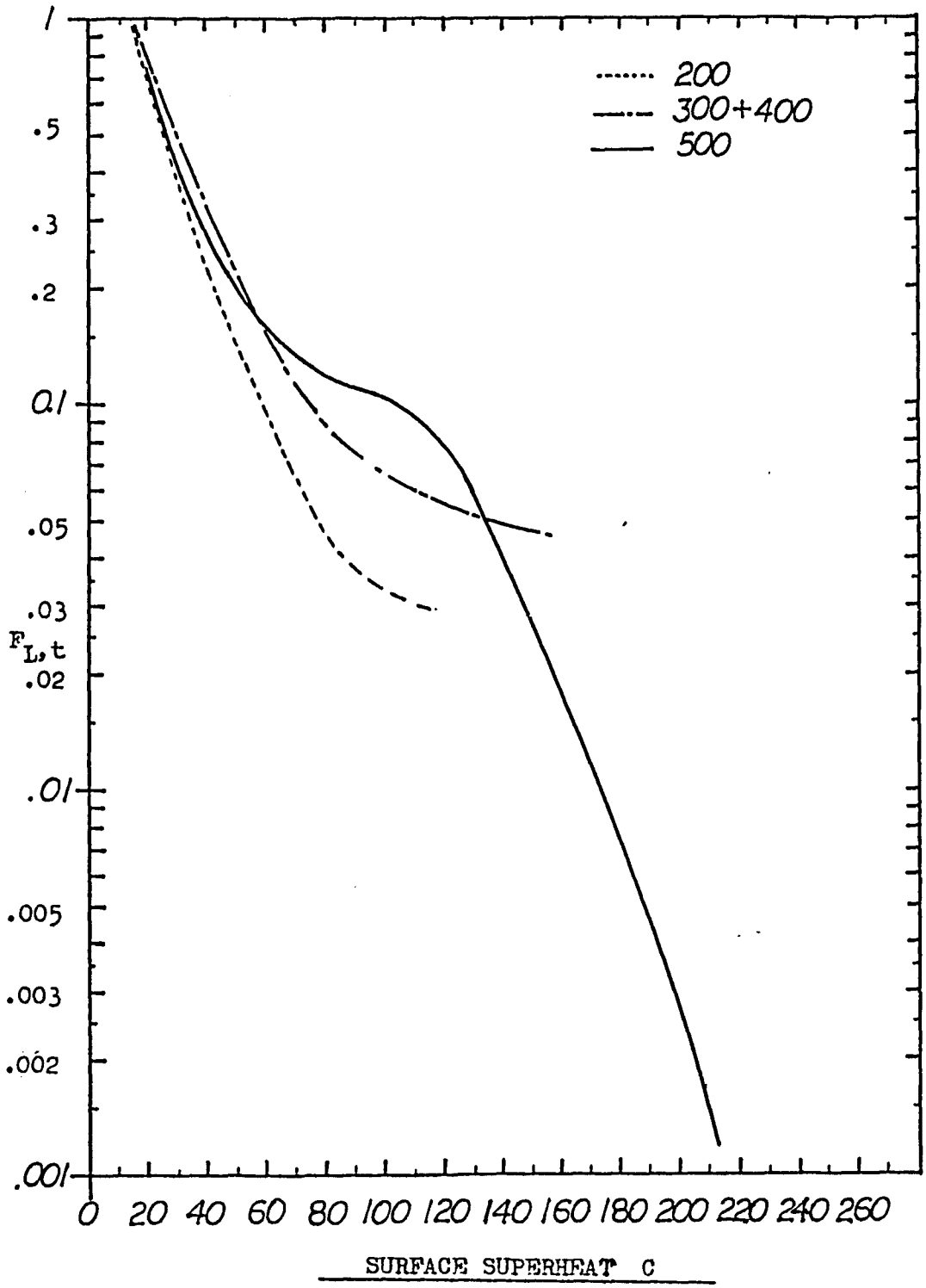

FIG. 27: Smoothed $F_{L,t}$ data, series I

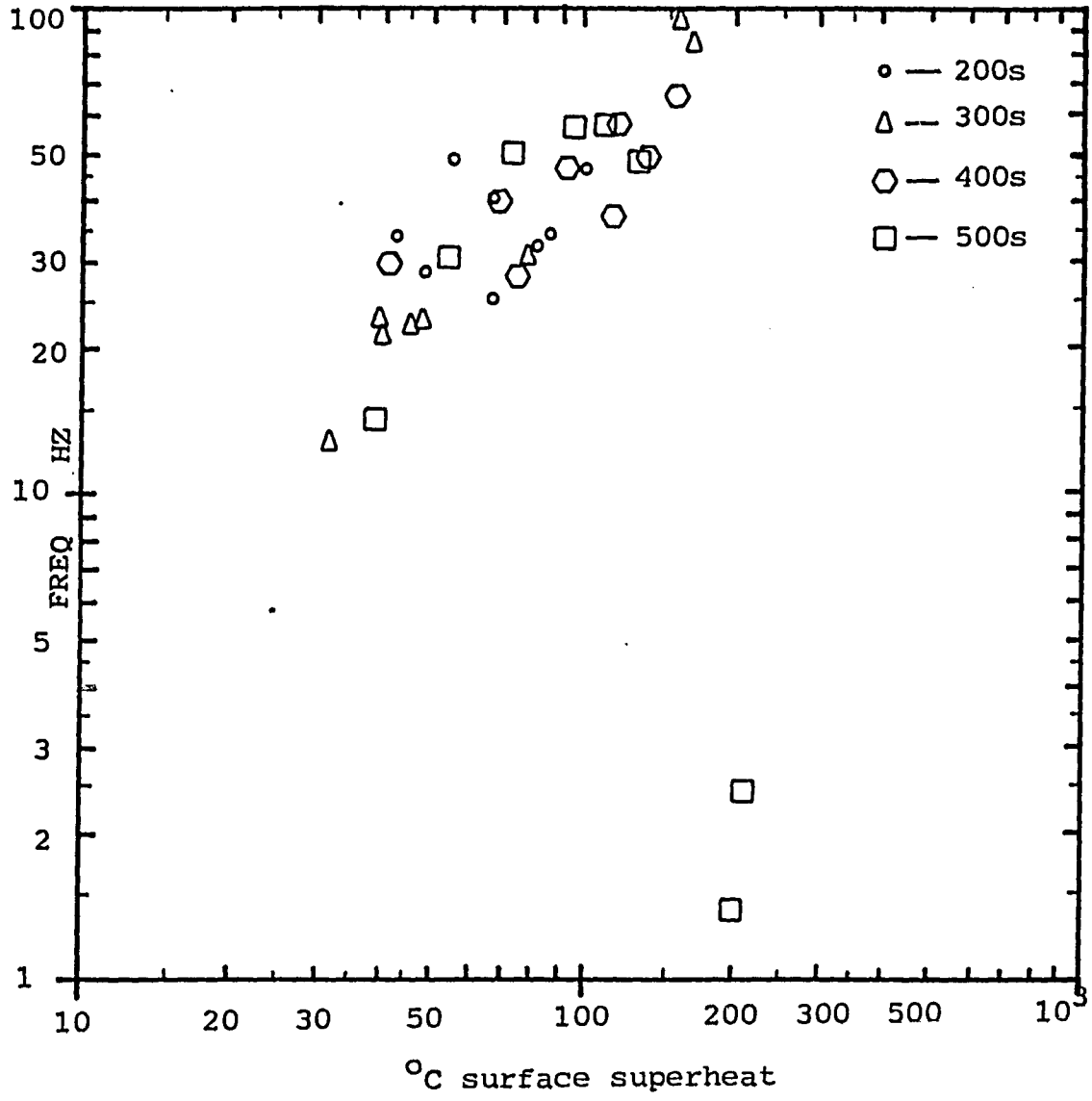

FIG. 28: Frequency of liquid contact, series I

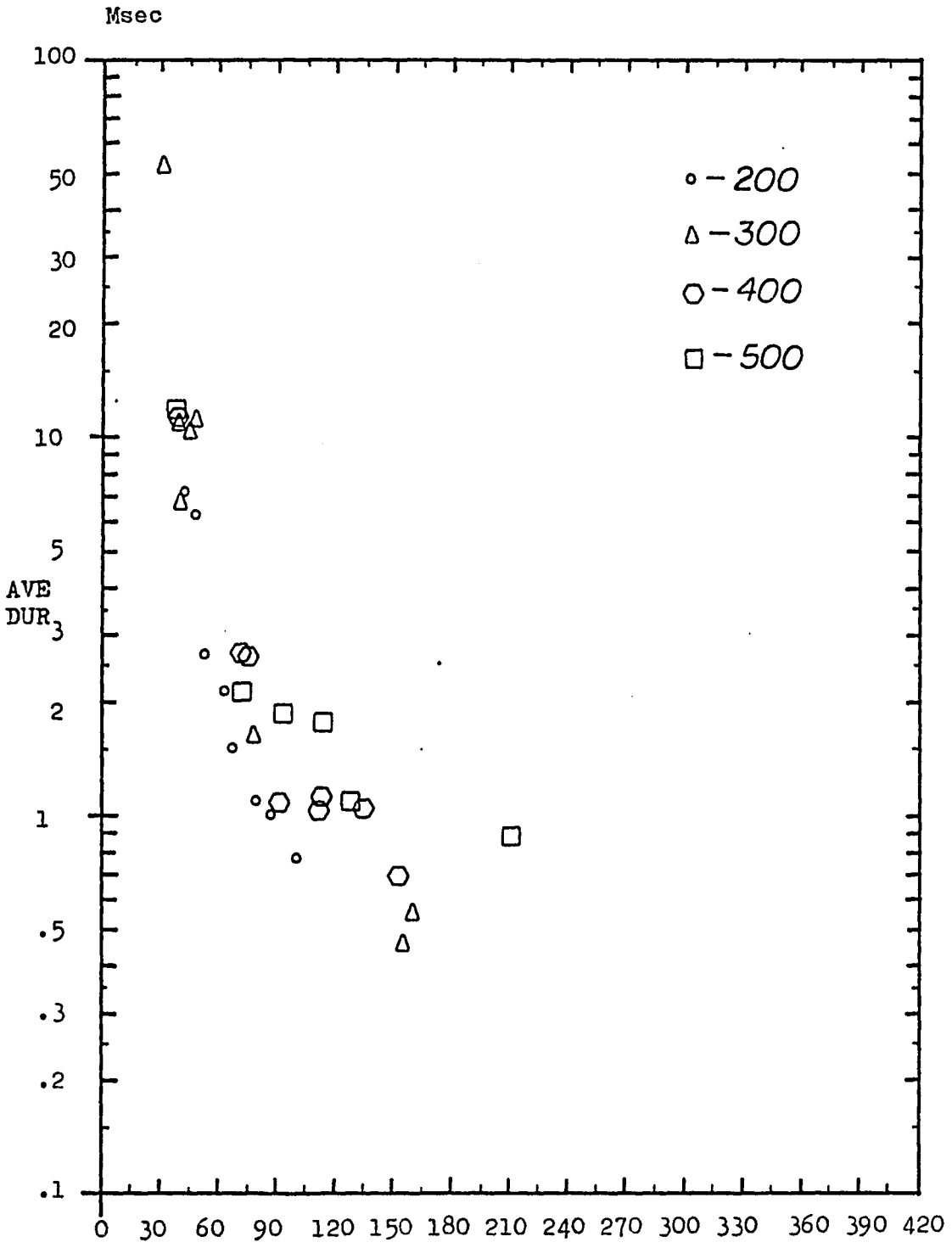

FIG. 29: Average contact duration, series I

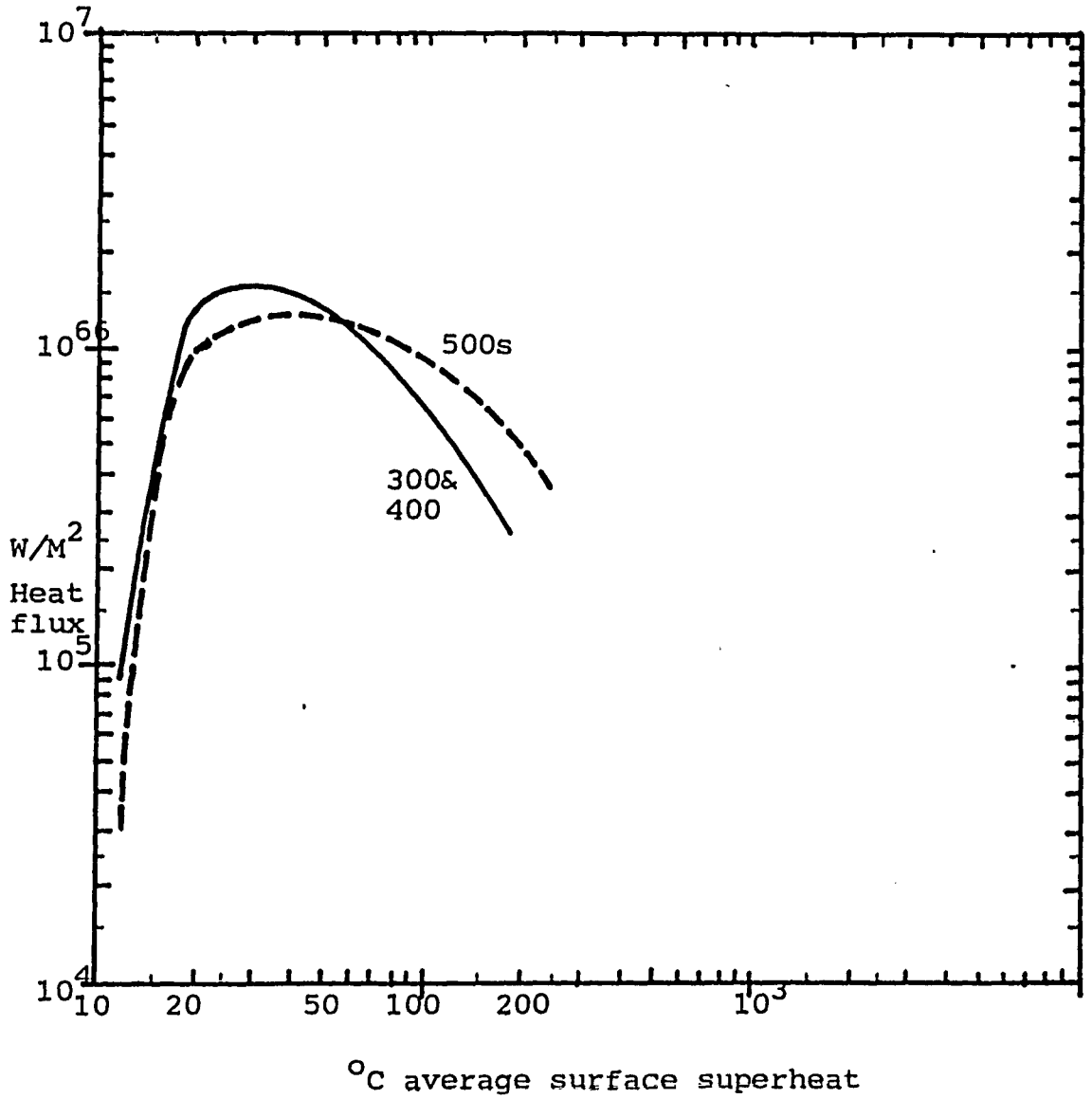

FIG. 30: Boiling curves, series I runs

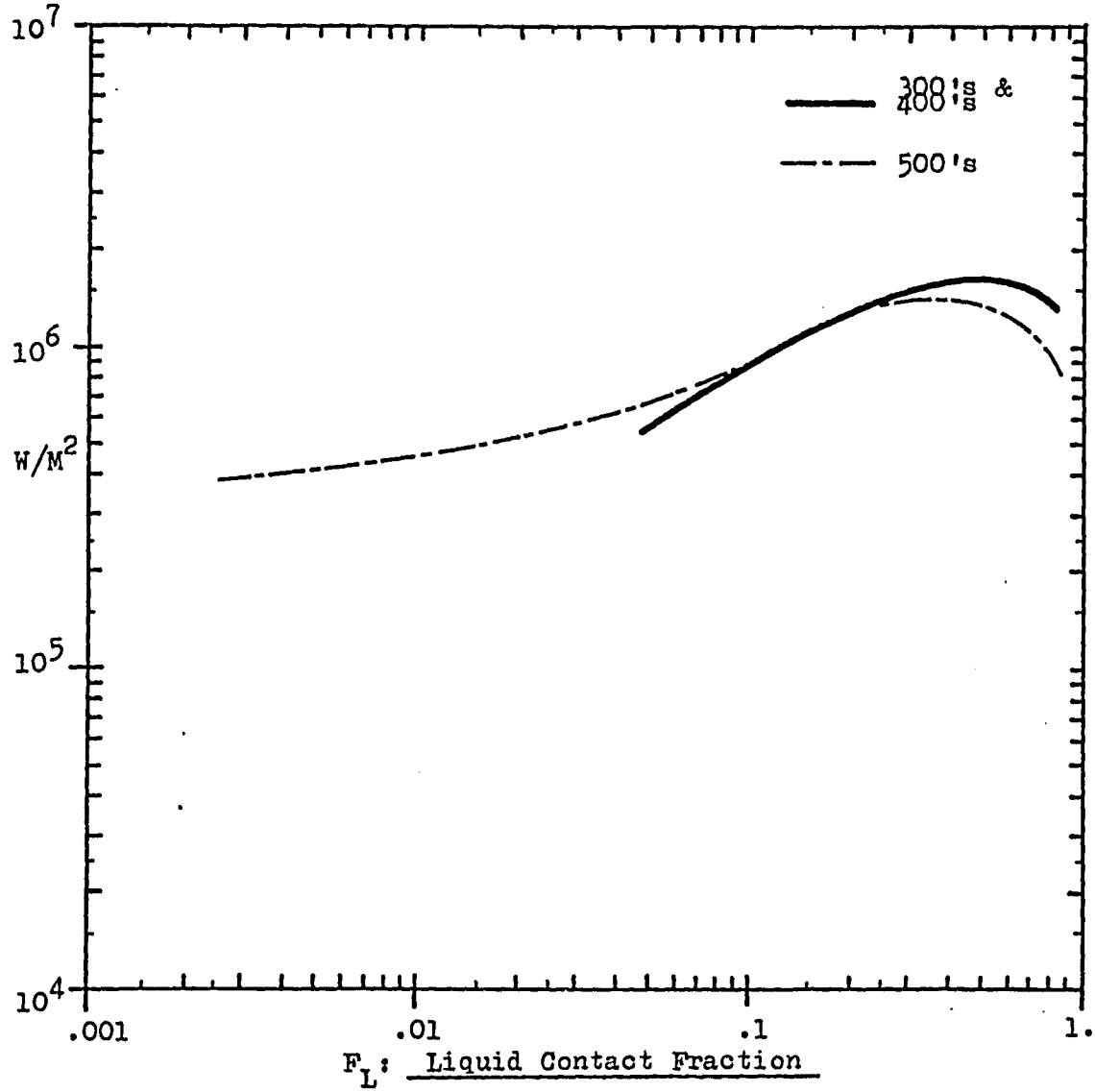

FIG. 31: surface heatflux vs. liquid contact fraction, series I runs

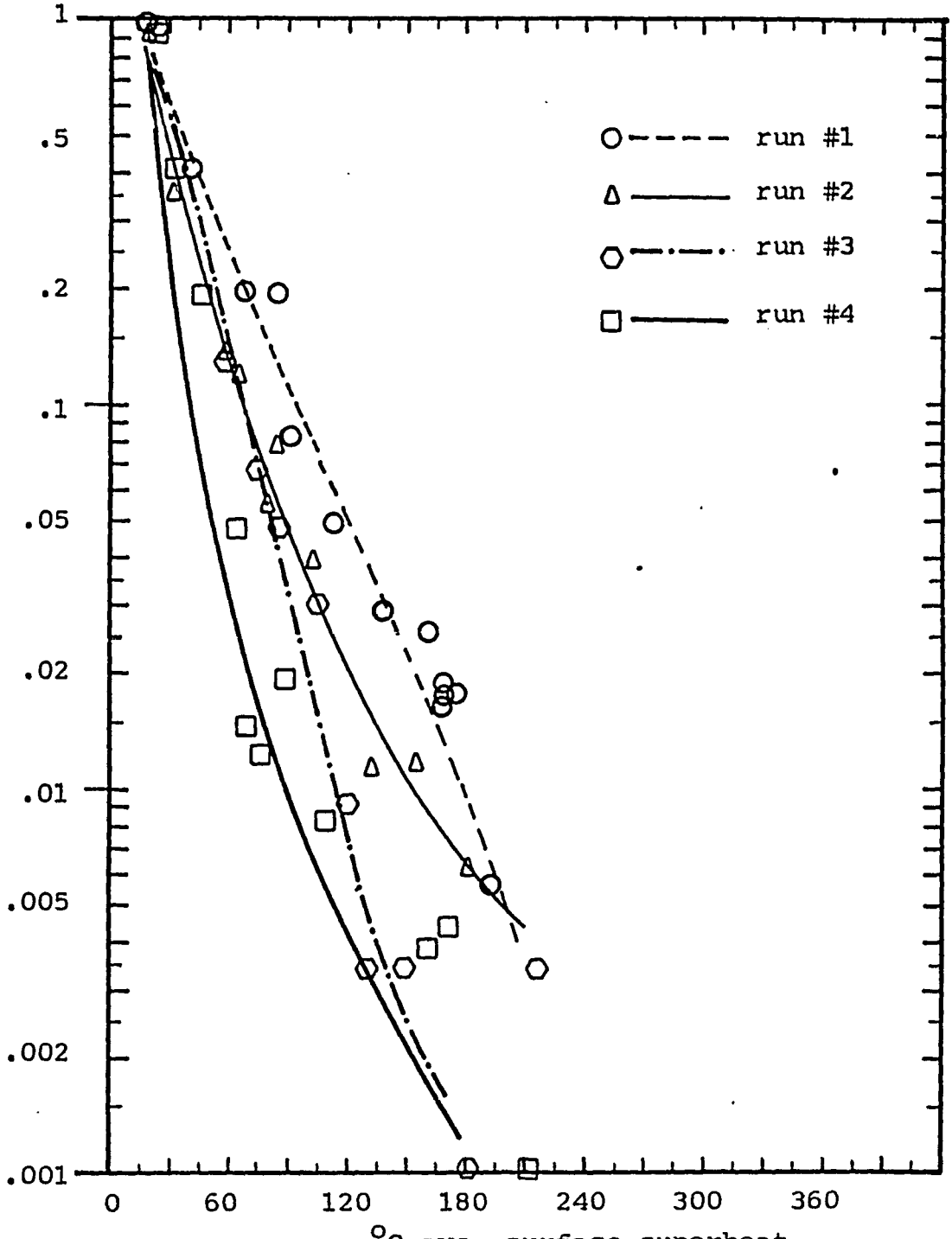

FIG. 32: $F_{L,t}$ data, series II

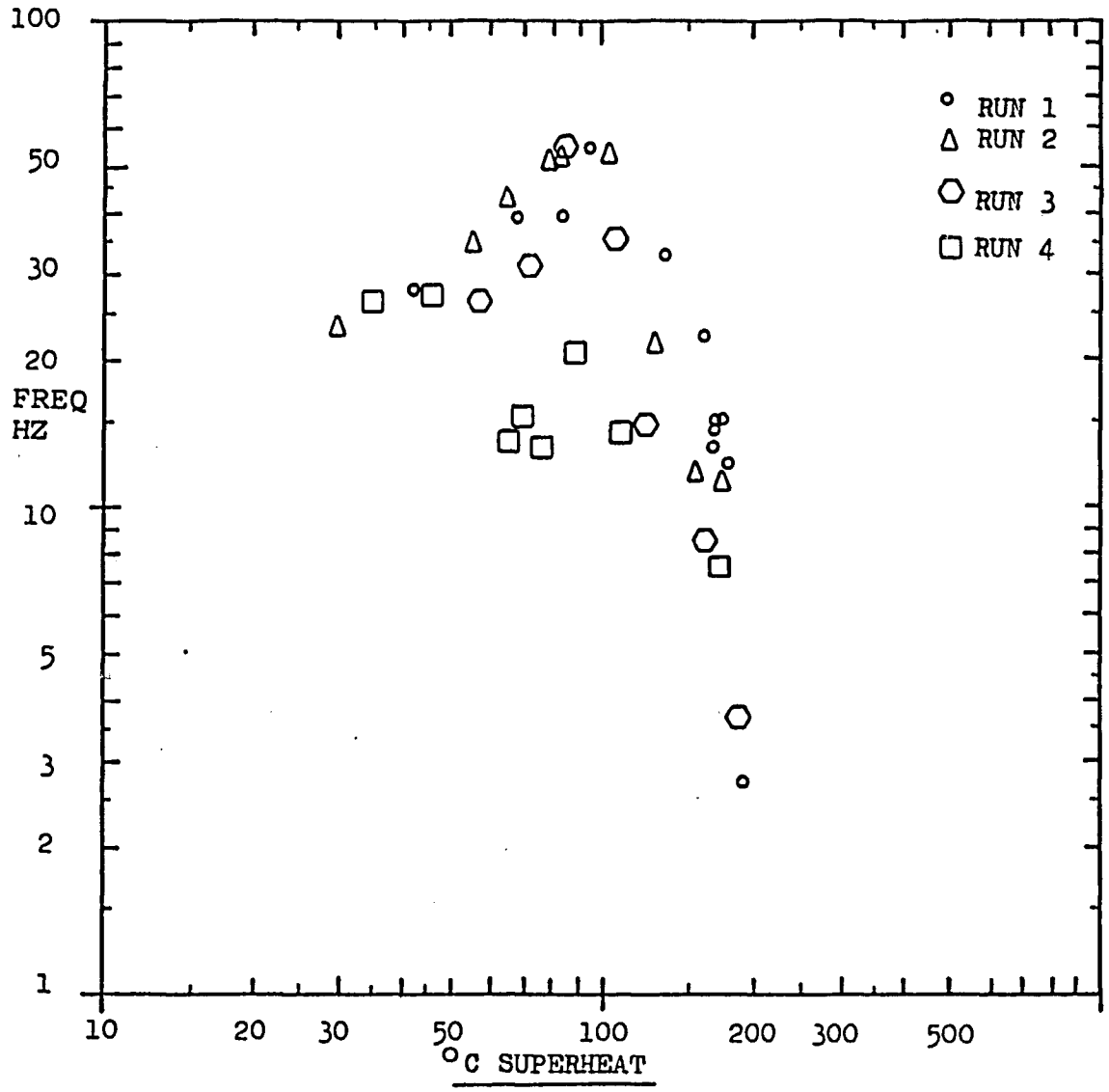

FIG. 33: Frequency of liquid contacts, series II runs.

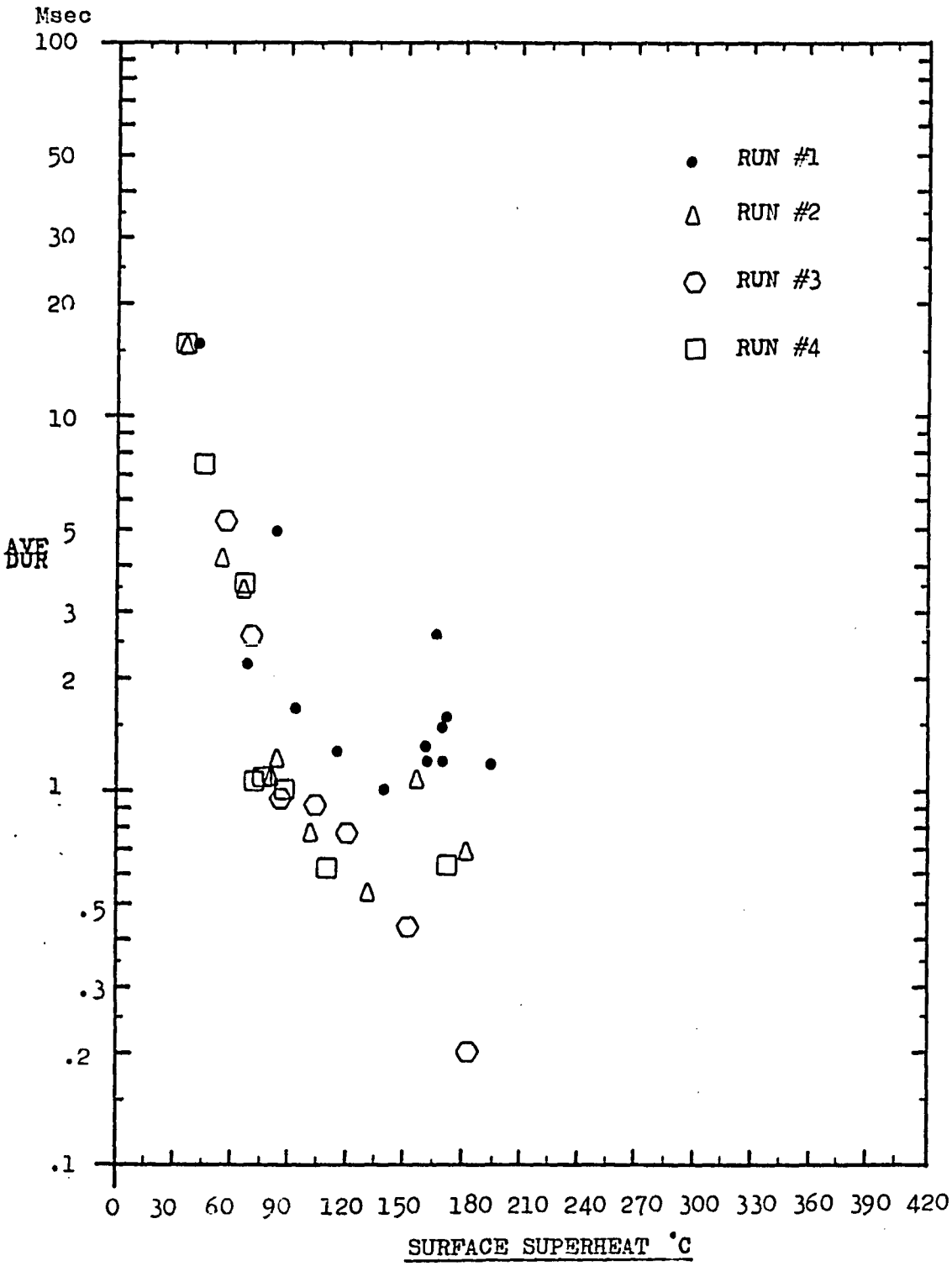

FIG. 34: Average contact durations, series II

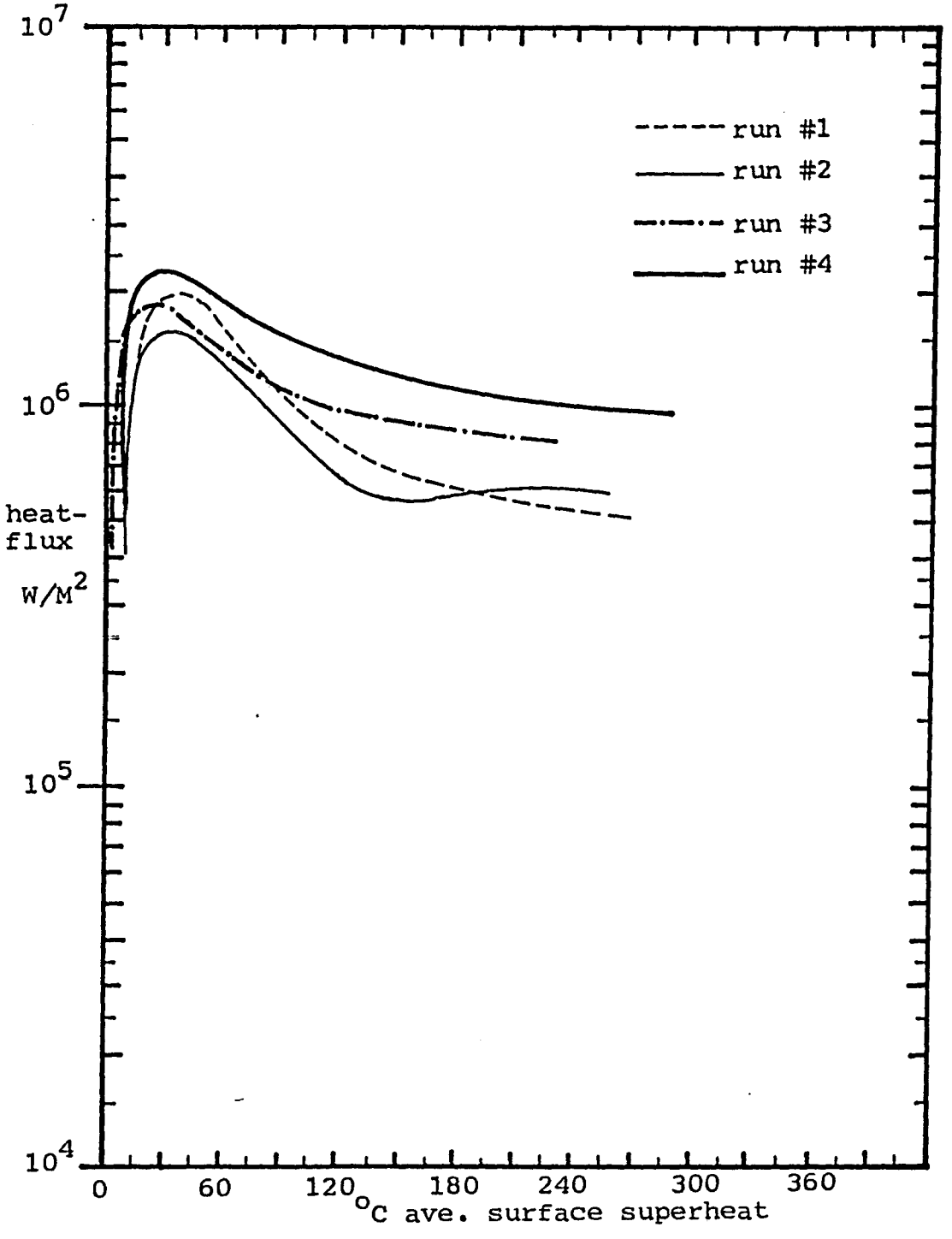

FIG. 35: Boiling curves, series II runs

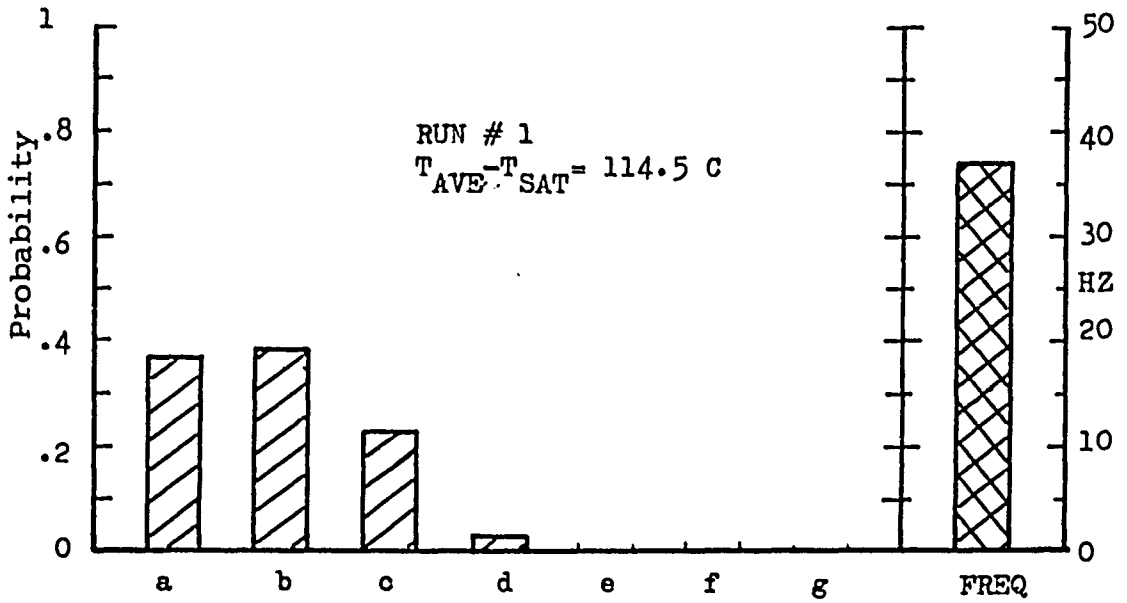

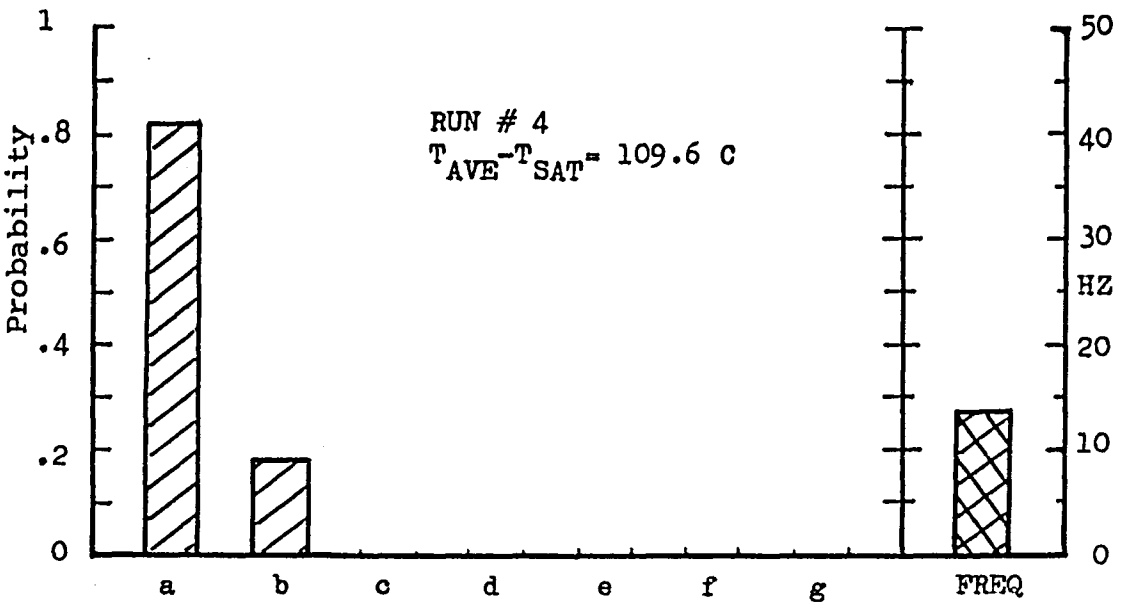

FIG. 36: Statistical distribution of contact durations, series II (run #1 & run #4)

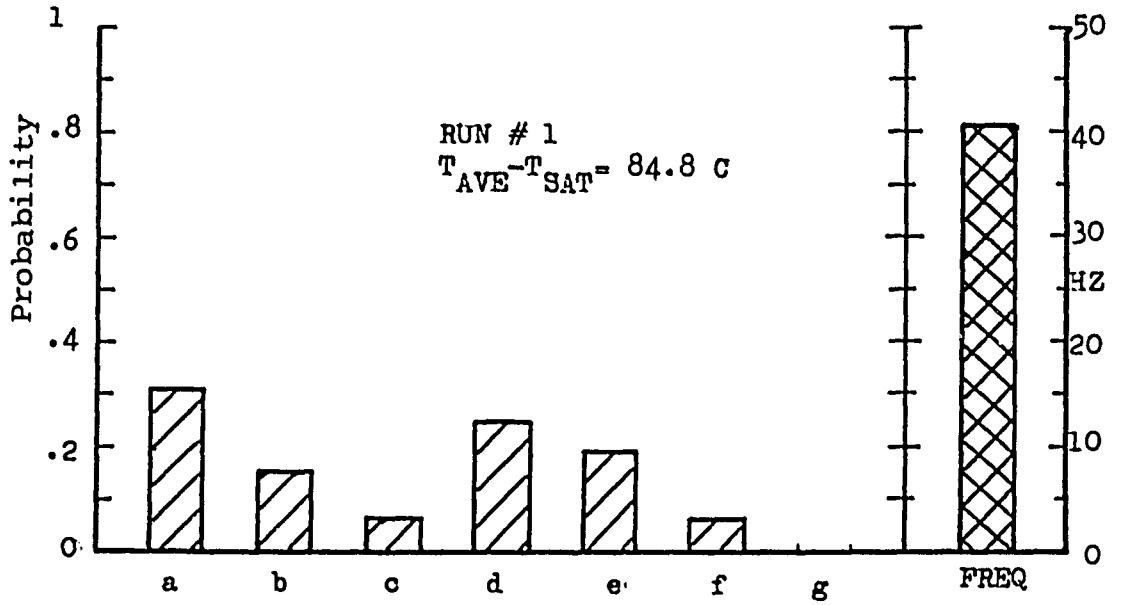

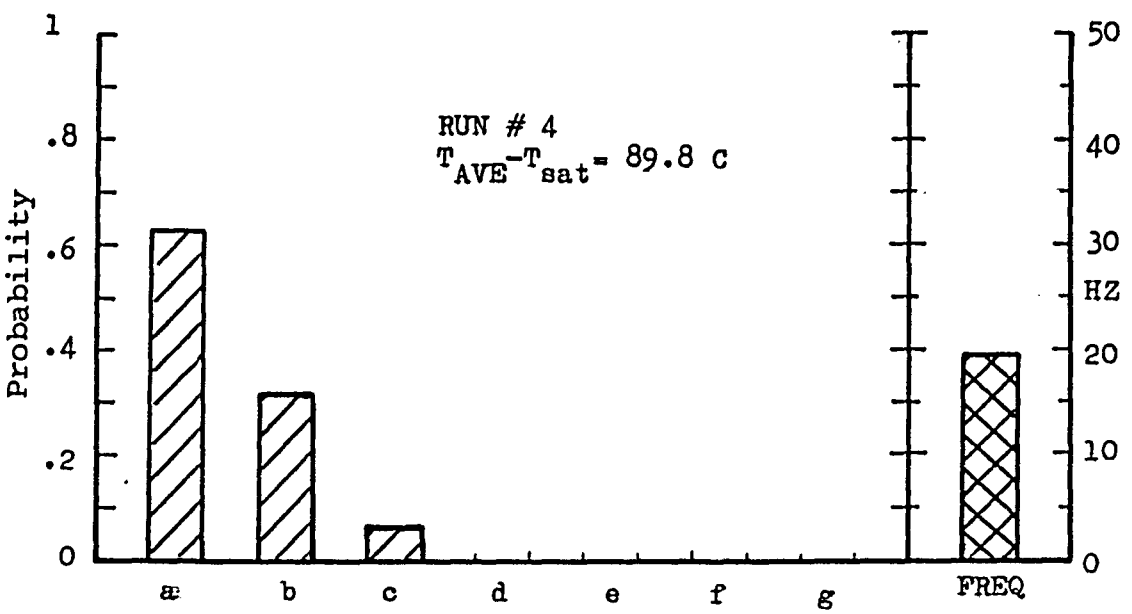

FIG. 37: Statistical distribution of contact durations, series II (run #1 & run #4)

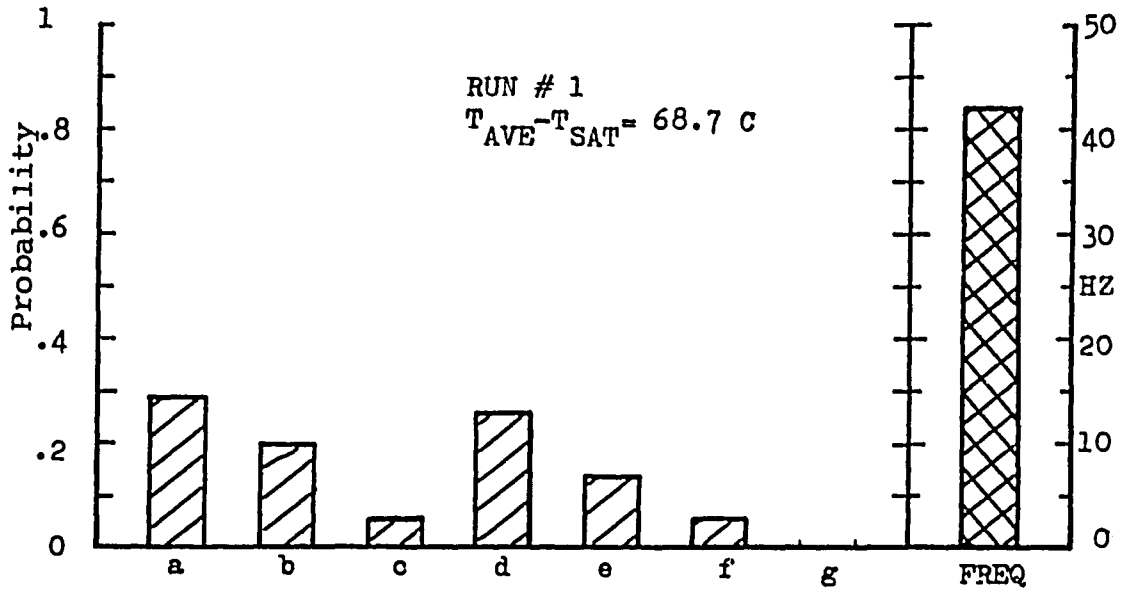

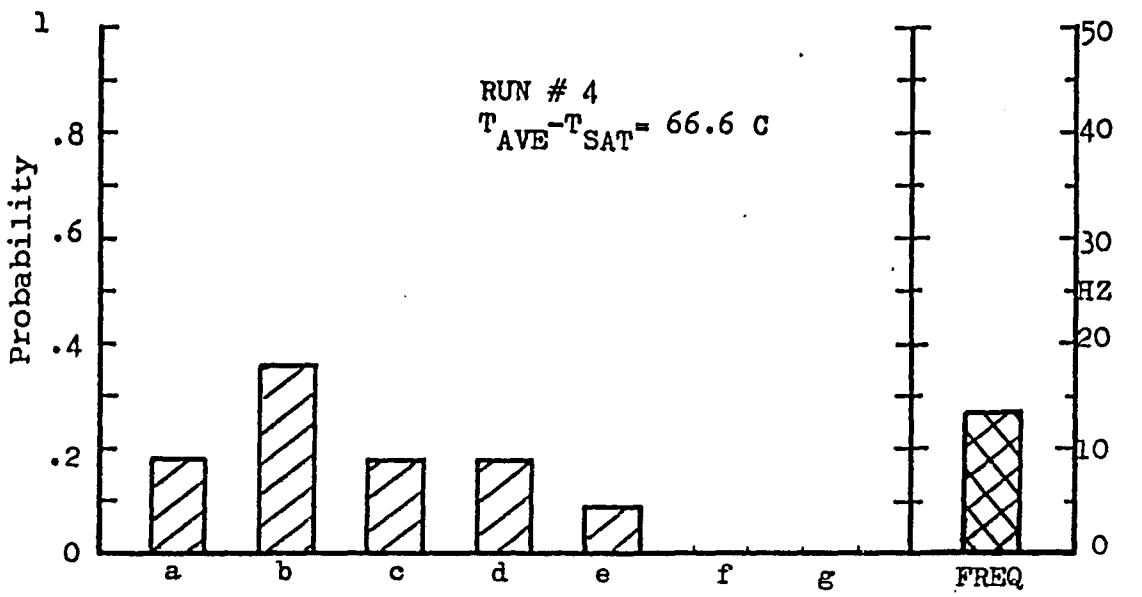

FIG. 38: Statistical distributions of contact durations, series II (run#1 & run#4)

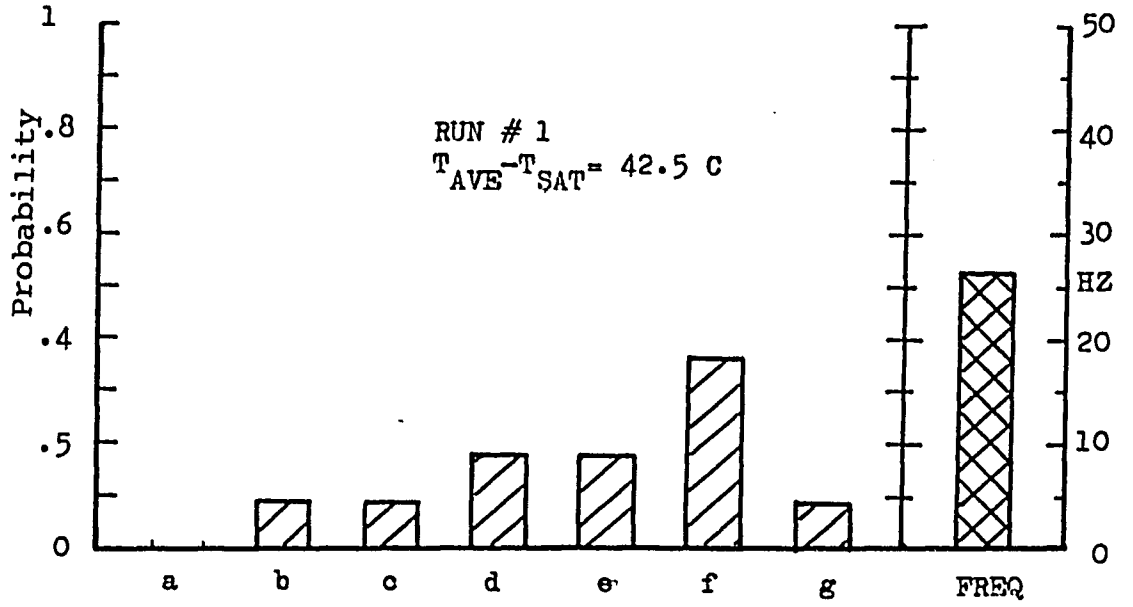

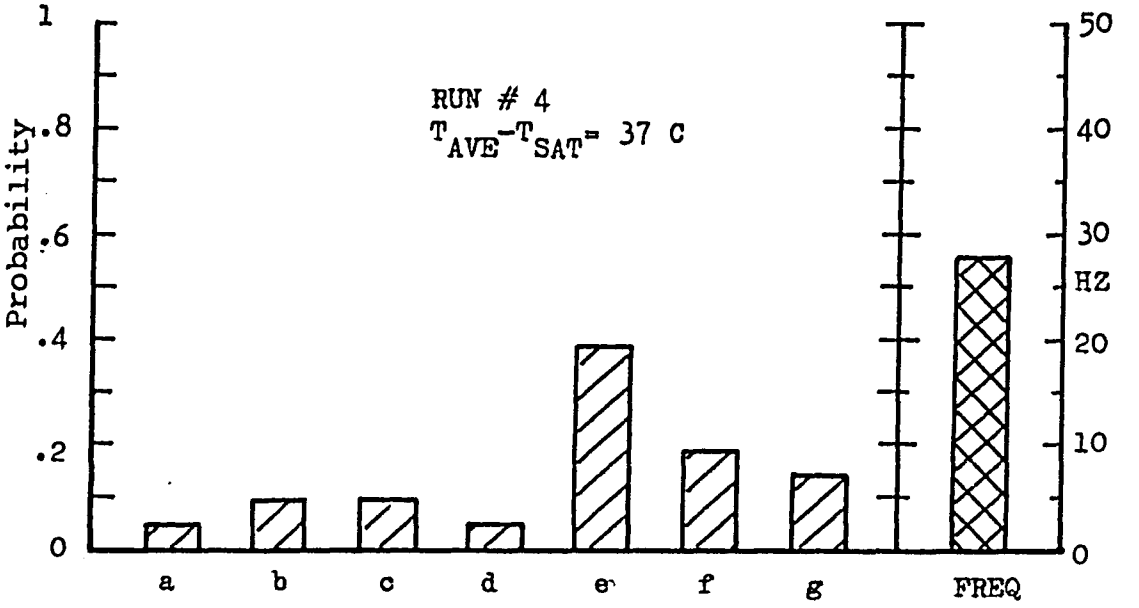

FIG. 39: Statistical distribution of contact durations, series II (run#1 & run#4)

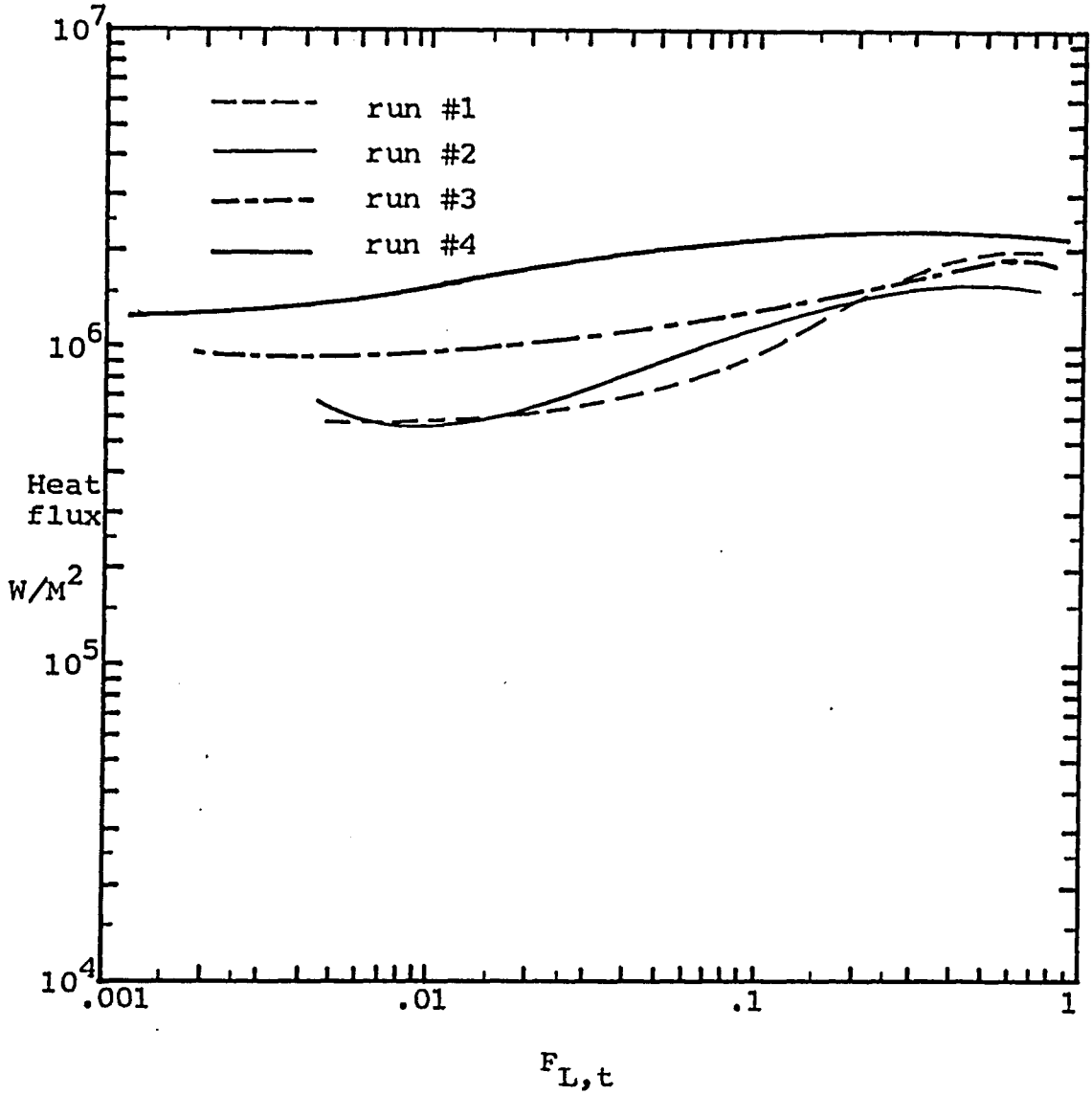

FIG. 40: Surface heatflux vs. $F_{L,t}$ for increasing surface aging effect (series II)

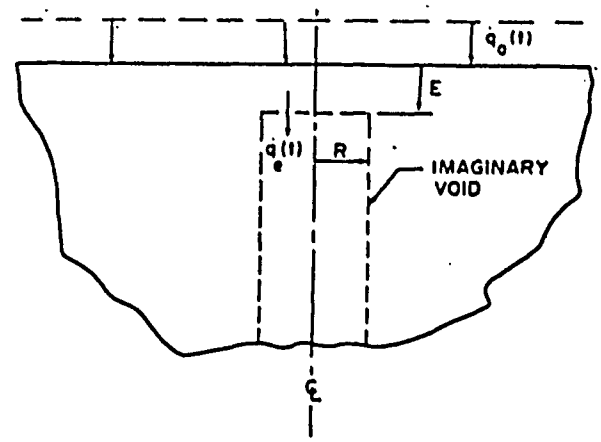

FIG 41: Boundary conditions of one-dimensional heat flow in a semi-infinite slab with imaginary void

From Beck [36]

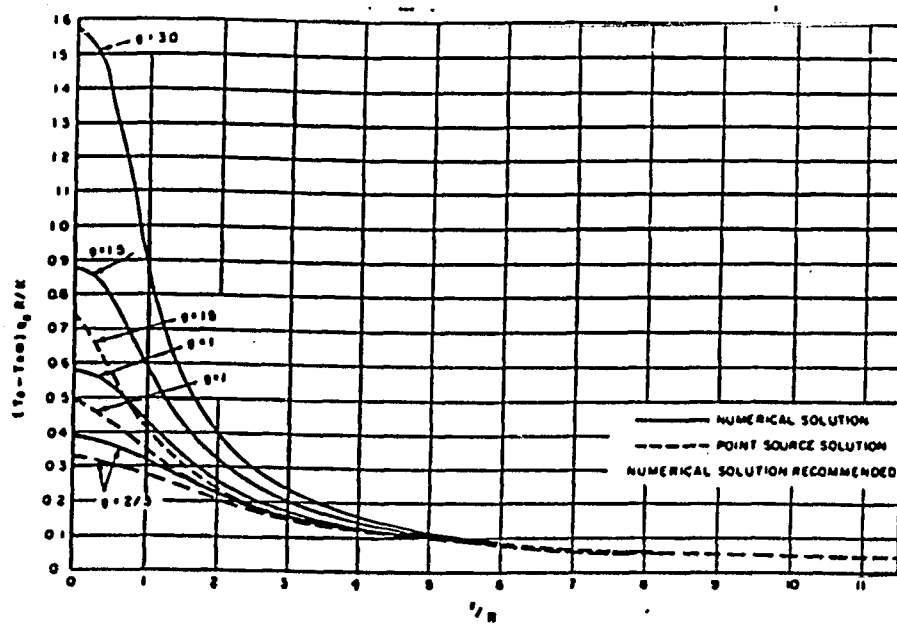

FIG 42: Steady-state numerical and point heat source solutions for the heat sink surface

From Beck [36]

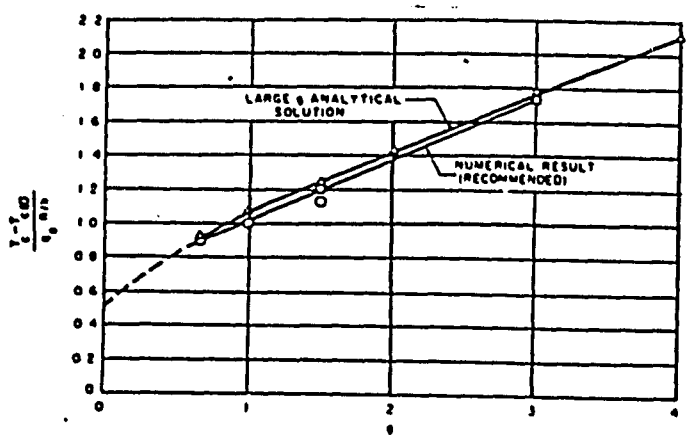

FIG 43a: Comparison of thermocouple temperature error results

From Beck [36]

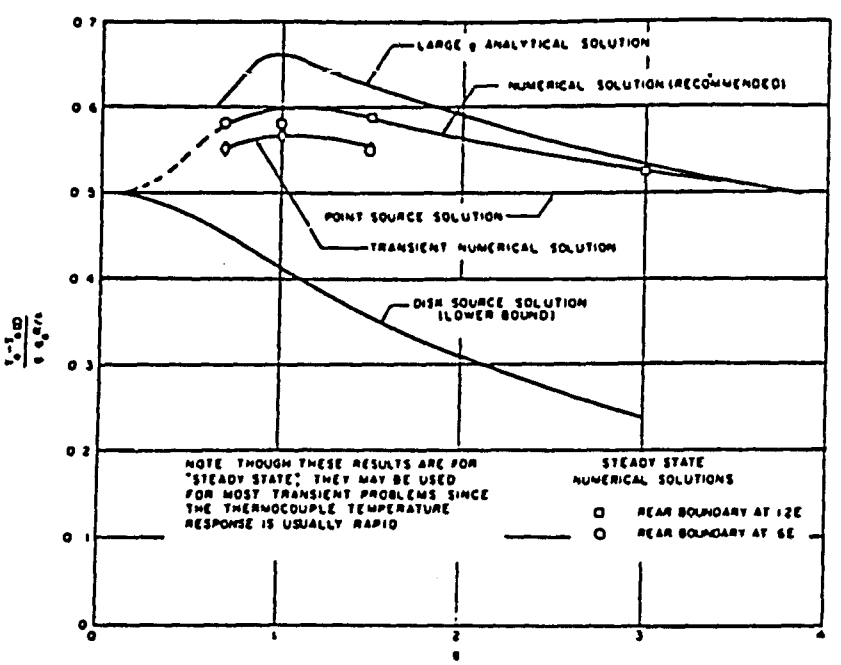

FIG.43b: Steady-state hot-spot results

FIG. 43: Thermal disturbance due to T.C. void.

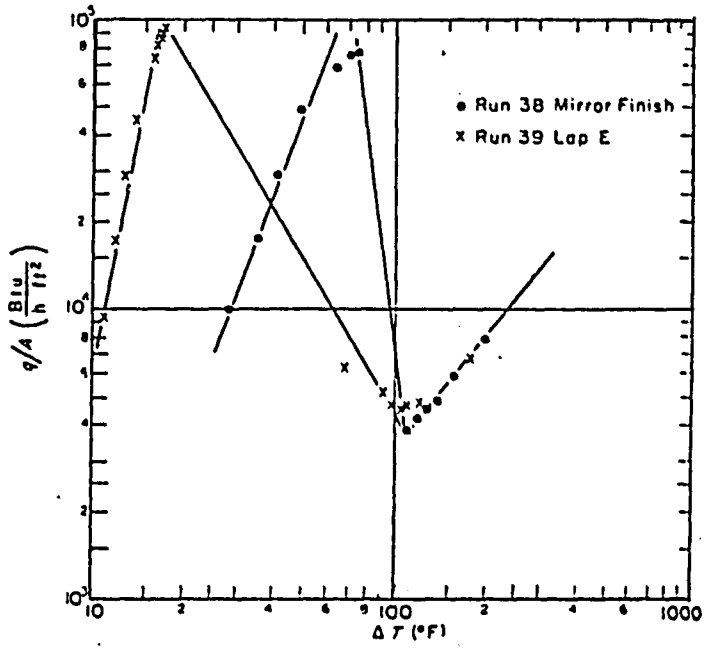

FIG. 44
Nickel-pentane test results: effect of roughness.

From Berenson [1]

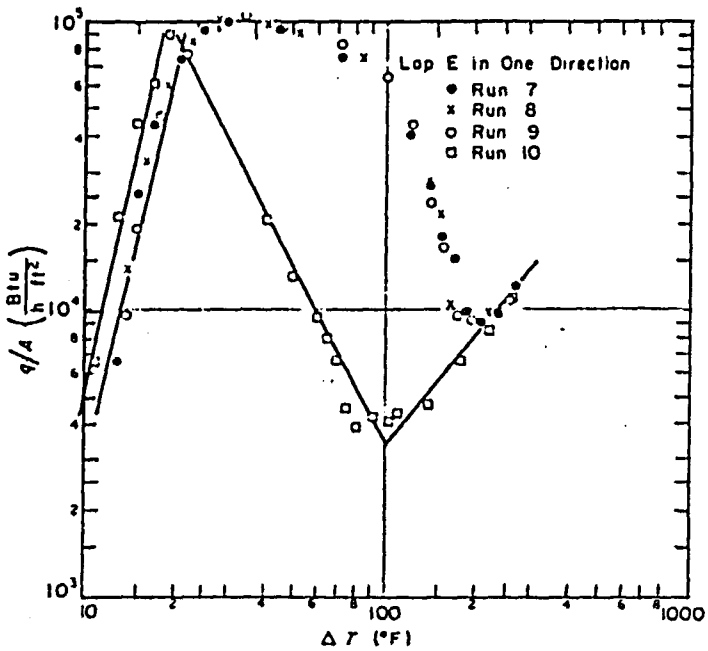

FIG. 45
Copper-pentane test results: effect of surface cleanliness.

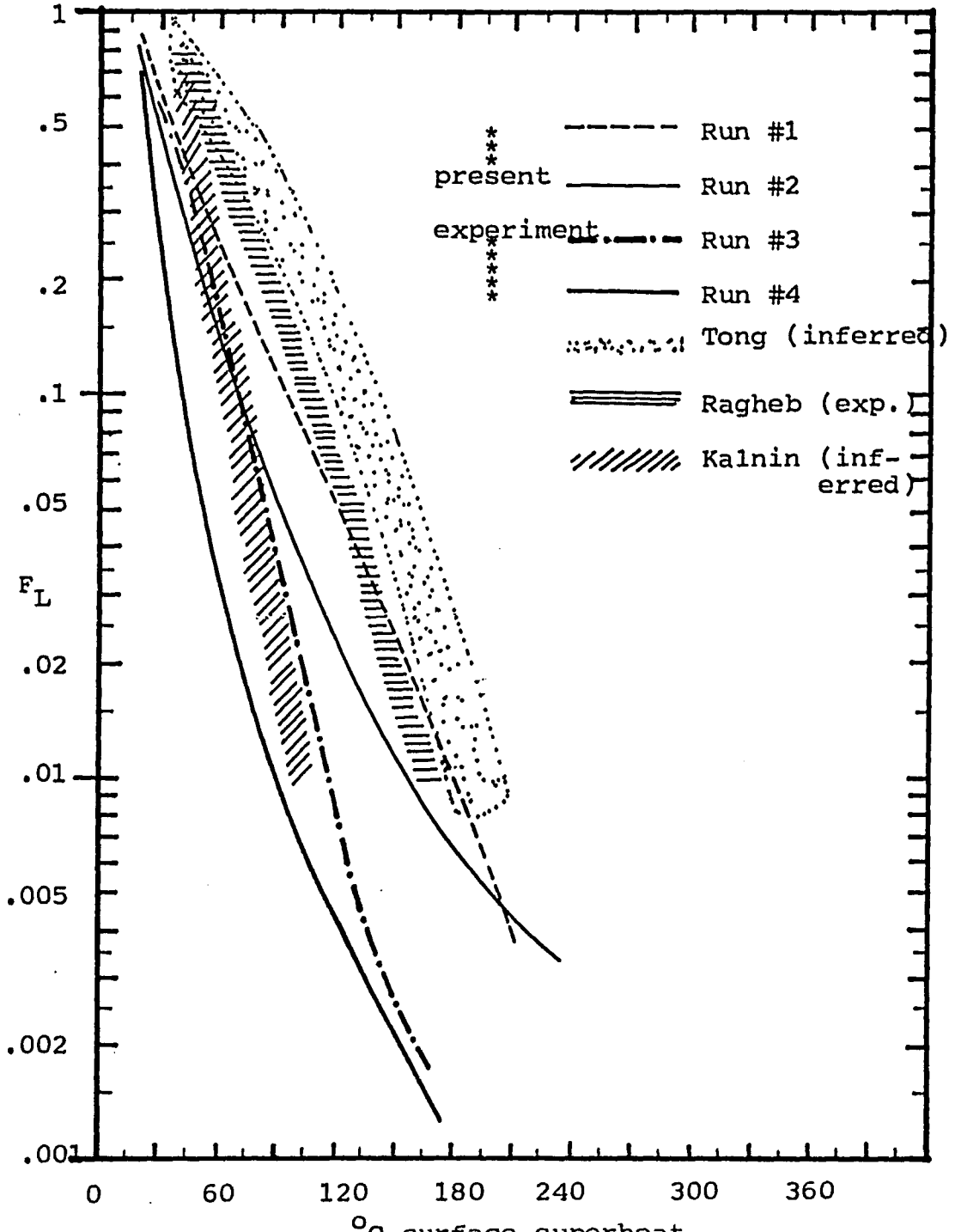

FIG. 46: A comparision of presentavailiable F_L data.

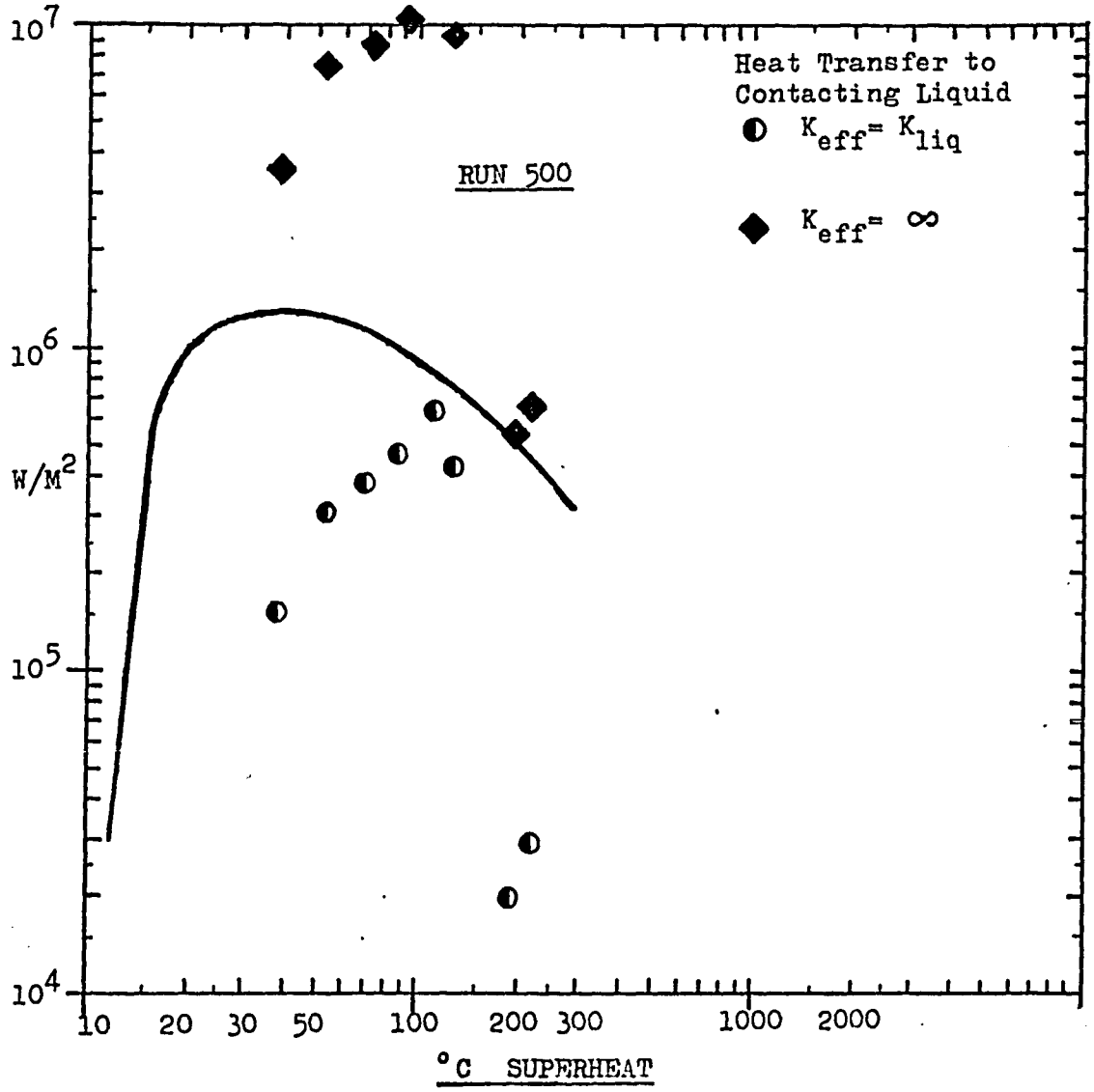

FIG. 47: Transient conduction liquid contact heat transfer contribution, series I

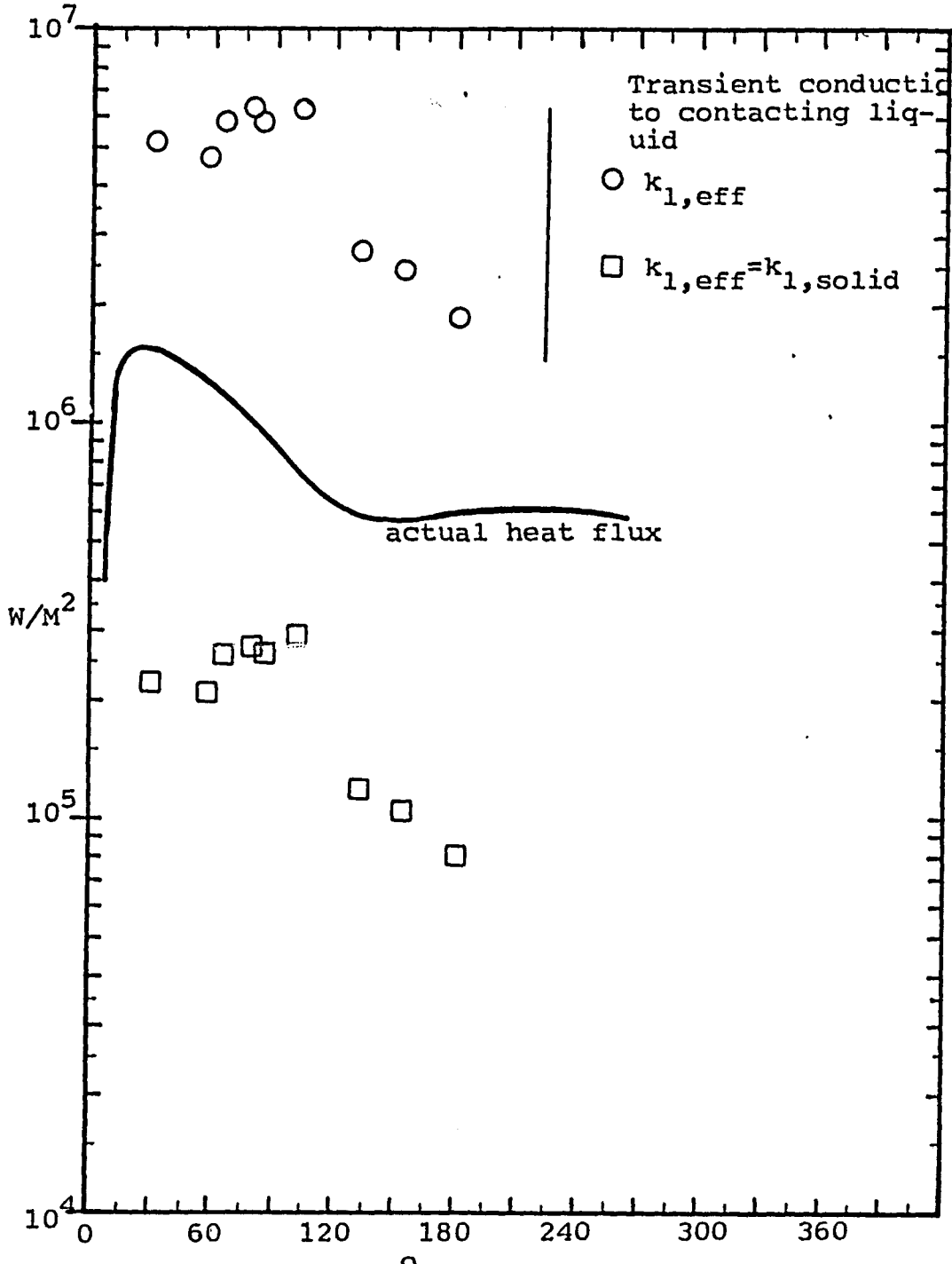

FIG. 48: Liquid contact heat transfer contribution by transient conduction, run2,series II

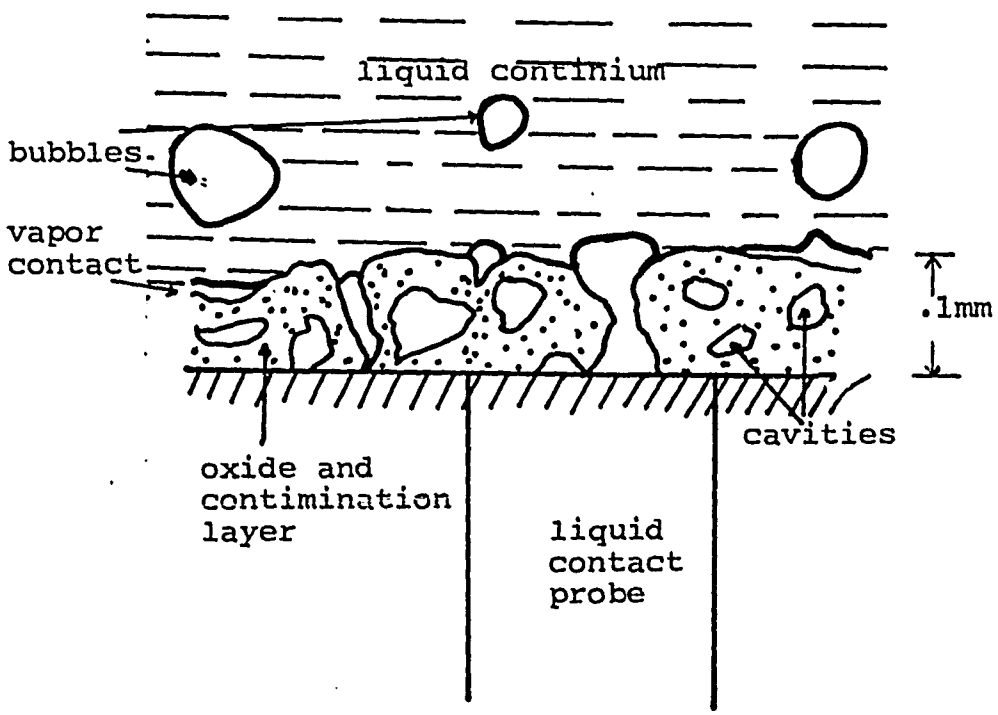

FIG. 49: A proposed model for high temp. boiling on oxidized surface

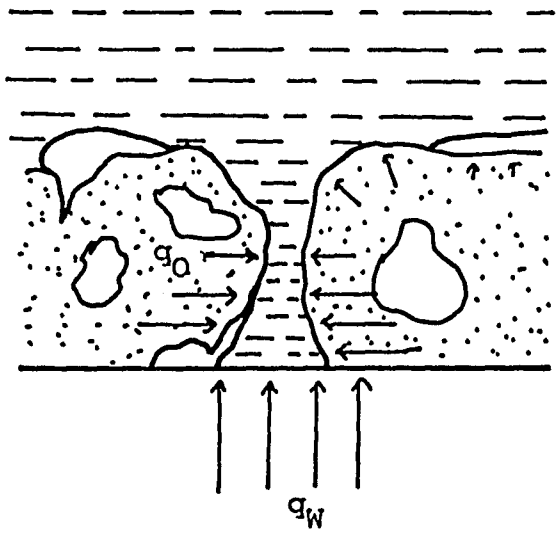

FIG. 50: Heat transfer path to liquid contact on oxide surface (high superheat)

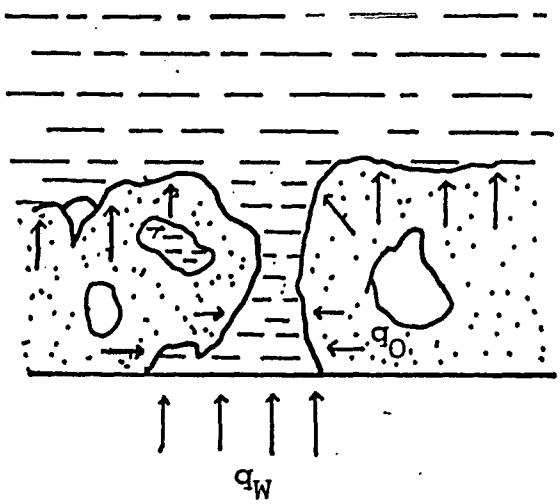

FIG. 51: Heat transfer path to liquid contact on oxide surface (low superheat)

APPENDIX I

Fabrication Techniques on Fast response flush mounted micro-thermocouple probe

Three steps were involved in the fabrication of the fast response thermocouple probe, they are:

(1) mounting the thermocouple into the test block.

(2) re-surfacing the probe-block surface.

(3) junction formation.

The three steps are discussed below:

(1) Due to the extreme delicacy of the micro-thermocouple (0.51mm OD) used, a protective 1.52 mm OD stainless steel tube was first put over the thermocouple sheath except very close to the probe tip. a 4.6 mm diameter hole was drilled at the center of the test block from the bottom up until the hole reaches 16mm from the top surface. A small 0.635 mm hole was drilled from the top center until the larger hole was matched.

After rigouous cleaning procedure, the probe assemble was then put through the hole with part of the thermocouple tip exposed. After filling the cavity with silver solder and flux, the whole copper block was supported invertedly in the oven.

The oven temperature was brought up to 750 ^{o}C and power was turned off when the block temperature reached 720 ^{o}C. With the oven lid removed, the block was cooled slowly to room temperature by radiation and natural convection.

Massive oxide scale was formed over the copper block. Some braising material was observed to flow through the clearance and clinged between the thermocouple tip and the copper block, good braize join was then concluded.

(2) The thermocouple tip was then cut flush and the top surface of the block was lapped down for a smooth finish. At this stage, the thermoxouple would have its leads exposed (Fig. 9)

(3) The junction of the micro-thermocouple probe can be formed by several different means; to get a smooth, homogeneous surface , electroplating and vacuum deposition techniques can be used.

a) Electroplating

Using brush electroplating technique, a thin layer of metal can be deposited on the block surface and between the two leads. Given enough time, the thin film of electroplated metal would merge and cover over the ceramic dielectric material. A thermocouple junctioncould thus be formed from the thin film of ele= ctroplated metal.

b) Vacuum vapor deposition.

Formation of a junction can also be achieved by vacuum vapor deposition technique. The whole metal block was put into a vacuum deposition chamber.

A small piece of metal was vaporized in a electrically heated tungsten basket. The metal vapor solidified on the contact to cold surfaces and a thin even layer of metallic, electrically conducting film was formed on the block surface. In general, the film thickness formed by the vapor deposite technique is less than $2x10^{-6}$ meter; to minimize thermal disturbance from the presence of the probe, multi-coating is needed to obtain a thicker, more rugged thermal junction.

The vapor deposited junction micro-thermocouple probe used in the series II had a junction thickness around $1.7x10^{-5}$meter. A maximum surface temperature fall rate of greater than 250°C was recorded on liquid-solid contact (surface superheat 150°C). The junction remain intact after the quench runs and it seemed an optimum trade-off between response time and junction ruggness was obtained.

APPENDIX II

Original and smoothed overall quench histories, series I & II.

IC OUTPUT IN MV
3.500
6.500
9.500
12.500
15.500
18.500
21.500
0.000
3.500
7.000
10.500
14.000
17.500
21.000
24.500
28.000
31.500X10
TIME IN SEC
Record 111, run series 300s

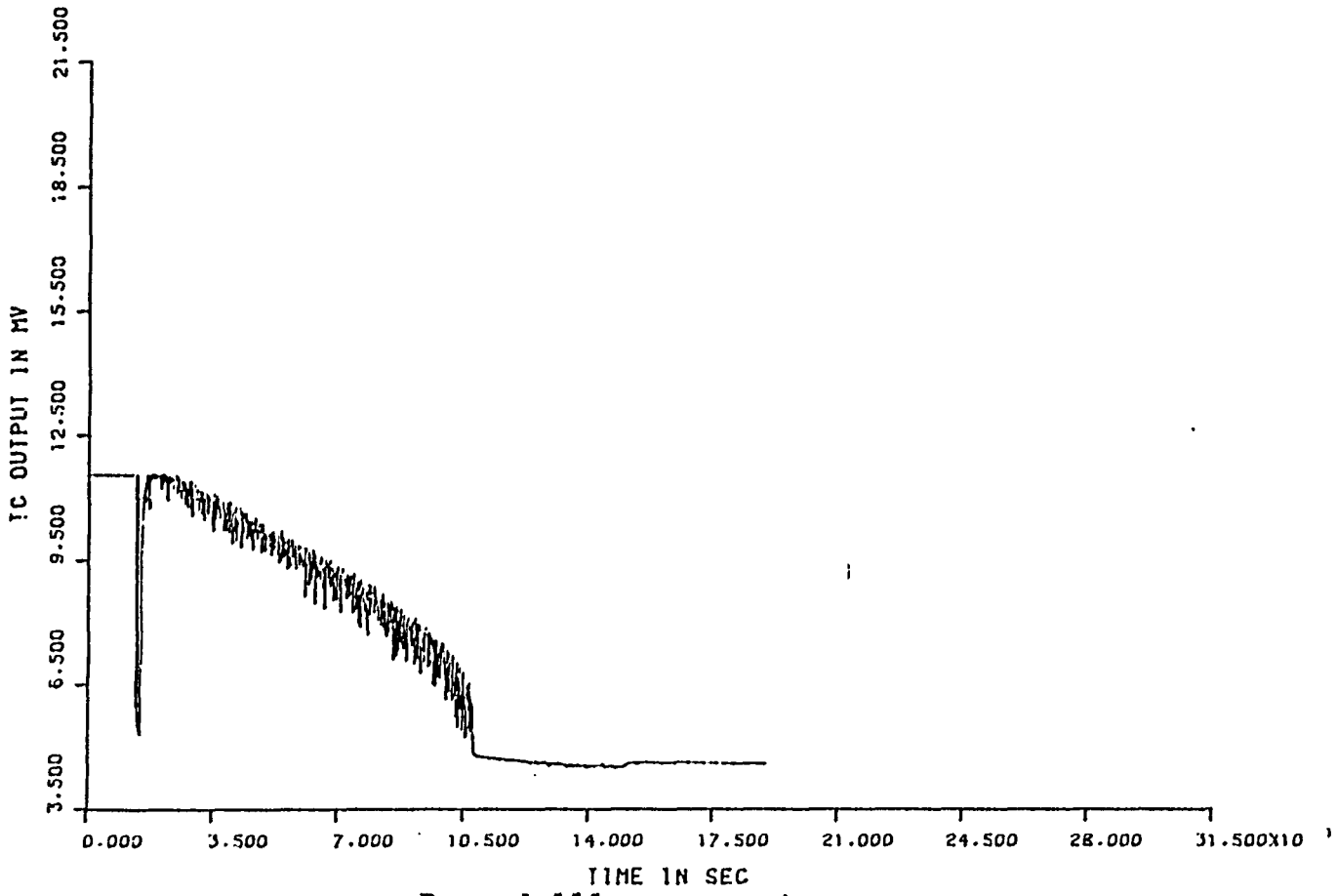

Record 111, run series 300s

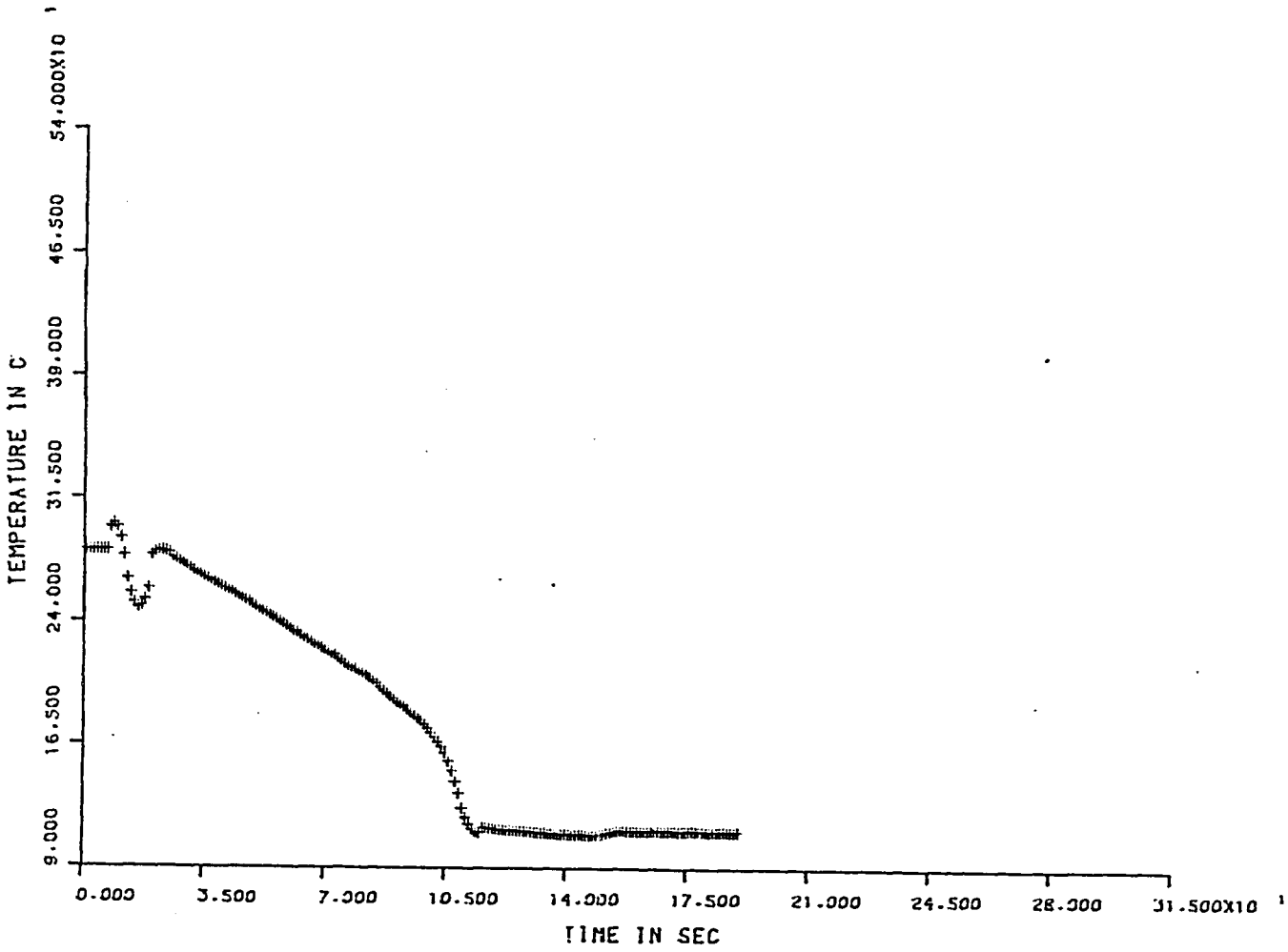

Record 111, smoothed, run series 300s

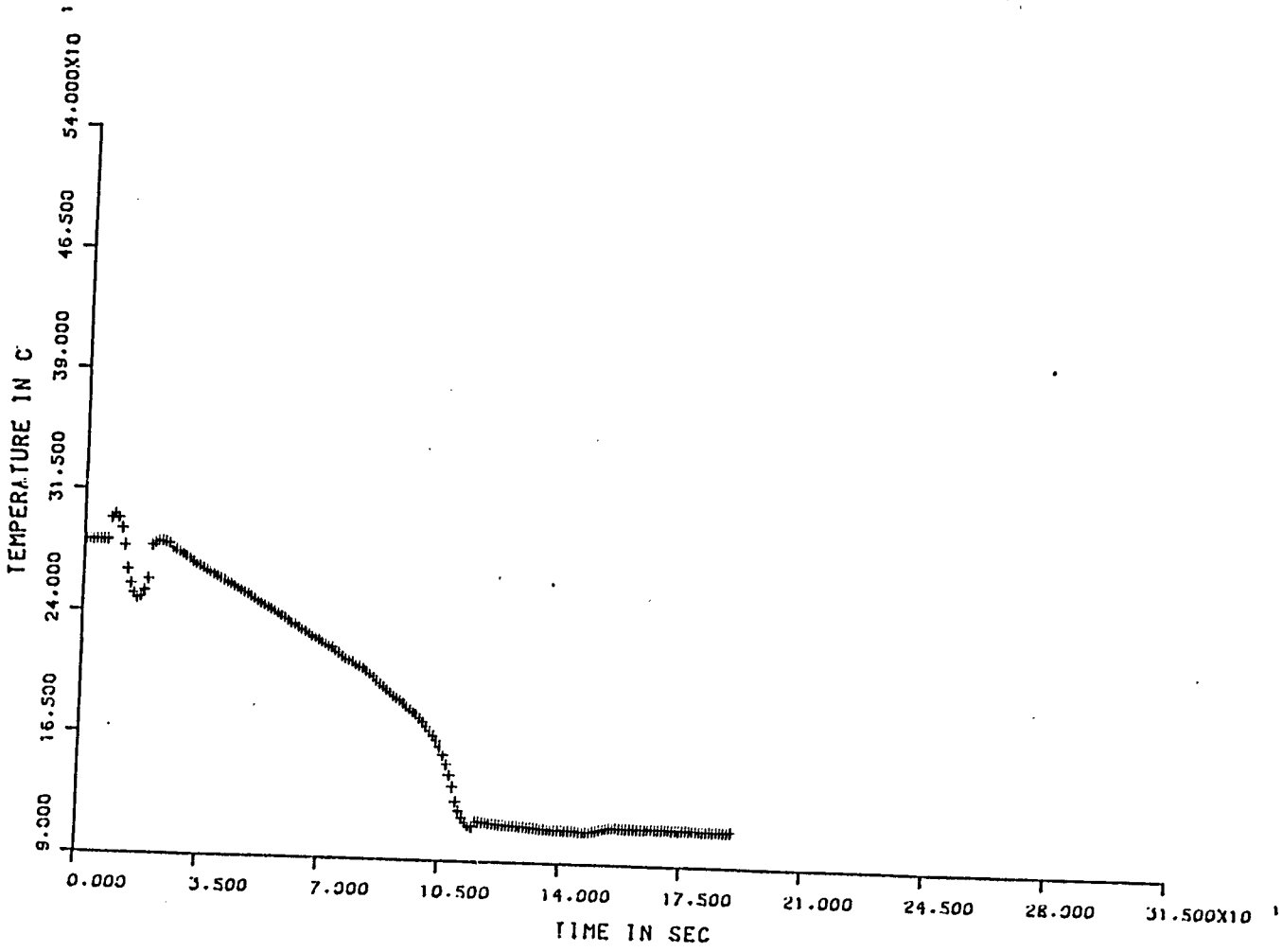

Record 111, smoothed, run series 300s

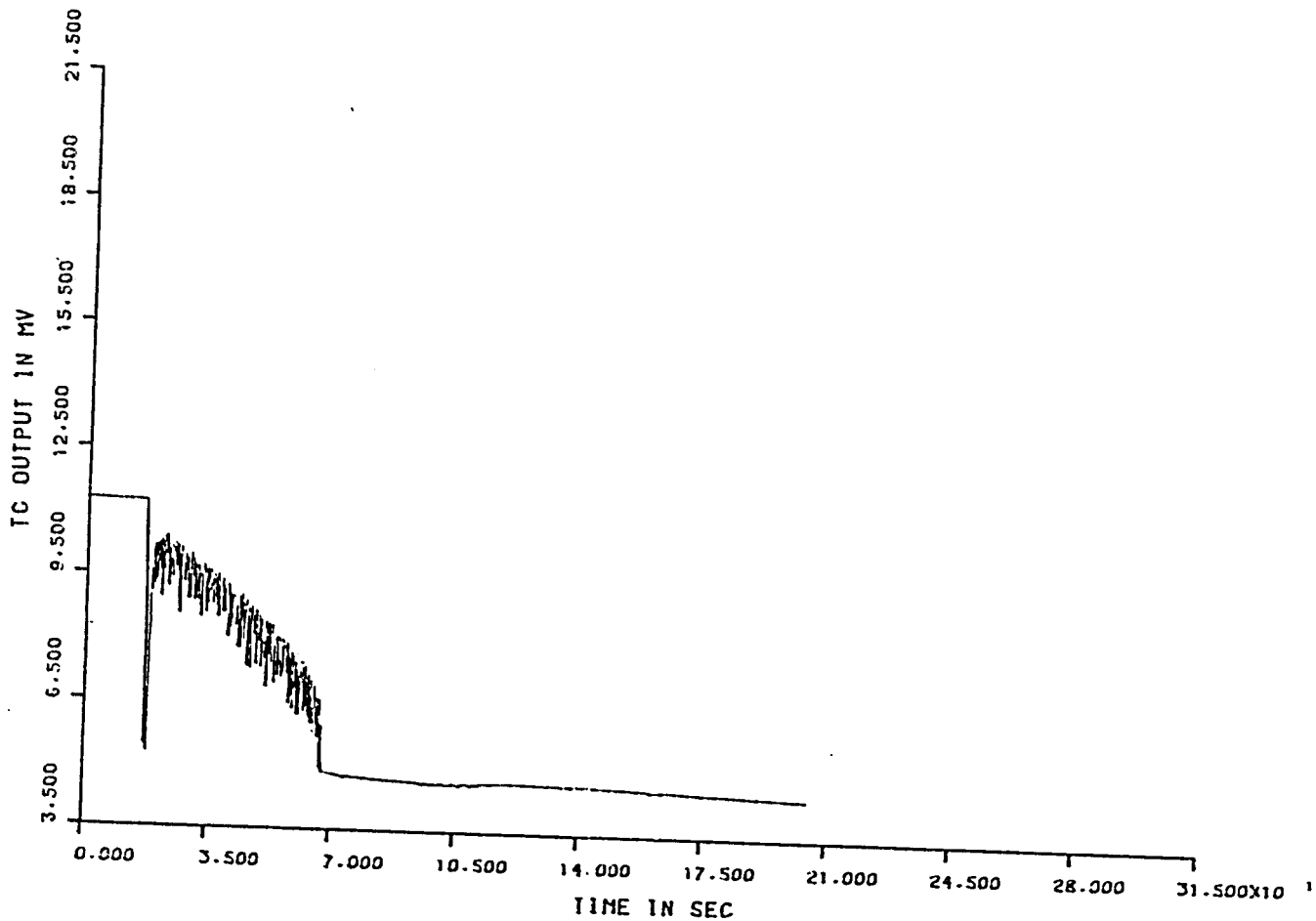

Rec 112, overall quench, run series 300s

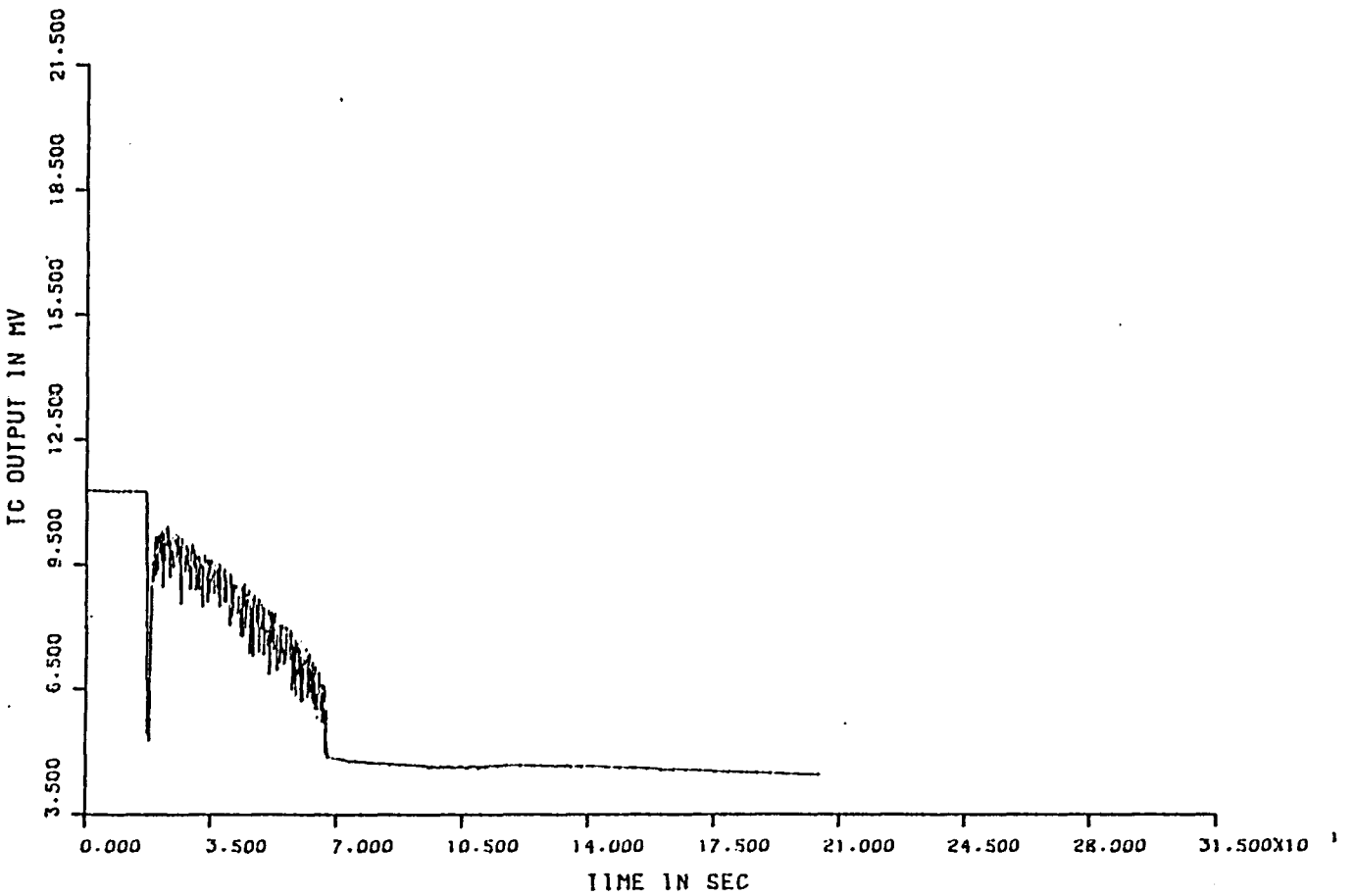

Rec 112, overall quench, run series 300s

Rec 112, smoothed overall quench, run 300s

Rec 112, smoothed overall quench, run 300s

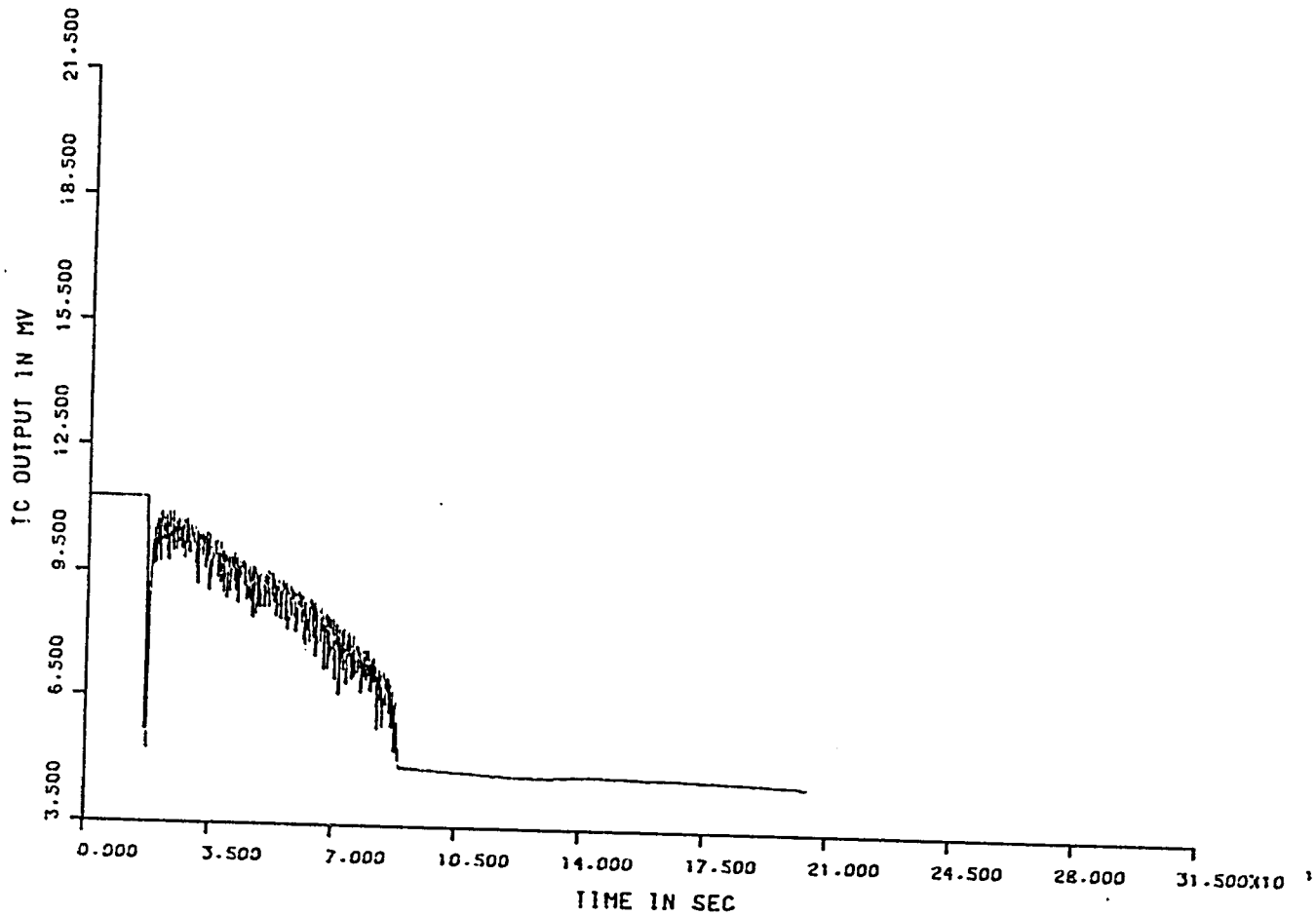

Record 115, overall quench, run series 400s

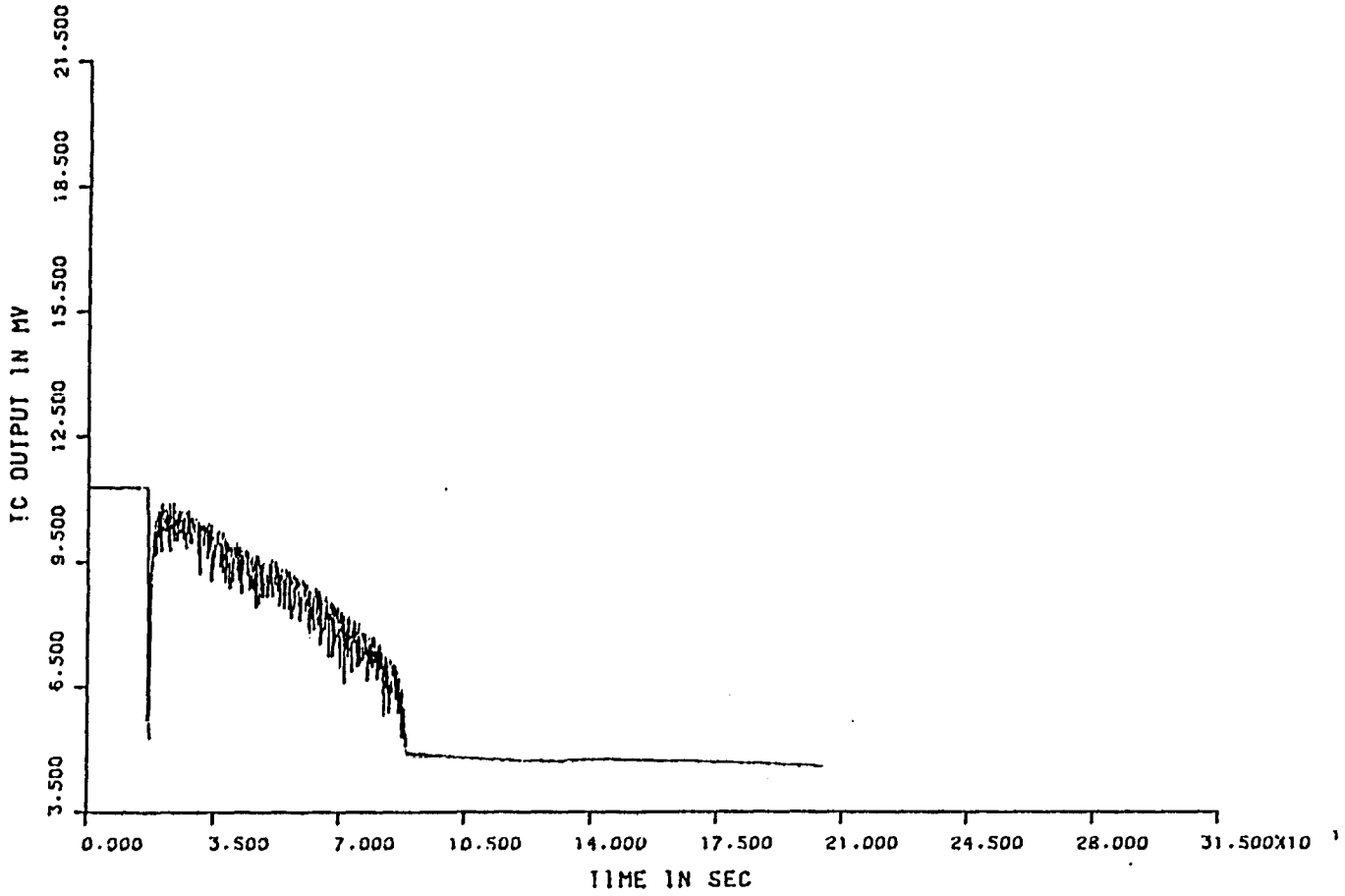

Record 115, overall quench, run series 400s

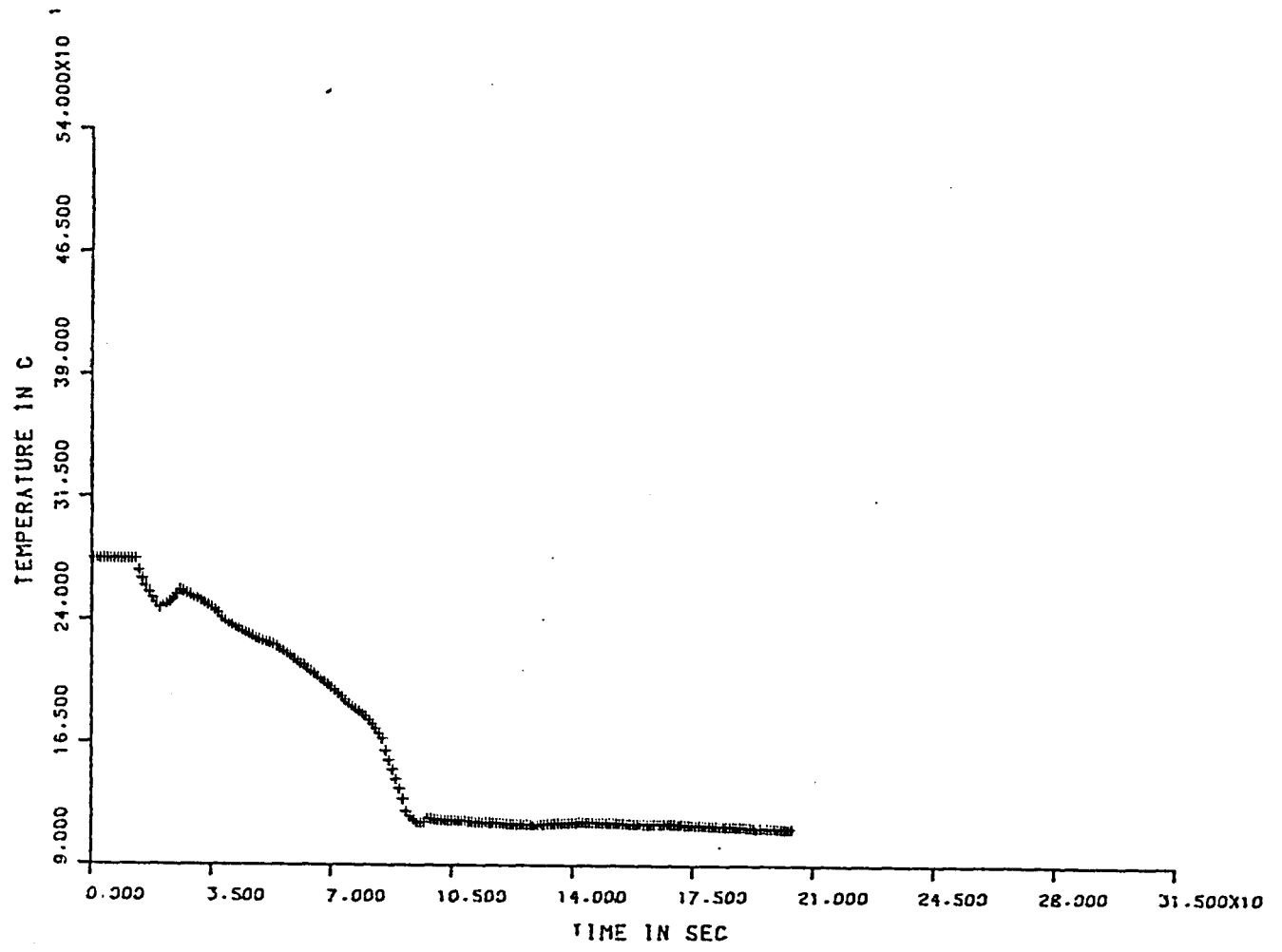

Record 115, smoothed overall quench, run series 400s

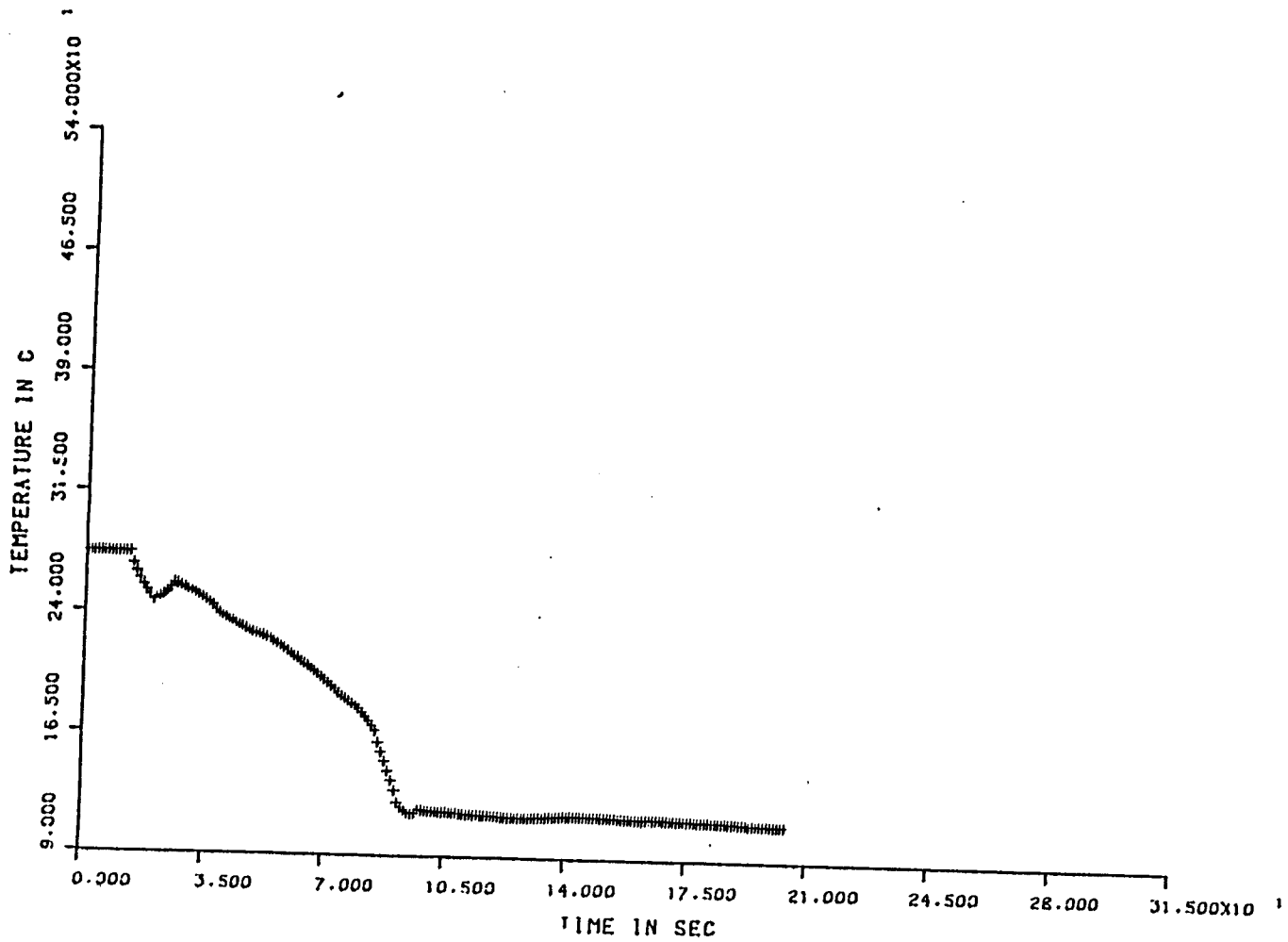

Record 115, smoothed overall quench, run series 400s

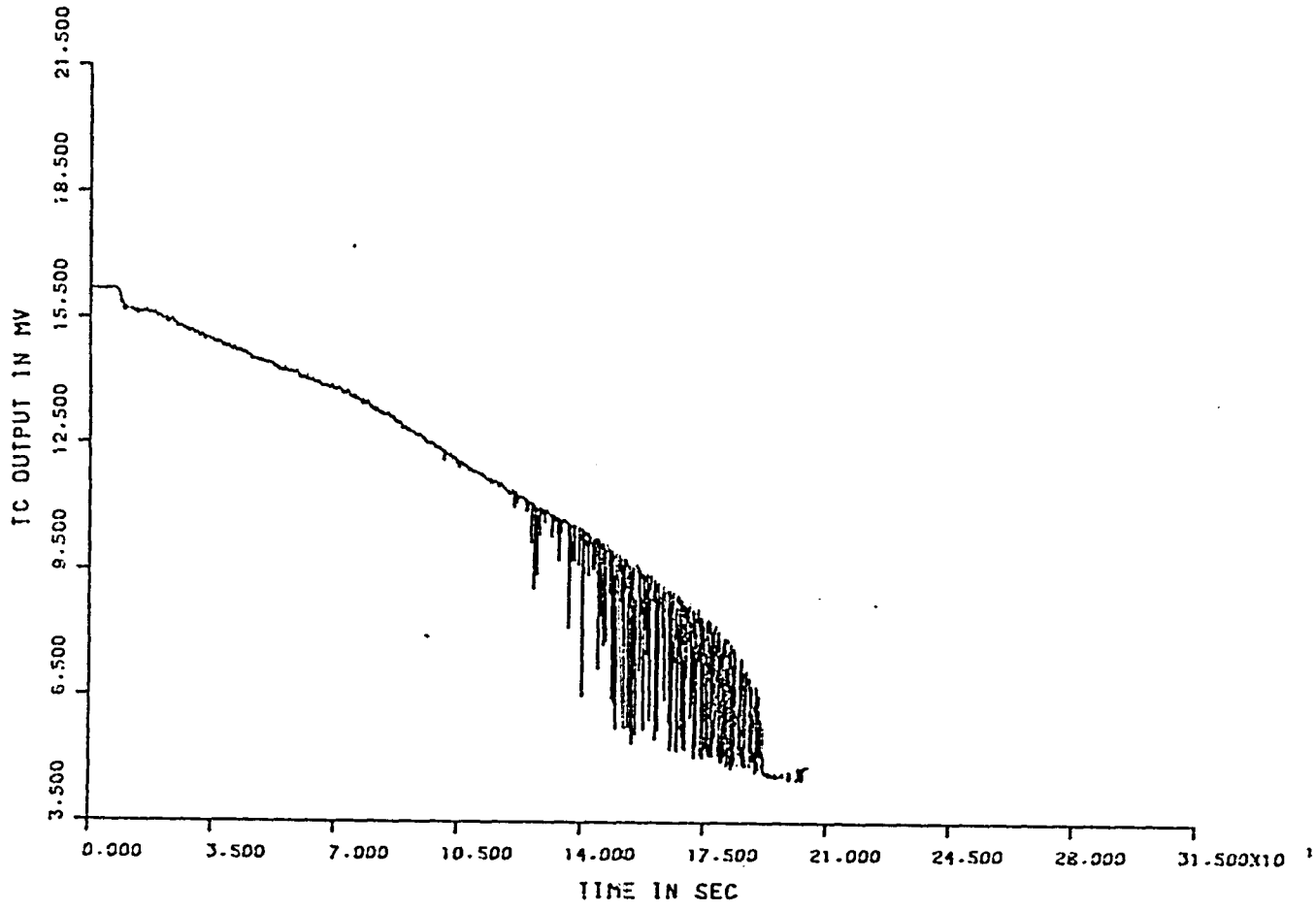

Record OQ, overall quench, run series 500s

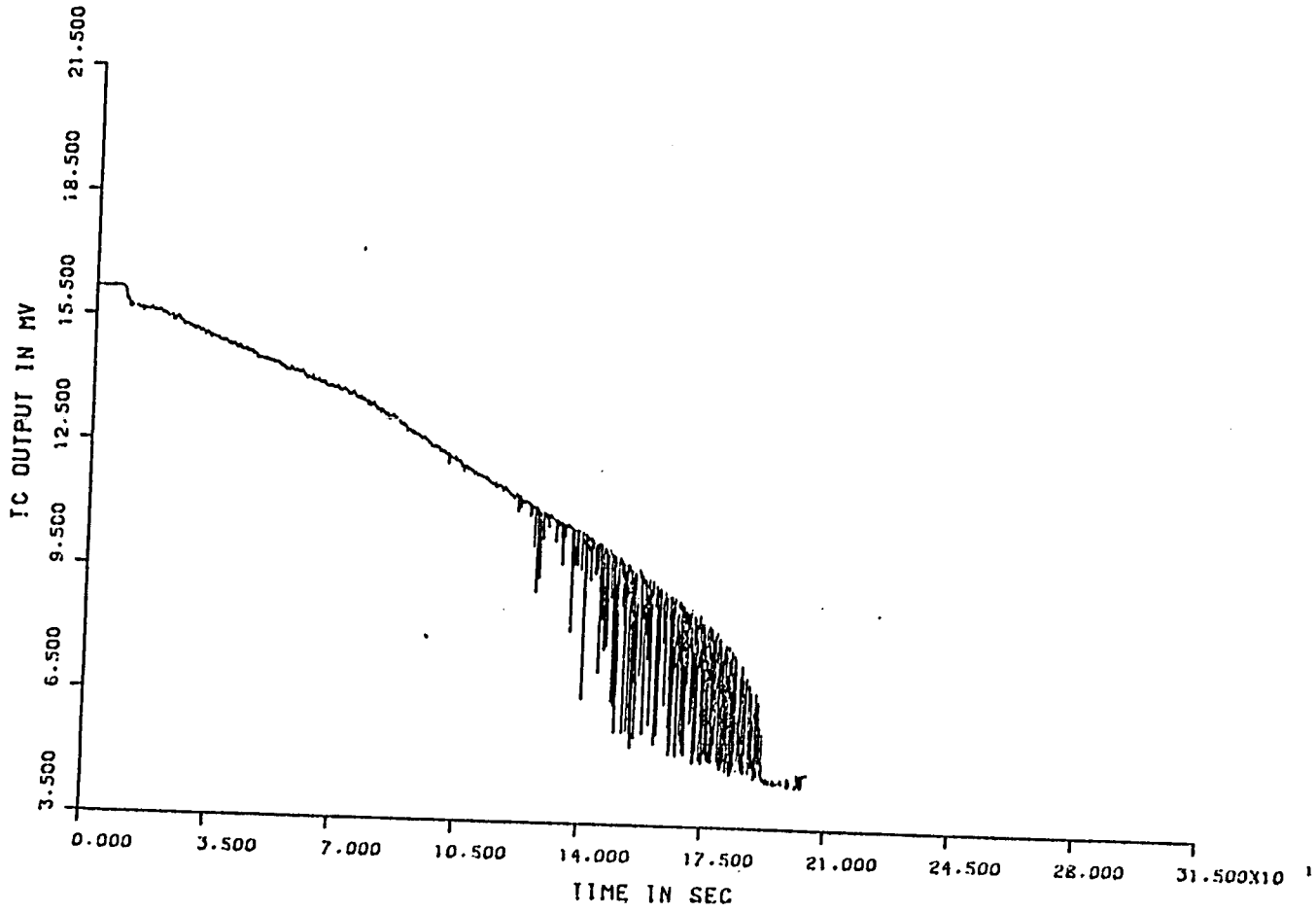

Record OQ, overall quench, run series 500s

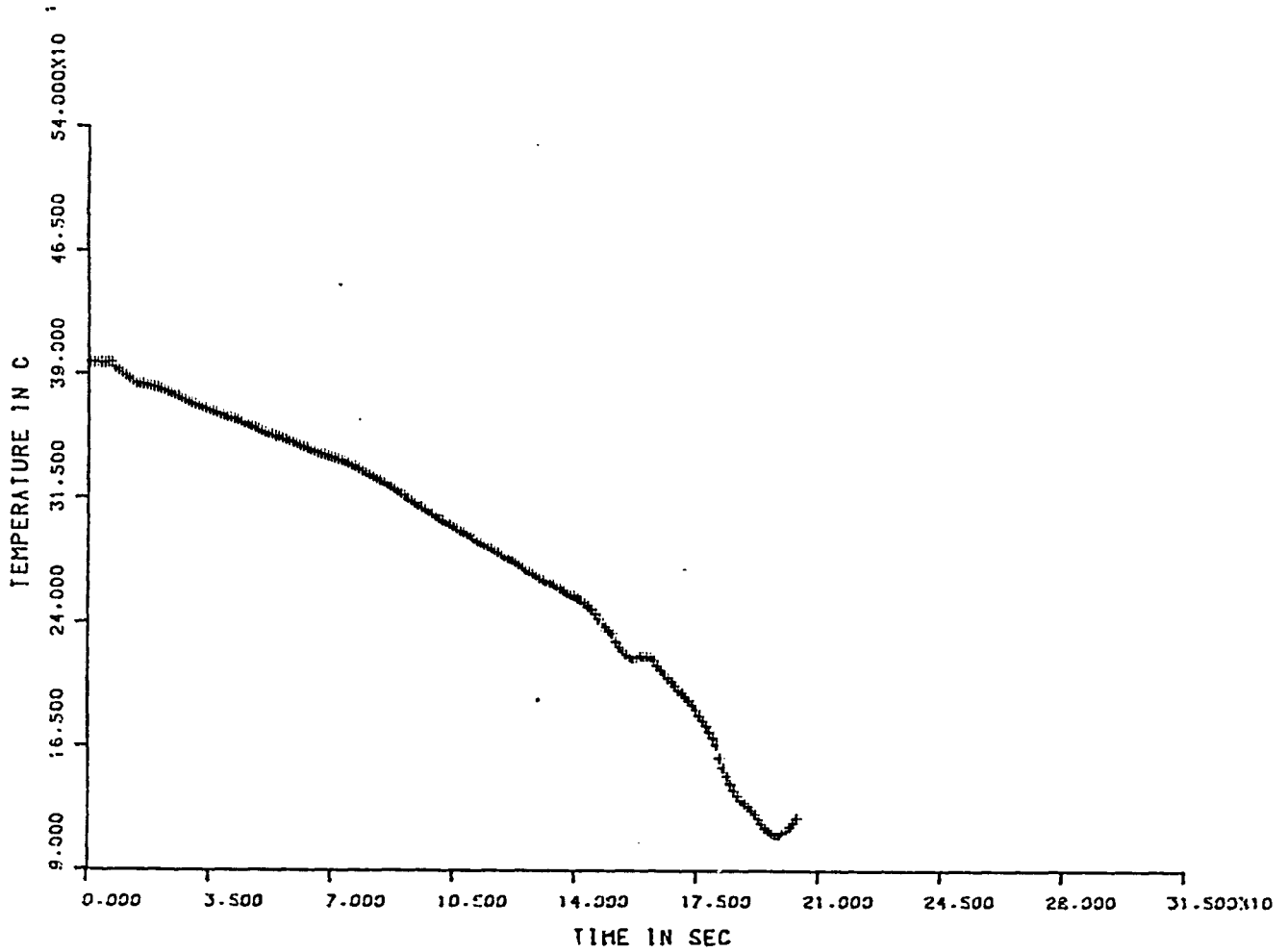

Record OQ, smoothed overall quench, run series 500s

Record OQ, smoothed overall quench, run series 500s

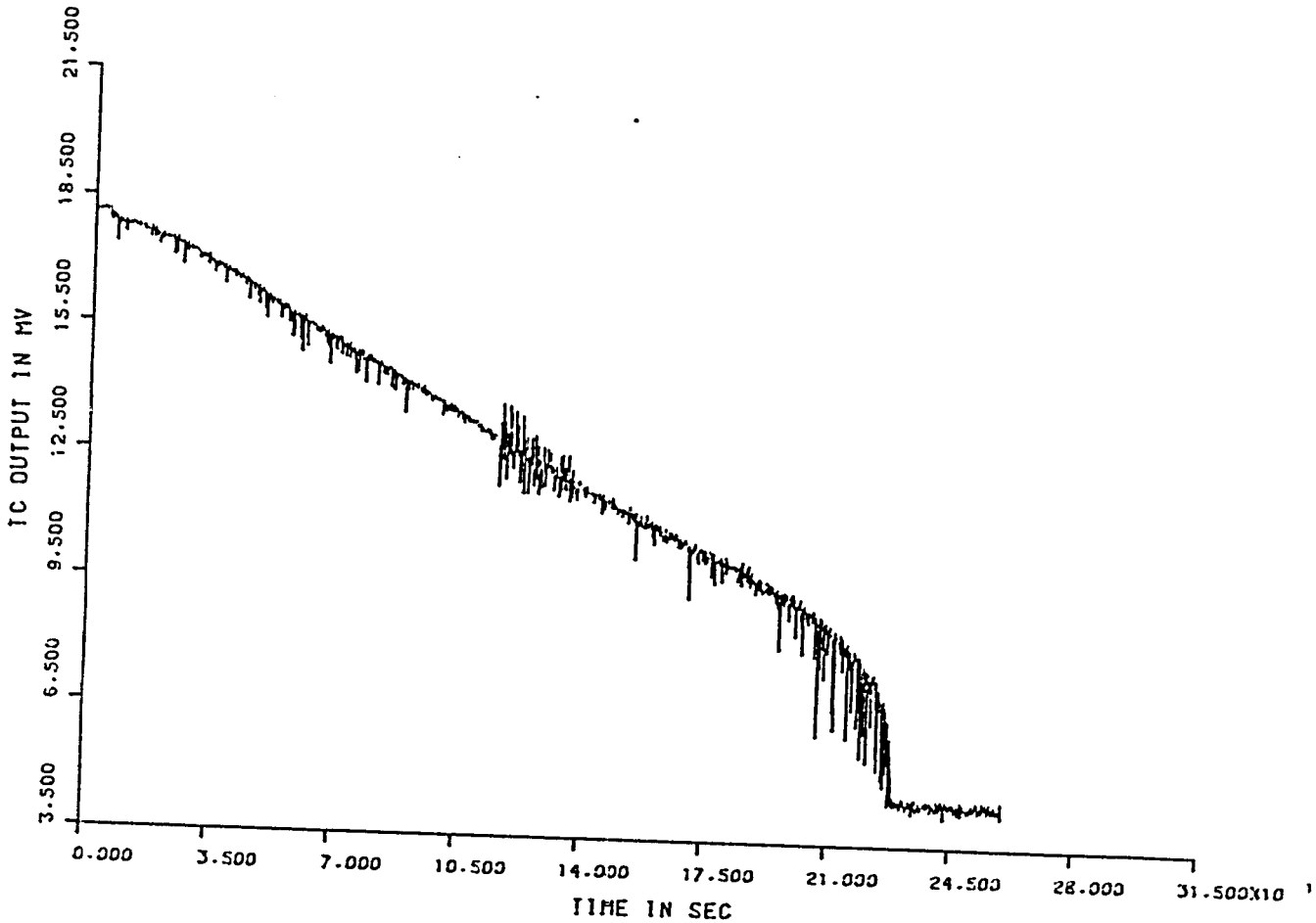

Run #2, overall quench, series II

III

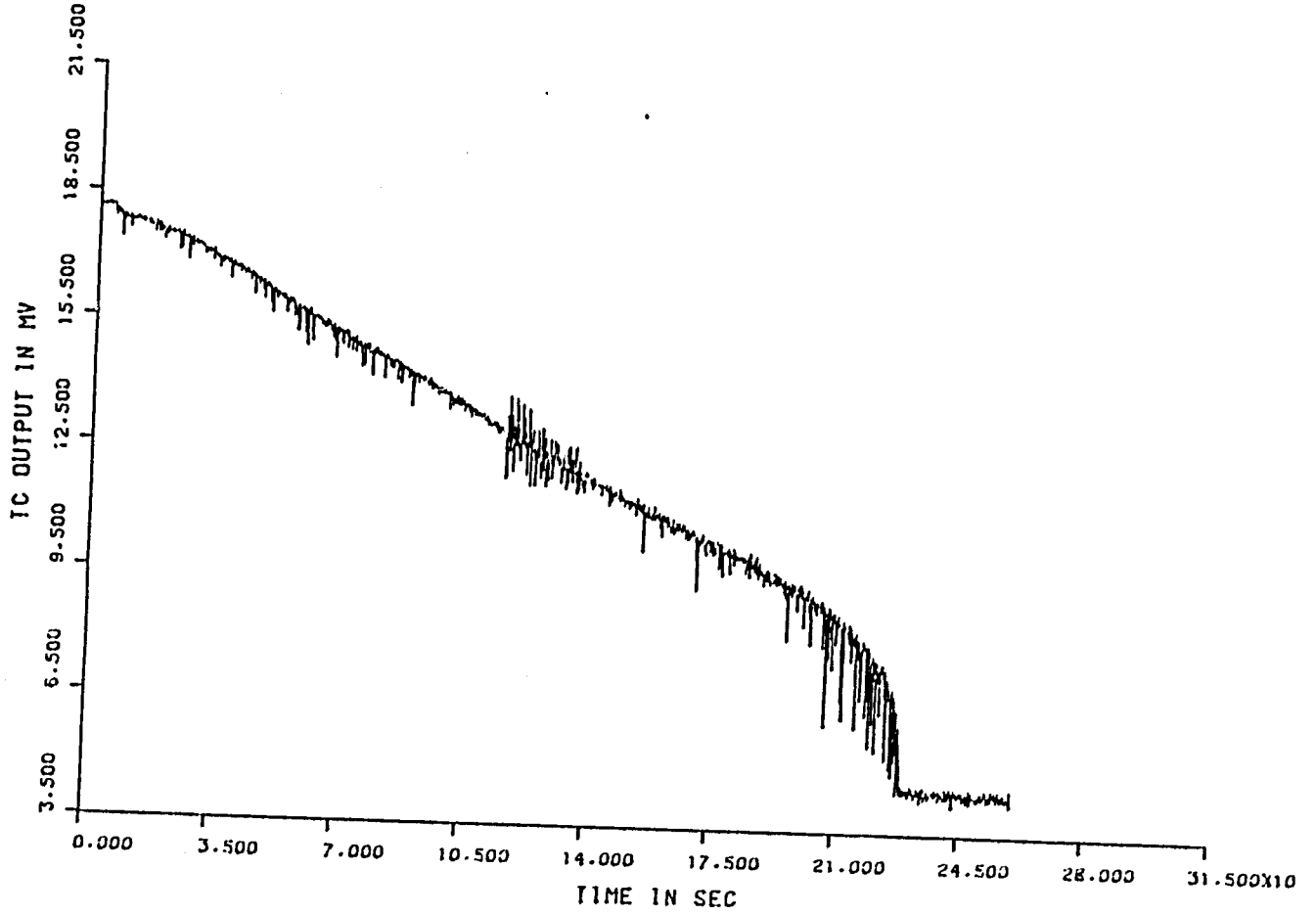

Run #2, overall quench, series II

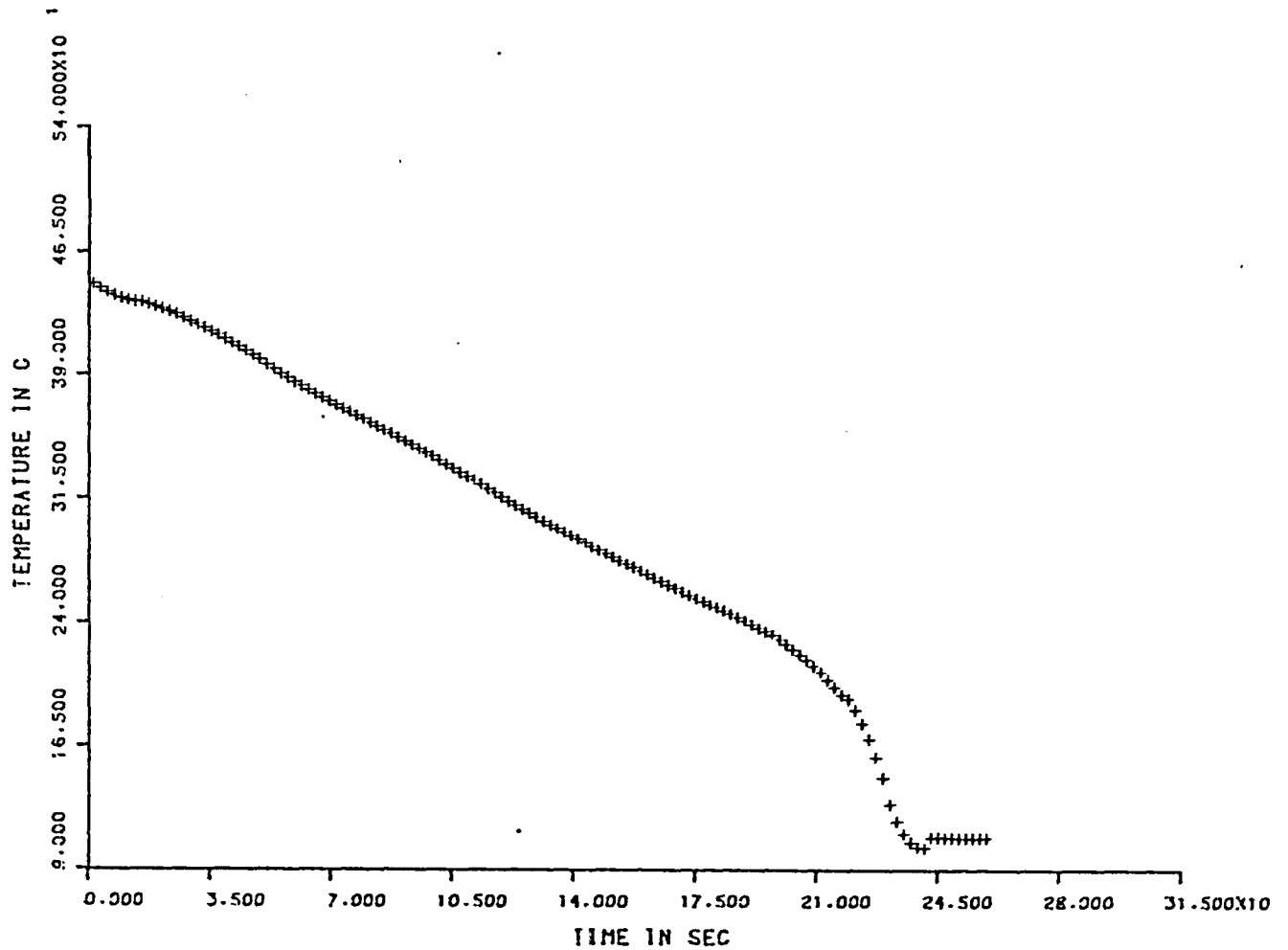

Run #2, smoothed overall quench, series II

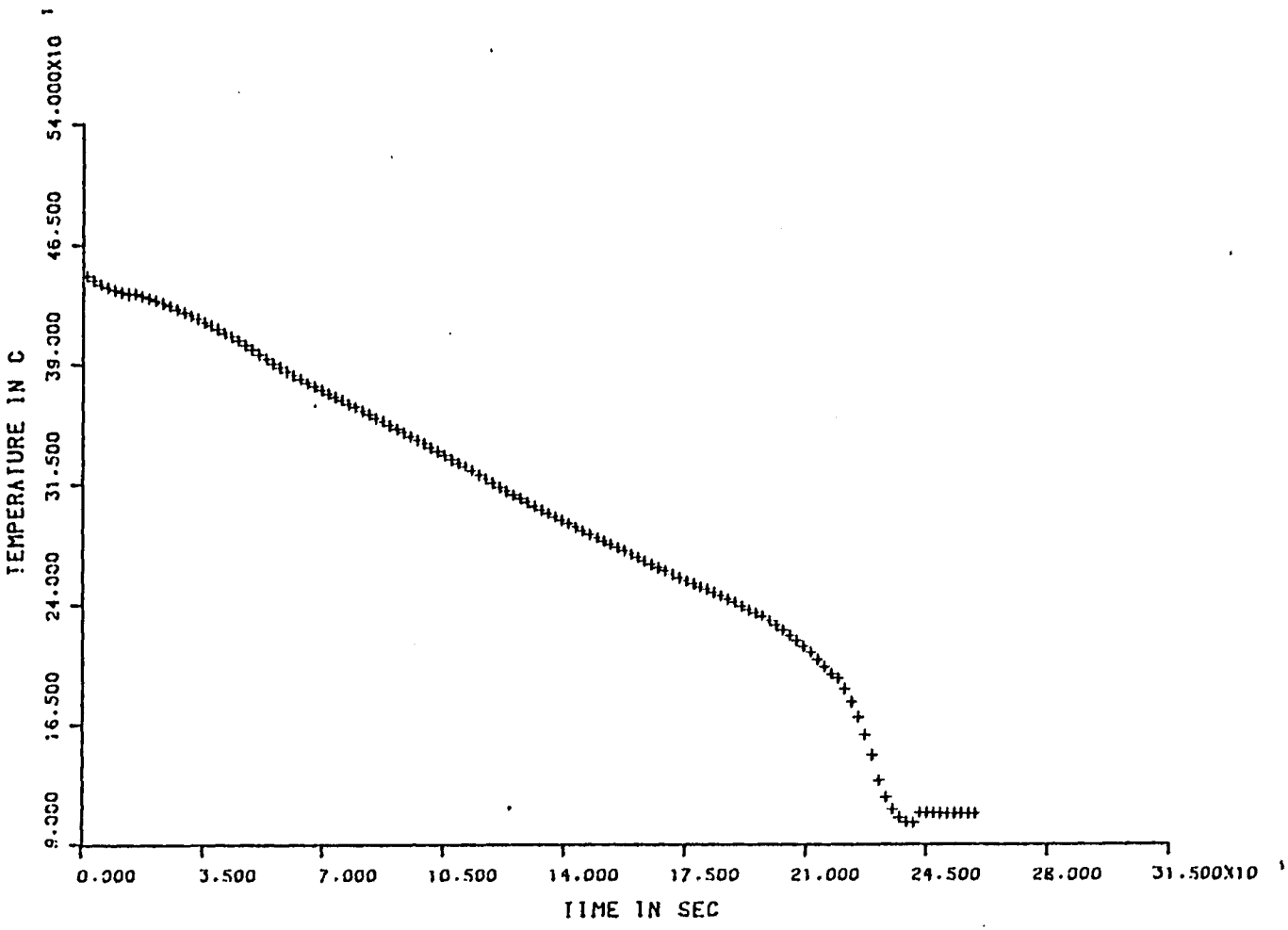

Run #2, smoothed overall quench, series II

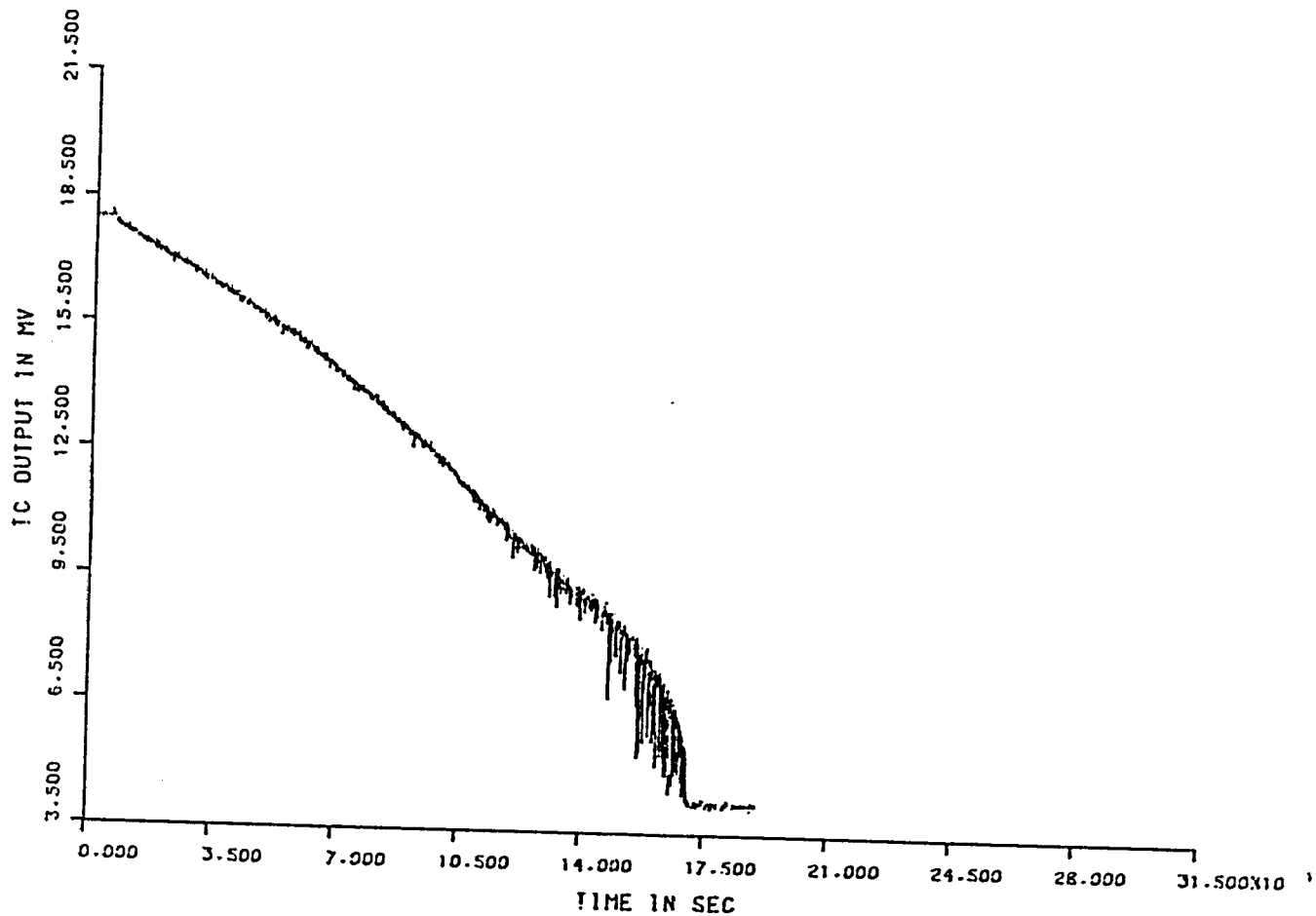

Run #3, overall quench, series II

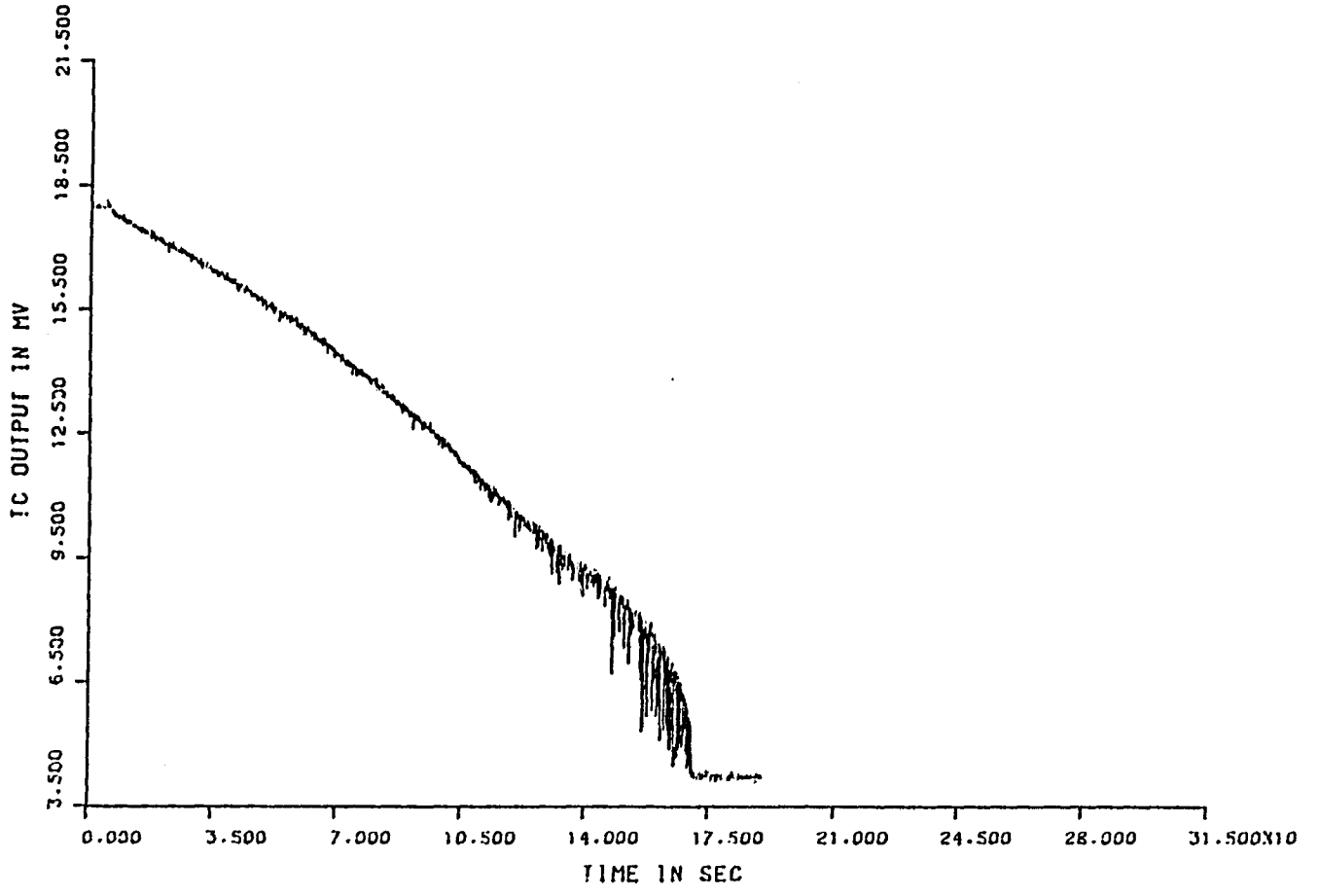

Run #3, overall quench, series II

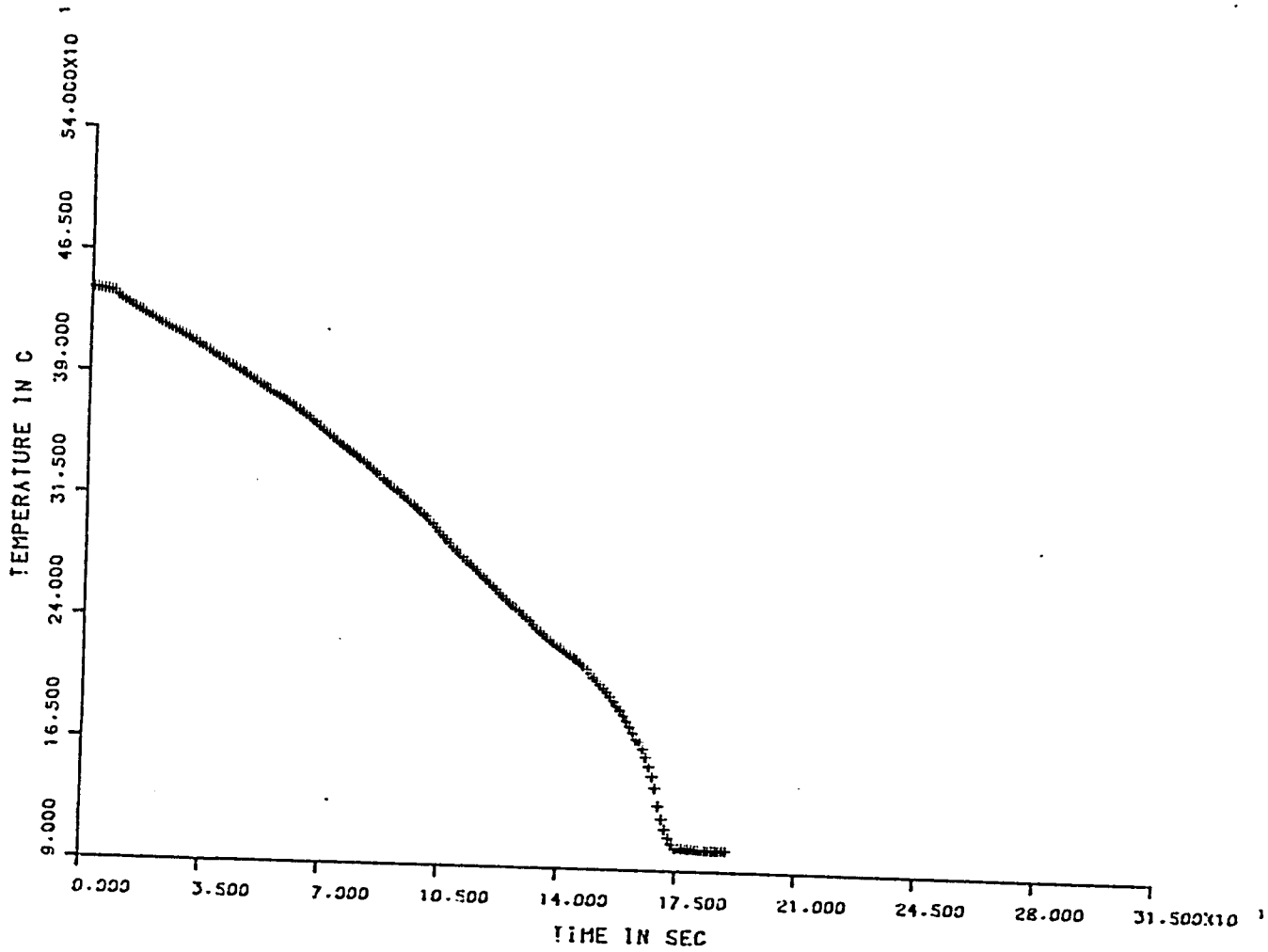

Run #3, smoothed overall quench, series II

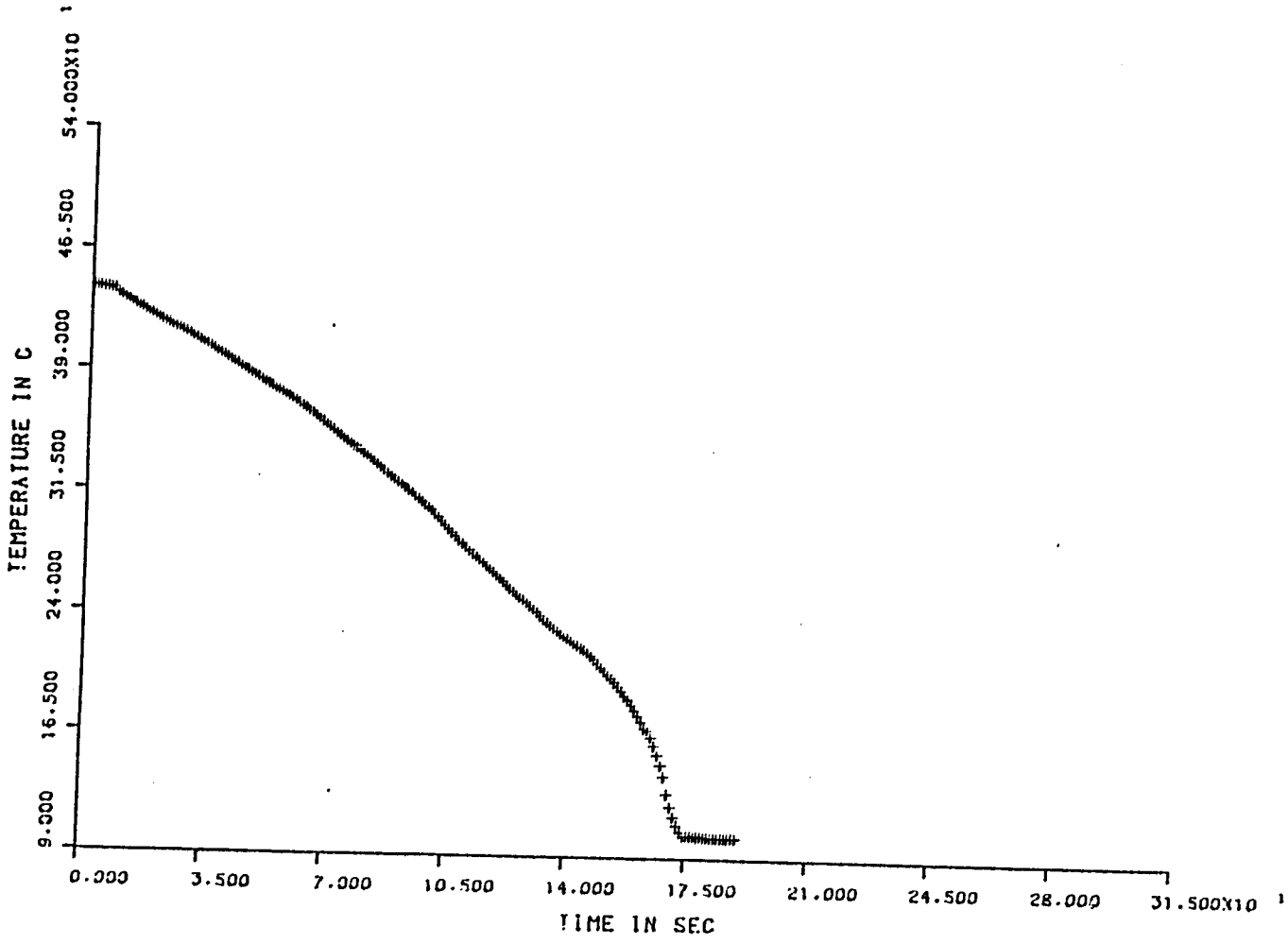

Run #3, smoothed overall quench, series II

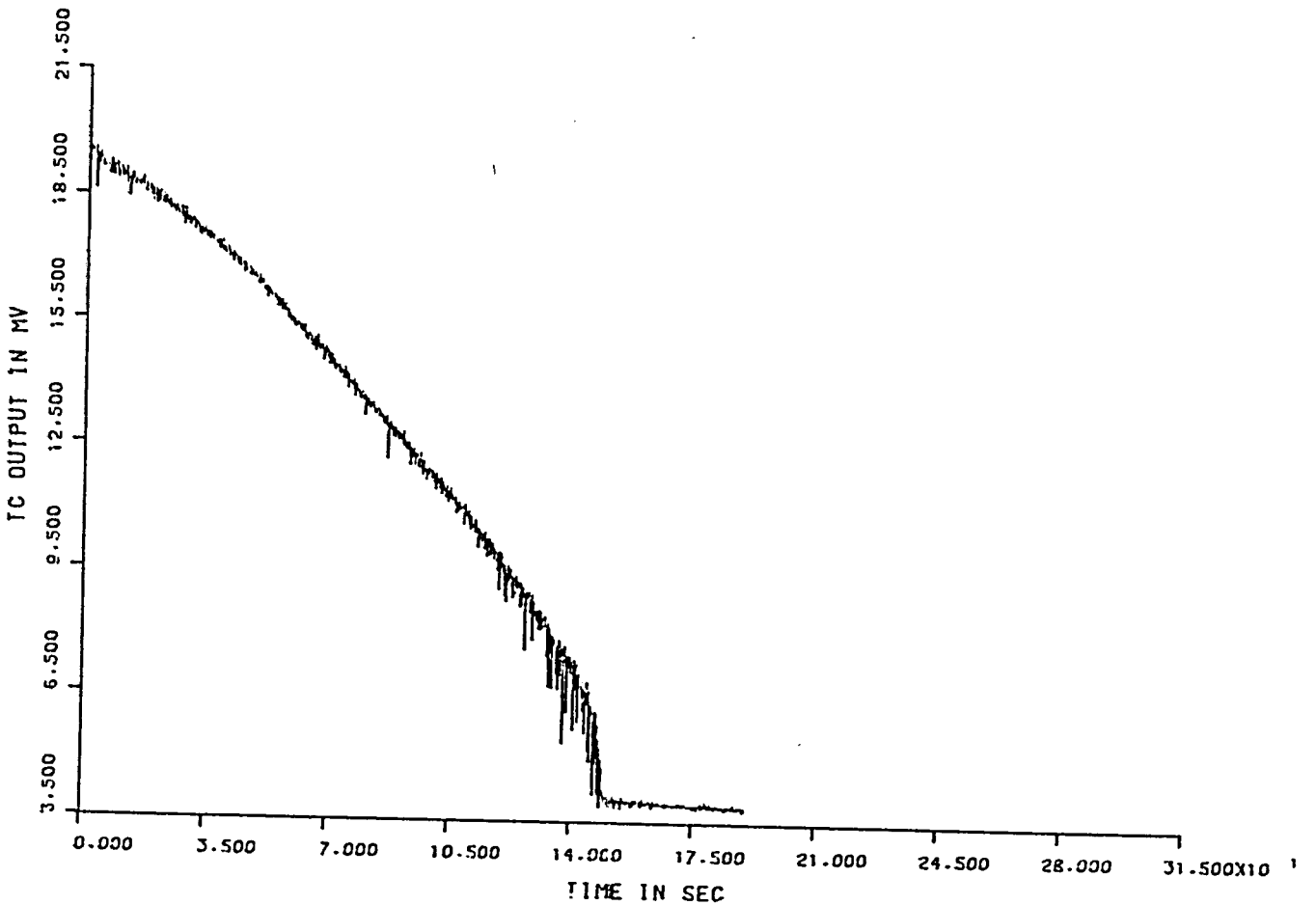

Run #4, overall quench, series II

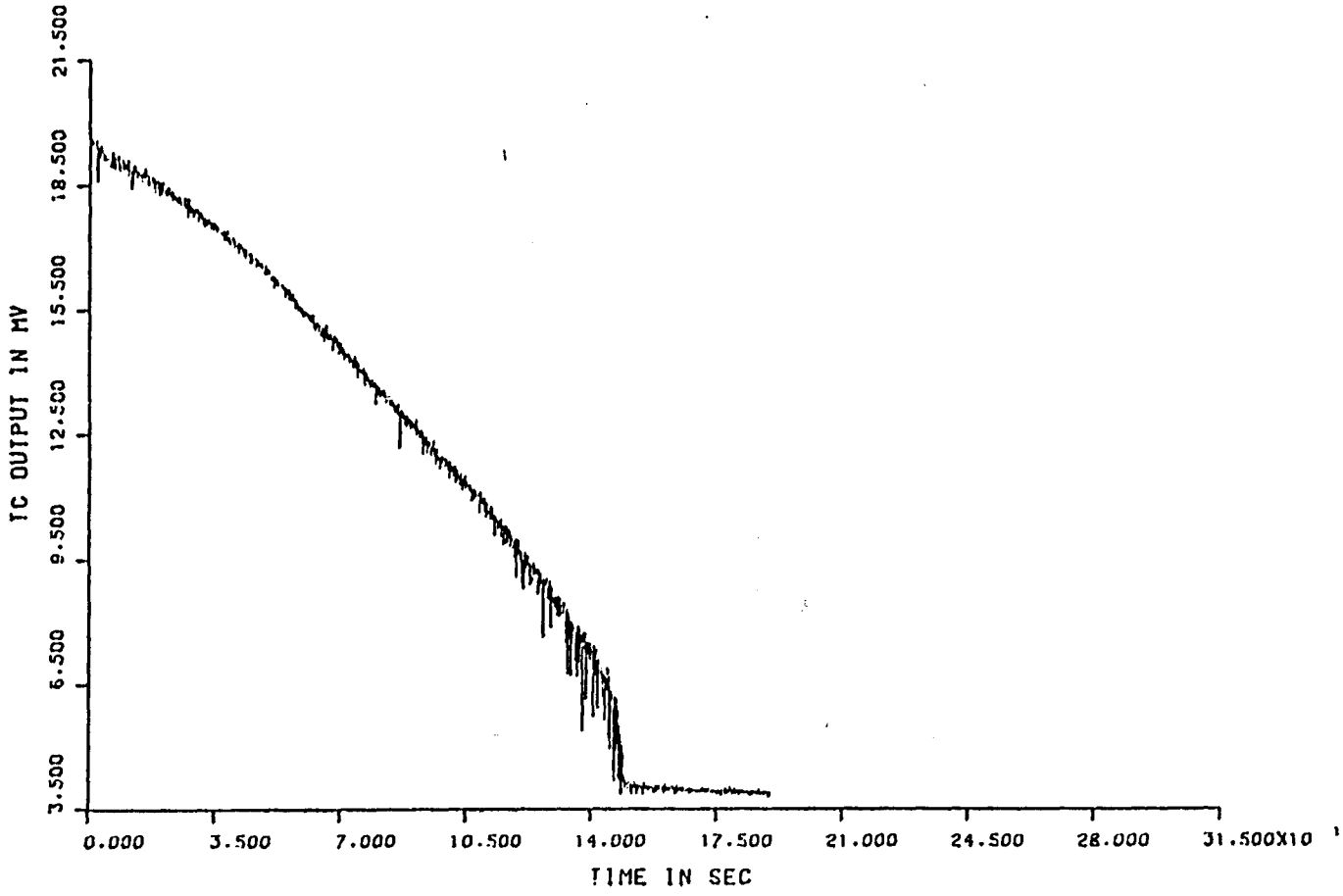

Run #4, overall quench, series II

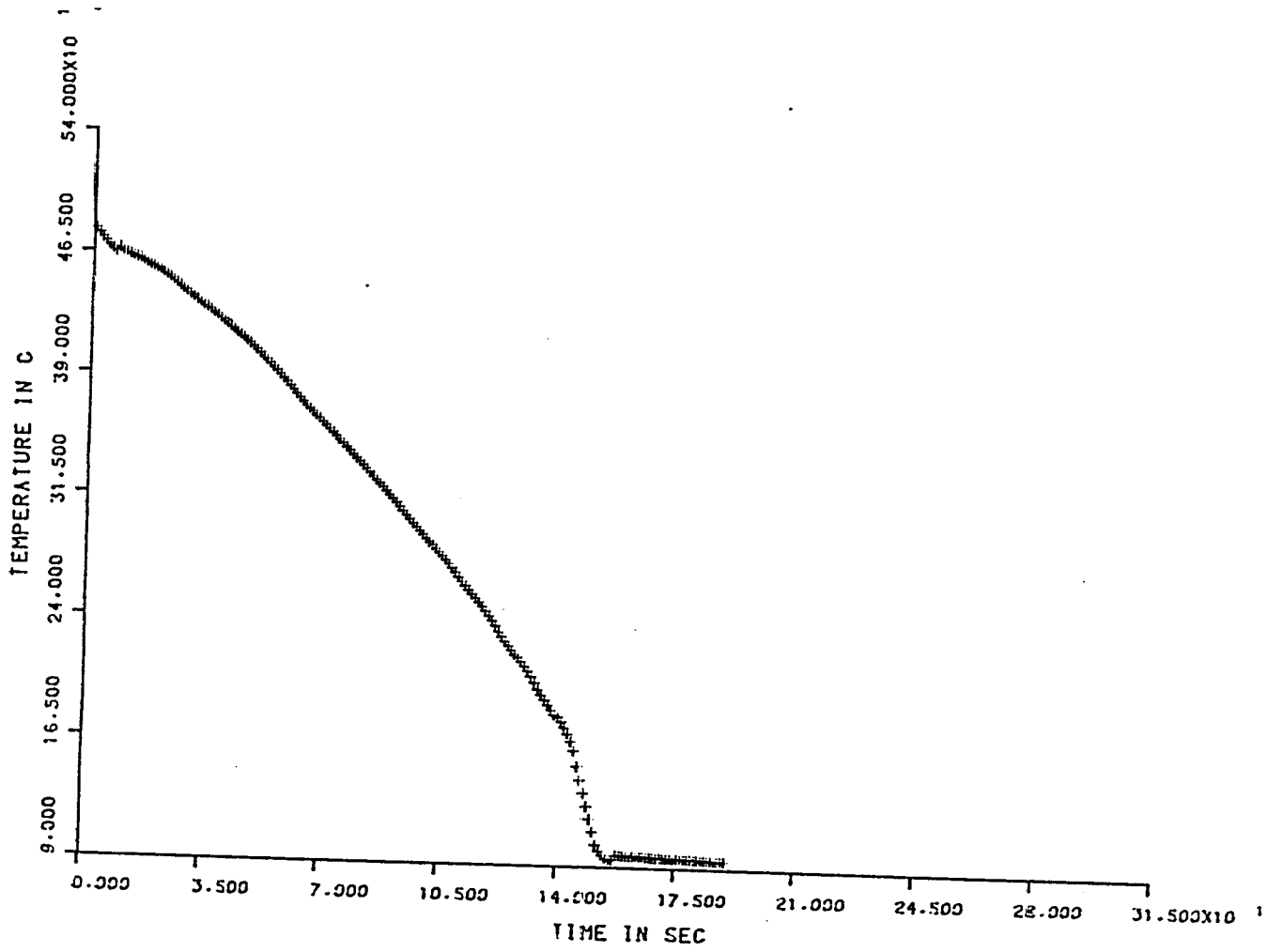

Run #4, smoothed overall quench, series II

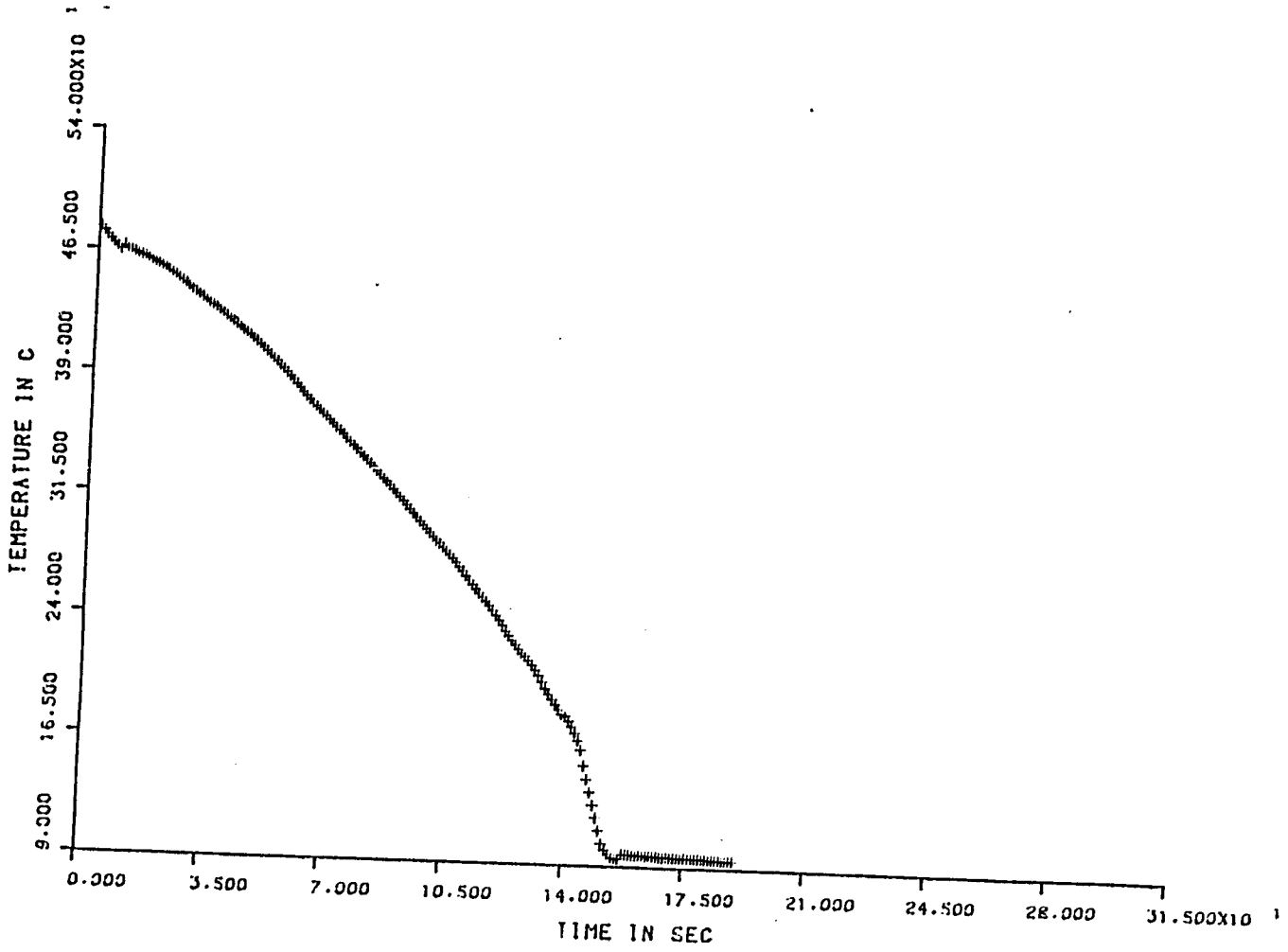

Run #4, smoothed overall quench, series II

VITA

Mr. Leo Yu-Wan Lee is the oldest son of Mr. Wang-Cheong Lee and Mrs. Char Kiu Lee. Born June 23, 1957 in Yuen Long of Hong Kong, he attended Yuen Long Public Middle School and the Diocesan Boy's School. In January, 1975, he attended Vincennes University (a junior college) in Indiana, and later obtained his B.S. degree in mechanical engineering at Cooper Union, New Yorik, in 1979. Currently he is completing his M.S. degree at Lehigh University with major studies in the field of thermo-fluids and heat transfer science.